Nanoscale Advances

REVIEW

View Article Online
View Journal | View Issue

Cite this: *Nanoscale Adv.*, 2026, **8**, 3035

Catalyst screening for electrochemical ammonia synthesis: a critical review

Dominik G. Jammal, *[a] Ricardo Bernardino, [a] Nuno Canha, [a] Cristina M. Cordas [ab] and Rui P. P. L. Ribeiro [ab]

Ammonia (NH_3) is a promising carbon-free energy carrier, and its synthesis is a key process in the chemical industry. While the Haber–Bosch process remains dominant, alternative approaches such as lithium-mediated nitrogen reduction (Li-mNRR), electrocatalysis, and photocatalysis are increasingly explored for sustainable NH_3 production. In this review, we systematically analyze 215 catalytic systems, evaluating production rates, faradaic efficiencies, and cost-performance. Key trends highlight the importance of transition-metal centers (*e.g.*, Mo, Ni, Cu), high-surface-area conductive supports (MOF- or MXene-based), and structural optimization *via* porosity, defect engineering, and doping. Our analysis identifies major gaps in standardized data reporting, particularly the frequent omission of turnover frequency, stability, and surface area, which hinder meaningful comparisons and limit machine-learning-driven catalyst design. We propose standardized metrics (*e.g.*, μmol cm^{-2} s^{-1}) and comprehensive reporting of key parameters to enable cross-catalyst comparison and the development of high-quality datasets. These insights provide practical guidelines for the rational design of efficient, stable, and scalable catalysts, with Mo-based systems, MOFs, and transition-metal nitrides/carbides emerging as particularly promising candidates for electrochemical and photocatalytic NH_3 synthesis.

Received 27th December 2025
Accepted 15th March 2026

DOI: 10.1039/d5na01170a

rsc.li/nanoscale-advances

1 Introduction

Ammonia (NH_3) is one of the most crucial chemicals in the global economy of the 21st century.[1] It is primarily used as a precursor for fertilizers and other essential industrial chemicals.[2] The importance of NH_3 is further underscored by its key role in sustaining global food production, with 40–50% of the global food supply depending on NH_3-based fertilizers.[3,4] With

[a]*HyLab- Green Hydrogen Collaborative Laboratory, Sines Central Termoelétrica, Estrada Nacional 120-1, Sines, 7520-089, Portugal. E-mail: dominik.jammal@hylab.pt*

[b]*LAQV-REQUIMTE, Department of Chemistry, NOVA School of Science and Technology, NOVA University Lisbon, Caparica 2829-516, Portugal*

Dominik G. Jammal

Dominik G. Jammal is a researcher at HyLab – CoLAB in Sines, Portugal, and a PhD candidate at the NOVA School of Science and Technology, Portugal. He earned his BSc in Chemistry from Julius-Maximilians-Universität Würzburg and his MSc in Chemistry from the University of Leipzig, Germany, with a specialization in organometallic catalysis. His current research focuses on the design and synthesis of electrocatalysts, with a particular emphasis on developing novel, nature-inspired materials for sustainable ammonia, hydrogen, and CO_2 conversion.

Ricardo Bernardino

Ricardo Bernardino is a researcher at HyLab – CoLAB in Sines, Portugal, where he focuses on assessing risks associated with hydrogen systems, including storage, transport, and utilization. He earned his BSc in Mechanical Engineering from Instituto Superior Técnico in Lisbon and completed his MSc in Mechanical Engineering, with a specialization in Energy Systems, at the same institution.

the population of the world projected to grow by approximately 9.8 billion people by 2050,[5] ammonia's significance in ensuring future food security will continue to increase.[6] Beyond its agricultural and industrial uses, ammonia is increasingly recognized as a promising hydrogen carrier and carbon-free energy vector.[7] With a hydrogen content of 17.6% by weight and existing infrastructure for storage and transport, NH_3 offers distinct advantages over molecular hydrogen (H_2), which requires either cryogenic (−253 °C) or high-pressure (up to 700 bar) storage. Its ease of liquefaction (−33.4 °C, 8–10 bar) and well-established distribution networks make NH_3 particularly attractive for large-scale energy applications.[8,9] Ammonia can also be directly utilized without prior cracking back to hydrogen, for example in microturbines or in ammonia fuel cells, where ongoing research demonstrates its potential as a zero carbon fuel.[10] While the exact comparison is case-dependent, some studies report that the energy penalty of converting H_2 to NH_3 and back is of the same order of magnitude as liquefying H_2. In addition to its storage and handling advantages, ammonia exhibits a favorable energy density compared to other carriers, and in particular H_2. In fact, liquefied hydrogen (LH_2) has an energy density of 2.36 kWh L^{-1}, whereas liquefied ammonia (LNH_3) reaches 3.53 kWh L^{-1}, representing a 33% higher volumetric energy content. Compared to carbon-based carriers like methanol (LMeOH = 4.39 kWh L^{-1}), ammonia provides a zero-carbon alternative with well-established logistics and reduced CO_2 emissions as depicted in Fig. 1.[11] These characteristics further highlight the potential of NH_3 as a versatile and sustainable candidate for both large-scale energy storage and direct energy use in a future hydrogen economy.[12] Ammonia production is commonly

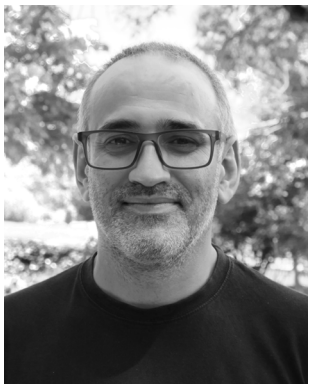

Nuno Canha

Nuno Canha is a Lead Researcher at HyLab – CoLAB (Green Hydrogen Collaborative Laboratory), where he coordinates the Safety and Risk Assessment Unit within the hydrogen end-use pillar. His research focuses on quantitative risk assessment and the experimental and numerical characterisation of hydrogen leaks and dispersion across operational contexts. His work also covers benchmarking and performance evaluation of hydrogen sensors for detection and safety applications. He holds a PhD in Environmental Sciences from Delft University of Technology and an MSc in Chemistry from Instituto Superior Técnico. His broader background includes air quality, exposure assessment, and environmental health research.

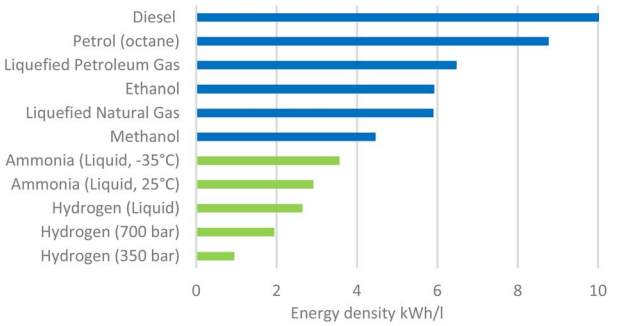

Fig. 1 Comparison of energy densities of zero carbon fuels (green) and carbon-based fuels.[11] Created using data reported in ref. 11. The Royal Society (2020).

Cristina M. Cordas

Cristina M. Cordas is an Assistant Professor in the Department of Chemistry at the NOVA School of Science and Technology and a researcher at LAQV-REQUIMTE. Her work focuses on interfacial electrochemistry, bioelectrochemistry, and sustainable energy systems, particularly green hydrogen production, electrolysis using low-quality water, and bio-inspired catalysts. She integrates fundamental electrochemical principles with advanced materials and enzymatic systems to address energy transition challenges. Cristina is actively involved in European research collaborations, project coordination, and advanced training, contributing to the development of innovative electrochemical technologies for clean energy and environmental sustainability.

Rui P. P. L. Ribeiro

Rui P. P. L. Ribeiro is an Assistant Professor at the NOVA School of Science and Technology (Portugal). His research focuses on adsorption processes and materials for gas separation and purification, with particular emphasis on carbon dioxide capture, biogas upgrading, hydrogen purification, and related sustainable energy applications. He has extensive experience in adsorption-based technologies such as Electric Swing Adsorption (ESA). More recently, he has been working on the shaping of porous materials through different approaches, including 3D printing. Rui Ribeiro's work aims to develop efficient systems and materials that contribute to decarbonization and the deployment of clean energy technologies.

categorized into three main routes: grey, blue, and green ammonia. Grey ammonia is obtained *via* conventional steam methane reforming (SMR) combined with the Haber–Bosch process, but it is associated with substantial CO_2 emissions. Blue ammonia follows the same production pathway yet integrates carbon capture and storage (CCS) technologies, lowering CO_2 emissions by approximately 9–12%.[13] In contrast, green ammonia represents a paradigm shift, as it relies on renewable energy sources such as wind, solar, or hydropower for hydrogen generation through electrolysis, and subsequent reaction with nitrogen (N_2), thereby offering a near carbon-free alternative.

To contextualize these advantages, it is useful to consider the current scale of ammonia production and the industrial processes that enable it. As depicted in Fig. 2, the global NH_3 production in 2023 reached *c.a.* 240 million tons annually, with a market value of USD 83.36 billion. This is expected to grow to around 290 million tons by 2030, reaching an estimated value of USD 129.63 billion.[14,15]

As mentioned, ammonia is industrially produced through the Haber–Bosch process since the 1910's, although throughout the 20th century, the process underwent continuous improvements, including a transition from coal to natural gas as the source for H_2 production.[16] Despite ongoing research into more eco-friendly methods, such as hydrogen production through electrolysis, the Haber–Bosch process using natural gas remains the industry standard due to its low costs and an overall energy efficiency of 66%.[17] The Haber–Bosch process involves reacting nitrogen obtained from air, typically through cryogenic air separation (ASU) or pressure swing adsorption (PSA), with hydrogen derived from natural gas, being described through the following exothermic reaction.[18]

$$N_2(g) + 3H_2(g) \rightleftharpoons 2NH_3(g)\ \Delta H^0 = -92.6\ \text{kJ mol}^{-1} \quad (1)$$

The formation of NH_3 is thermodynamically favoured at low temperatures. However, kinetic limitations under those mild conditions, implies the industrial Haber–Bosch process to be carried out at temperatures between 400–500 °C to achieve an efficient production rate.[19,20] The extremely high activation energy (E_a) required to break the triple bond (945 kJ mol^{-1}) necessitates these high temperatures to facilitate efficient dissociation.[21] Equilibrium calculations reveal that at temperatures above 400 °C and a pressure of 0.1 MPa, more than 99% of NH_3 decomposes.[22] To address this challenge, the Haber–Bosch process operates under a compromise, utilizing moderately high temperatures of 400–500 °C combined with high pressures of 20–40 MPa.[23] High operating pressures shift the equilibrium towards NH_3 production, while the temperatures are sufficient to overcome the kinetic barrier without causing excessive decomposition. Typically, only about 15% of the reactants convert to NH_3 in a single reaction pass, but the unreacted N_2 and H_2 are recycled back into the Haber–Bosch production cycle. This recycling approach, combined with the integration of heat recovery systems, leads to an overall conversion rate of ~97%. The produced NH_3 is liquefied at −33.4 °C and maintained under pressures of 8–10 bar to ensure safe storage and distribution.[24] Fig. 3 shows the process flow diagram of the Haber–Bosch process based on steam methane reforming.[25,26]

The high efficiency of this process is due to both optimal reaction conditions but also the utilization of highly effective catalysts that significantly enhance NH_3 production. In particular, iron (Fe) and nickel (Ni) catalysts are widely used in the process because of their catalytic activity, availability, and cost-effectiveness (Fe ~ $107 per ton, Ni ~ $16,300 per ton).[18,26–28] The incorporation of ruthenium (Ru) catalysts also proves to be beneficial in the Haber–Bosch process as these catalysts are highly efficient owing to their exceptional selectivity and long-

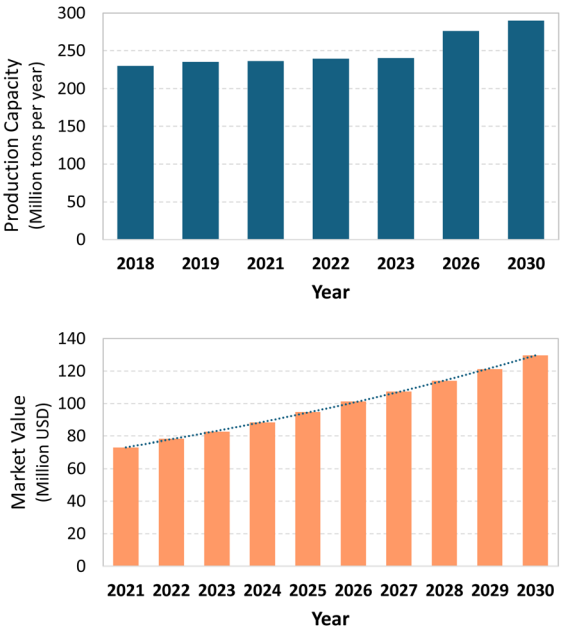

Fig. 2 NH_3 Production capacity in million tons per year from 2018 to 2023 (above), along with forecasts for 2026 and 2030 (above). Ammonia market value in billions USD from 2021 to 2024, Best wishes, Joe Busby along with projection to 2030 (down).[15] Created using data reported in ref. 15. IEA (2021). Licence: CC BY 4.0.

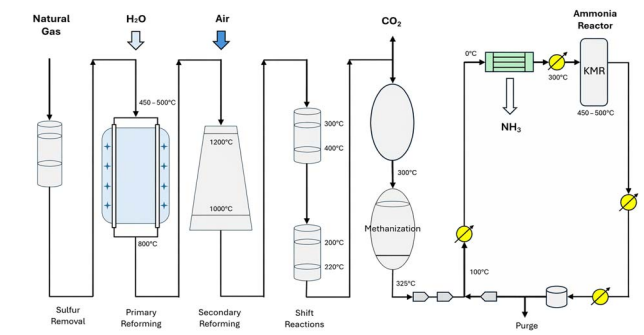

Fig. 3 Process flow diagram of the SMR reforming based Haber–Bosch process: Key stages from natural gas desulfurization, primary and secondary reforming and shift reactions to the methanation and ammonia synthesis loop.[25,26] Adapted from ref. 26 with permission Elsevier

term stability.[26,29] Their main drawback is their high cost (*e.g.* Ru ~ $13 million per ton). Although a range of d-metal catalysts—including Co, Cr, Mn, Mo, Pd, Pt, Rh, W, and V—are under continuous investigation, Fe and Ni are particularly notable for their favourable balance between catalytic performance and cost, whereas Ru is distinguished mainly by its superior intrinsic activity. Typically, these catalysts are combined with various activators and support materials to enhance their performance. Alumina (Al_2O_3) and potassium oxide (K_2O) for instance serve as activators to improve the catalysts' efficiency and stability.[27] Additionally, support materials like alumina (Al_2O_3) and silicon dioxide (SiO_2) increase the catalyst's surface area, thereby enhancing overall effectiveness by improving reactant accessibility and promoting better dispersion of the active sites.[30–32]

1.1 Efficiency and CO_2 emissions of the Haber–Bosch process

The Haber–Bosch process, utilizing H_2 from natural gas through Steam Methane Reforming (SMR), remains the more economically viable option. Continuous improvements in this process have achieved an energy consumption of 28 GJ per ton of NH_3 (with a practical minimum around 22 GJ per t NH_3 (Fig. 4)).[33] With global natural gas prices ranging from $0.00728 to $0.0425 per kWh, the cost of producing one ton of NH_3 is estimated to be between approximately $44 and $330.[34,35] However, the high CO_2 emissions associated with this process—approximately 2.4 tons per ton of NH_3, accounting for about 1% of global CO_2 emissions—underscore the need for cleaner ammonia production methods.[36] With green H_2 produced by water electrolysis, CO_2 emissions can be dramatically reduced. While the current electrolysis-based Haber–Bosch process consumes around 38 GJ per t NH_3 in practice, the theoretical minimum energy required for NH_3 synthesis itself is approximately 21 GJ per t NH_3. This theoretical value represents the energy needed solely for the chemical conversion of N_2 and H_2 into NH_3 and is lower than the practical minimum of the conventional HB process because it does not include energy losses from H_2 production.[36]

As renewable energy prices continue to decline—currently around USD $0.0490 per kWh for photovoltaic (PV) power—the estimated cost of producing green NH_3 is projected to be approximately USD $520 per t NH_3.[35] Despite these advancements, independently from the H_2 source, the Haber–Bosch process remains energy-intensive due to the high temperature and pressure requirements. Furthermore, the optimal Haber–Bosch process operates continuously which adds complexity when working with intermittency of the conversion of renewables into H_2.[37] Consequently, there is an ongoing effort to develop alternatives to the HB process. A promising approach is the production of NH_3 through (photo)-electrocatalysis, as these methods offer a cleaner alternative with potential reduction of CO_2 emissions from 1.6 tons to around 0.1 tons per ton of NH_3. A comparative overview of the performance of conventional and emerging NH_3-production routes is provided in Table 1, which summarizes the most relevant efficiency metrics and operational characteristics. These alternative approaches will be further explored in Chapter 3.[38]

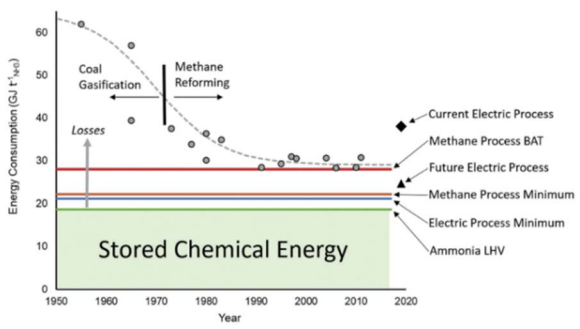

Fig. 4 Efficiency improvements in NH_3 production are shown, comparing real plant data with BAT, energy minima for methane- and electrolysis-based routes (H_2, LHV basis), and current versus projected electric processes. LHV indicates the lower heating value of NH_3, with excess energy reflecting losses.[33] Reproduced from Ref. 33 via Creative Commons CC BY 3.0 licence.

1.2 State-of-the-art and scope of this review

In recent years, several comprehensive review articles have addressed electrochemical and photo(electro)chemical nitrogen reduction reactions (NRR), reflecting the rapidly growing interest in sustainable ammonia synthesis. Key reviews published between 2022 and 2025 have focused on distinct but complementary aspects of this research. For instance, Ahmed *et al.*, 2023 (ref. 44) and Mangini *et al.* (2024)[45] systematically analyzed Li-mNRR, discussing catalysts, electrolyte formulations, reactor designs, and strategies to enhance faradaic efficiency. Biswas *et al.* (2022)[46] and Mahmood *et al.* (2024)[47] focused on catalyst design principles for electrochemical NRR, mechanistic insights, and performance benchmarking using transition metal-based systems. Meanwhile, Ješić *et al.* (2024)[48] and Shen *et al.* (2022)[49] examined photo(electro)catalytic routes, highlighting the role of light absorption, charge carrier dynamics, and defect engineering in enhancing catalytic activity. In addition, emerging material classes such as metal–organic frameworks (MOFs) have gained increasing attention due to their high surface areas, structural tunability, and the large density of accessible catalytic sites, which are particularly beneficial for N_2 adsorption and activation. The growing relevance of MOFs for electrocatalytic NRR has been comprehensively summarized in "*Recent Advances in Metal–Organic Frameworks and Their Derivatives for Electrocatalytic Nitrogen Reduction to Ammonia*" (2022), highlighting both pristine MOFs and MOF-derived materials as promising catalyst platforms. In the present review, the analysis is intentionally limited to pristine MOF-based catalysts. MOF-derived materials with substantially altered compositions or morphologies are excluded, as their complex transformation pathways and heterogeneous structures hinder a consistent and quantitative comparison of production rates (PR), faradaic efficiencies (FE), and catalyst costs (CC) across different NH_3 synthesis routes.

Table 1 Comprehensive evaluation of the process performance of different ammonia production technique

Process performance overview	SMR HB-process	Benchmark electrolysis HB-process	Electrochemical synthesis (aqueous NRR purge)	Lithium mediated NRR (Li-mNRR)
Energy consumption per ton of NH_3 [a] (GJ per kWh)	28/7778 (ref. 39)	38.4/11 000 (ref. 39)	~67/19 000 (ref. 39)	190/50 000 (ref. 39)
Efficiencies (%) [b]	61–66 (ref. 40)	65	Not reported	Not reported (ref. 41)
Faradaic efficiencies (%)	~97 (ref. 42)	Not reported	~**73** (ref. 42)	**78.2** [d,43]
Costs (USD $ per t NH_3) [c]	55–330	520	910	2500
CO_2 emissions per t NH_3	2.4	0.1	0.1	0.1
TRL	9	7–9	1–3	1–3

[a] Energy consumption values include all major process operations: heating, distillation, the NRR electrolyzer, the H_2 electrolyzer, air separation units, and O_2 compression. [b] Overall efficiencies for electrochemical ammonia synthesis and lithium-mediated NRR are not provided, as standardized and reproducible efficiency metrics for these emerging technologies are not yet available. [c] Reported costs reflect the energy consumption in kWh per ton of NH_3, calculated using the current electricity price of USD 0.0490 per kWh as well as Natural gas price range (0.0073–0.0425 USD $ per kWh). [d] Ambient conditions.

While these prior reviews provide valuable insights into catalyst development, reaction mechanisms, and reactor concepts, they predominantly focus on either catalytic activity metrics or mechanistic trends, with techno-economic aspects largely treated qualitatively. In contrast, the present work systematically integrates PR, FE, and CC for 215 catalytic systems, enabling direct, cross-platform comparison across lithium-mediated, electrochemical, and photo(electro)catalytic NRR systems. To our knowledge, no previous review has benchmarked such a large number of catalytic systems across multiple quantitative performance metrics, including techno-economic considerations. By adopting a harmonized, quantitative assessment, this review provides a coherent overview of current progress, elucidates performance trade-offs, identifies promising catalyst-process combinations, and establishes a structured basis for guiding future research toward scalable, energy-efficient, and economically viable NH_3 production technologies.

1.3 Selection criteria and methodology for catalytic systems

The 215 catalytic systems analyzed in this review were selected based on a systematic, literature-driven approach. The initial basis was established from recent review articles, particularly the work of Castillejos and Garcia-Bordejé (2024),[50] which provided an overview of relevant catalysts and reaction routes. Building upon this foundation, primary research articles published between 2022 and 2025 were screened to capture the most current developments in Li-mNRR, electrochemical, and photo(electro)catalytic NRR. Inclusion criteria required that each system have verifiable literature references consistent with the source review tables, clearly reported performance metrics (PR, FE, and, where available, CC), and applicability to contemporary research directions. Systems were excluded if literature references were inconsistent, data were incomplete, or the study predated 2022, ensuring a focus on the state-of-the-art. This methodology enabled the compilation of a large, comparable dataset, allowing the identification of performance trends, trade-offs, and promising catalyst-material combinations across different NRR approaches. The SI (Table S1) provides a comprehensive overview of all 215 collected catalysts, including the original literature references and the normalized performance scores derived from PR, FE and CC.

2. Fundamentals of ammonia synthesis

The development of improved approaches for ammonia synthesis must be supported by a strong understanding of the process fundamentals. Advances in catalysts and novel optimized synthetic methods are built upon the underlying mechanistic steps, key inspirations, and thermodynamics of NH_3 synthesis.

2.1 Nature-inspired enzymes

Nitrogen fixation is a natural process in which gaseous N_2 undergoes chemical reactions to be transformed into valuable compounds such as ammonia, nitrates, or nitrites. In biological systems, one of the enzymes catalysing such processes is nitrogenase that catalyzes H_2 reduction into NH_3 with sunlight serving as the driving force for the reactions shown in eqn (2.1)–(2.3).[51,52] These enzymatic nitrogen reduction reactions (NRR) demonstrate remarkable efficiencies up to 66%, utilizing, in the case of the Fe–Mo nitrogenase (nitrogenase using an iron–molybdenum (FeMo cofactor) structure as the active site), eight protons, eight electrons and 16 equivalents of Adenosine triphosphate (ATP) to convert one mol of N_2 into two moles of NH_3.[53] The energy requirement for this conversion is 244 kJ mol^{-1}, which is significantly lower than the 520 kJ mol^{-1} needed for the Haber–Bosch process, highlighting the superior energy efficiency of biological nitrogen fixation. Iron (Fe), molybdenum (Mo), and vanadium (V) are recognized as crucial metal centers in biological nitrogen fixation. Fig. 5 shows the three main types of nitrogenase enzymes' active centers: Fe–Mo–S, Fe–V–S, and Fe–Fe–S nitrogenases.[54] Although their cluster structures are identical, they differ in the metals in the catalytic active sites, leading to varying energy requirements for the N_2 fixation.[50,53]

Due to the highly selective and efficient conversion of N_2 to NH_3 by these enzymes, there is increasing interest in mimicking

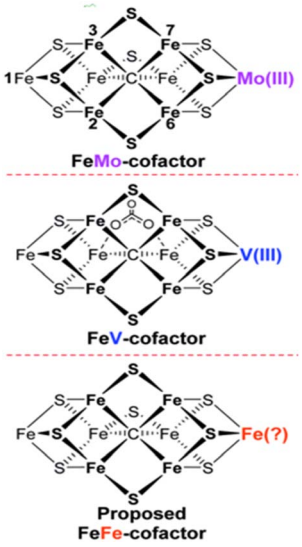

Fig. 5 Fe-Mo-S nitrogenase, Fe-V-S-nitrogenase and Fe-Fe-S-nitrogenase.[54] Adapted from ref. 54 *via* Creative Commons CC BY 3.0 licence.

nitrogenase enzymes for synthetic NH_3 production.[51,52] Research is now focused on replicating these enzymes with either heterogeneous or homogeneous (electro-)catalysts to understand and utilize their catalytic sites, structures and mechanisms, aiming to achieve similar high selectivity and efficiency.[55] These enzymatic insights are not only relevant from a biological perspective but also serve as guiding principles for synthetic catalyst design. To translate this understanding into practical applications, theoretical approaches such as Density Functional Theory (DFT) have been applied to elucidate the fundamental reaction mechanisms of NRR.[56]

$$\text{Mo-nitrogenase: } N_2 + 8H^+ + 8e^- + 16ATP \rightarrow 2NH_3 + H_2 + 16ADP + 16P \quad (2.1)$$

$$\text{V-nitrogenase: } N_2 + 12H^+ + 12e^- + 24ATP \rightarrow 2NH_3 + 3H_2 + 24ADP + 24Pi \quad (2.2)$$

$$\text{Fe-nitrogenase: } N_2 + 24H^+ + 24e^- + 48ATP \rightarrow 2NH_3 + 9H_2 + 48ADP + 48Pi \quad (2.3)$$

2.1.1 Mechanism of the NRR. A detailed understanding of the reaction pathways in NRR is essential to enable its optimization. Therefore, DFT calculations have been employed, allowing for the identification of key transition states and the rate-determining step.[57] Calculations of the free energy differences (ΔG) for the elementary reactions provided valuable insights into the stability of the system and possible surface intermediates.[58] These theoretical results were consistent with experimental observations and led to the classification of two general reaction pathways, based on coordination sites and specific binding interactions at the catalytic surface: (I) the associative pathway, which can be further divided into distal (Fig. 6a), alternating (Fig. 6b), and enzymatic (Fig. 6c) mechanisms, and (II) the dissociative pathway (Fig. 6d).[59] The coordination mode of N_2—end-on or side-on—plays a crucial role in molecule–surface interactions and the design of efficient metal catalysts. Distal and alternating pathways are typically associated with side-on adsorption, whereas the enzymatic pathway proceeds *via* an end-on configuration. Insights from DFT calculations and adsorption studies have elucidated the corresponding free-energy profiles, although the detailed mechanism of nitrogen fixation remains not fully understood.[58–61]

2.1.1.1 Associative pathway. In the associative pathway, N_2 adsorbs onto the catalytic surface and undergoes stepwise protonation and hydrogenation, facilitated by the catalyst's provision of electrons and protons.

This pathway comprises three distinct mechanisms: distal, alternating, and enzymatic.[58] In the distal pathway (Fig. 6a), N_2 is adsorbed in a side-on configuration and sequentially hydrogenated. Initial protonation elongates the N–H bond, weakening the N≡N triple bond and forming intermediates such as diazenido, nitrido, and imido species. The first NH_3 molecule desorbs, followed by a second cycle of protonation and NH_3 formation.[59–61] The alternating pathway (Fig. 6b) involves hydrogenation of both nitrogen atoms in an alternating manner. The process involves both side-on and end-on

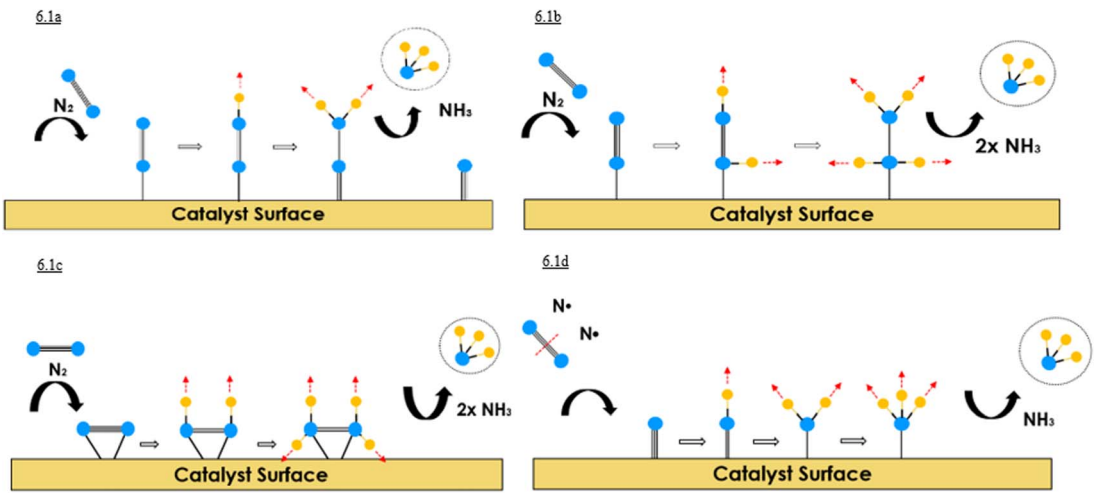

Fig. 6 General NRR pathways highlighting coordination modes and binding interactions.[50,53]

interactions of H_2, leading to symmetric and asymmetric weakening of the N≡N bond. Key intermediates include diazene, hydrazido, and hydrazine, with N_2H_4 formation identified as a potential rate-limiting step.[58,59] The enzymatic pathway (Fig. 6c) closely resembles the alternating mechanism but proceeds *via* end-on coordination of N_2 to the nitrogenase active site. Electron and proton transfer is facilitated by the enzyme, gradually converting N_2 into NH_3. The reduction of NH_2^* to NH_3 is suggested as the rate-limiting step.[58]

2.1.1.2 Dissociative pathway. In the dissociative pathway, the N≡N bond is completely cleaved upon adsorption, requiring significant energy (~945 kJ mol^{-1}). Subsequent hydrogenation of individual nitrogen atoms leads to NH_3 formation. Although feasible, this pathway is energetically less favourable compared to associative mechanisms.[58,60]

2.2 N_2-binding

Understanding how N_2 interacts with metal catalysts—including different binding modes and their energy requirements—enables the targeted selection and optimization of catalysts for specific applications, enhancing activity and clarifying reaction mechanisms. This optimization strategy requires a systematic analysis of catalytic materials, which can be classified into four categories: (a) non-noble metals, (b) noble metals, (c) alkali metals and (d) metal–organic compounds. The aim is to gain insight into the interaction between catalysts and N_2, with a focus on optimizing adsorption and desorption characteristics. For efficient NRR, catalysts need to have well-balanced binding properties—neither too weak nor too strong—to ensure optimal performance. The use of (a) non-noble d-metals as catalysts is inspired by natural processes (*e.g.*, Fe, Mo, V) and has proven effective in industrial applications such as the Haber–Bosch process (*e.g.*, Fe).[52] Their catalytic activity originates from the destabilization of the N≡N bond through effective orbital overlap between the metal and the nitrogen atom, which enhances electron density at the metal's d-orbitals and facilitates bond weakening.[62] Among the d-metals explored in NRR, titanium (Ti), vanadium (V), chromium (Cr), iron (Fe), cobalt (Co), nickel (Ni), and molybdenum (Mo) are particularly valuable due to their electronic properties, which are crucial for N_2 activation and subsequent reduction.[63] The interaction mechanism of these metals follows the principles of metal–ligand bonding.[64] Specifically, σ-donation from the sp-hybridized orbitals of nitrogen contributes with electron density to the vacant d-orbitals of the metal centre, while π-back bonding occurs through interactions between the metal's filled d-orbitals and the nitrogen's empty π* orbitals. This synergistic combination of σ-donation and π-back bonding reduces the electron density of the N_2 triple bond, leading to its elongation and weakening. Consequently, the molecule becomes more susceptible to activation and reduction (Fig. 7).[64,65]

Among these categories, (b) noble metals such as ruthenium (Ru), rhodium (Rh), palladium (Pd), iridium (Ir), osmium (Os), platinum (Pt), gold (Au), and silver (Ag) follow the same metal–ligand bonding principles as non-noble transition metals. Although their orbital overlap resembles that of non-noble metals, their unique electronic structures give rise to distinct bonding characteristics. Owing to their filled d-orbitals, noble metals display reduced reactivity toward air and moisture, which enhances their electronic stability and lowers their tendency to undergo undesired side reactions. These properties make noble metals valuable in catalytic applications, including the Haber–Bosch process, where ruthenium-based catalysts have been widely applied for improved performance.[66] In contrast, (c) alkali metals such as lithium (Li), sodium (Na), and potassium (K) represent a different type of catalyst. Their interaction with nitrogen is not governed by classical covalent orbital overlap, but rather by ionic interactions. Among them, lithium stands out due to its high reactivity and efficiency in NRR, whereas sodium and potassium, although catalytically active, generally exhibit lower performance. The oxidation of lithium into Li^+ ions facilitate the electron transfer to N_2, weakening the N≡N triple bond and enabling the formation of Li–N complexes and subsequent $Li_xN_yH_z$ intermediates. These intermediates play a crucial role in further transformation steps, ultimately leading to the formation of NH_3.[67,68] In contrast to both transition and alkali metals, (d) hybrid metal–organic compounds (MOCs) represent a fundamentally different class of catalysts, in which the metal centre is coordinated by organic ligands that strongly influence its electronic properties and catalytic activity. MOCs encompass a wide range of molecular structures, with Metal–Organic Frameworks (MOFs) and metal-porphyrins being prominent examples due to their stability and tunable properties.[69,70] The activation of N_2 in metal–organic compounds involves several key steps in the binding mechanism. Initially, the metal centre binds the N_2 molecule through coordinative interactions, typically in either the η^1 (end-on) or η^2 (side-on) mode, depending on the electronic and steric

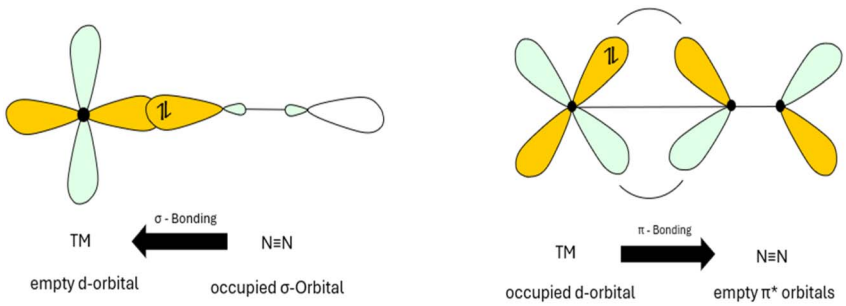

Fig. 7 Metal–ligand bonding interactions between transition metals and nitrogen.

properties of the complex. In the η^1 mode, N_2 binds *via* one nitrogen atom, whereas in the η^2 mode, it coordinates through both nitrogen atoms. These binding modes enable electron donation from the metal to the N_2 molecule, weakening the strong N≡N triple bond and altering its electronic structure. This activation enhances the reactivity of N_2, facilitating subsequent chemical transformations. In catalytic systems for ammonia synthesis, further steps such as stepwise protonation led to NH_3 formation. The ability of metal–organic catalysts to weaken the N≡N bond and promote protonation is critical in emerging electrocatalytic and photocatalytic approaches for sustainable ammonia production.[71,72]

3 Emerging green ammonia production technologies

Modern ammonia synthesis aims to reduce CO_2 emissions and energy consumption compared to the traditional Haber–Bosch process. The following sections present four of the most promising methods for greener ammonia production.

3.1 Mechanochemistry

Mechanochemistry enables chemical reactions by applying mechanical force, commonly through processes like ball milling. In this approach, a rotating ball mill activates a solid catalyst (commonly Fe, Co, or Ru), often promoted with alkali metals such as Na, Cs, or K. The reactants, either solid, liquid, or gaseous, are introduced into the milling vessel, where reactions occur on the surface of the activated catalyst. Fig. 8 illustrates the working principle, showing how mechanical activation facilitates these reactions.[73] Interest in mechanochemistry for ammonia synthesis is based on its advantages over traditional methods, operating under milder conditions with significantly lower temperature and pressure than the Haber–Bosch process. Additionally, this method avoids the use of solvents, making it more environmentally sustainable and scalable. In 2021, J-B. Baek *et al.*[74] reported significant advances in mechanochemical ammonia synthesis using ball milling with an Fe-based catalyst. The mechanical impacts generate a high density of surface defects, which markedly improves the activation and dissociation of N_2. During the subsequent hydrogenation steps, these activated sites promote the formation and release of NH_3. Under mild conditions (45 °C and 1 bar), the reaction yielded ammonia concentrations of up to 82.5 vol% in the reaction mixture.[74] In the same year, Schüth *et al.*[75] demonstrated continuous ammonia production over 50 hours using a mechanocatalytic flow setup. An Fe catalyst promoted with cesium (Cs) enabled sustained NH_3 generation under these conditions. By increasing the Cs content to 4.2 mol% and operating at 20 bar while lowering the reaction temperature, the system maintained stable, continuous ammonia synthesis for nearly 90 hours—representing one of the longest mechanocatalytic gas-phase reactions reported to date. These studies demonstrate that the Cs-promoted iron catalyst has potential for sustained and efficient ammonia production under optimized mechanochemical conditions, though further research on scalability and purification remains necessary. Despite achieving high ammonia concentrations in the reaction mixture, the overall yield remained low (0.44% after 72 hours), indicating that a large fraction of reactants remained unconverted opening space for its recovery and recycling.[75] While these results show the viability of mechanochemical ammonia synthesis, the method is still in its early stages and not yet suitable for industrial application. The reaction mechanisms are not fully understood, requiring further optimization of reaction time, efficiency, and scalability. Although the energy demand at the laboratory scale is relatively low—about 4.5×10^{12} J per ton of NH_3 compared to 228×10^{12} J for the electrified Haber–Bosch process, mechanochemical methods still require substantial development to become industrially viable.[76]

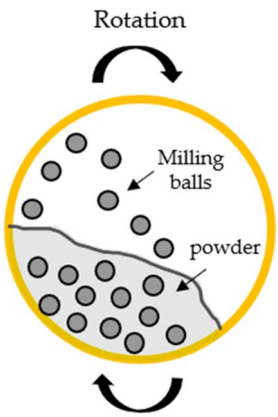

Fig. 8 Schematic representation of ball milling for NH_3 synthesis.[73] Adapted from ref. 73 *via* Creative Commons CC BY 4.0 licence. © 2022 by the authors. Licensee MDPI, Basel, Switzerland.

3.2 Non-thermal plasma

Non-thermal plasma (NTP) is a physical method that activates reacting gases by generating partially ionized plasma through the breakdown of gas when an electric field is applied. This high-energy ionized gas promotes chemical reactions, as illustrated in Fig. 9.[77] A key advantage of NTP is its potential to lower energy consumption and reduce environmental impact compared to traditional processes, which typically require high temperatures (400–500 °C) and pressures (20–40 MPa).[78] The microwave plasma produces highly energetic electrons capable of activating N_2 and H_2, the primary feedstock components for this process. This activation leads to the formation of ions and free radicals, significantly enhancing ammonia formation efficiency. However, NTP technology faces significant challenges: (i) the activation of nitrogen gas due to the cleavage of its strong triple bond (E_a (N_2) = 945 kJ mol^{-1}) and (ii) the prevention of NH_3 decomposition. Addressing these issues necessitates developing and selecting catalysts with enhanced plasma-synergistic activities, specifically tailored for relevant plasma conditions.[78,79] Recent research highlights promising results in catalyst performance for ammonia synthesis. In 2023, NTP using Ru/MgO catalyst, achieved an NH_3 productivity of 2.67 mmol g_{cat}^{-1} h^{-1}, with an energy demand of 4.20 kJ L^{-1}.

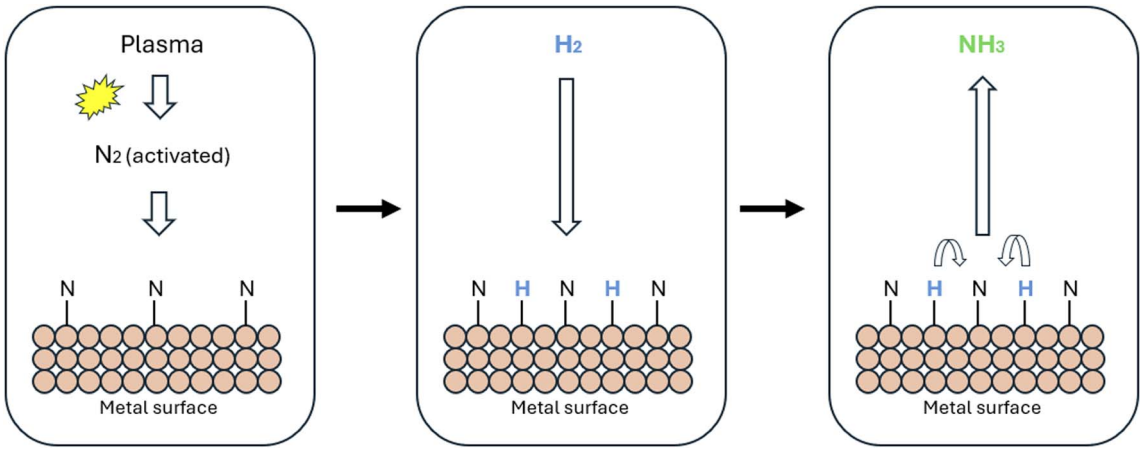

Fig. 9 Suggested mechanism for plasma-assisted catalytic ammonia synthesis through plasma induced N_2 dissociation.[77,79]

Furthermore, innovative methods using seawater as a feedstock yielded results comparable to those achieved with pure H_2, underscoring the critical role of the Co/SiO_2 catalyst (energy demand: 3.2 g NH_3 kW^{-1} h^{-1} at 2 W) in determining NH_3 productivity.[78,80] In this approach, H_2 is generated from seawater *via* electrolysis. Simultaneously, N_2 and H_2 are activated using NTP, enabling ammonia synthesis under milder conditions. This method integrates the conventional Haber–Bosch process with plasma activation to improve energy efficiency and environmental sustainability. While NTP represents a promising environmentally friendly approach, the energy demands associated with this process are currently high when compared to the traditional SMR Haber–Bosch process. Experimental data revealed that the NTP process, particularly when integrated with an electrified Haber–Bosch approach, requires approximately 155 GJ of energy, significantly exceeding the 28 GJ needed by the traditional SMR Haber–Bosch method. In summary, substantial challenges in the industrial application of NTP for NH_3 synthesis persist, including energy demand, scale-up, reactor design, and the stabilization of ammonia to prevent its decomposition. Tackling these issues is crucial for positioning NTP as a viable option for ammonia synthesis.[81]

3.3 Electrochemical route

3.3.1 Electrocatalysis. Another significant methodology that has gained importance in recent years is the electrochemical production of green ammonia.[82] With the anticipated decrease in renewable electricity costs, electrochemical approaches are set to become increasingly viable, offering considerable advantages over traditional methods.[83] These techniques allow for on-site ammonia synthesis, which not only reduces dependence on centralized production facilities but also minimizes transportation-related CO_2 emissions, making them an attractive solution for sustainable NH_3 production.[50] The fundamental reaction in electrochemical ammonia synthesis involves the reduction of N_2 to NH_3 in a catalytic cell, with H_2 sourced from purified water (H_2O). At the cathode (Cat.), H_2O is split to produce H_2 and electrons (e^-). At the anode (Anod.), N_2 is reduced to NH_3, typically in the presence of a suitable catalyst. This process completes the electrochemical cycle, where the reduction of nitrogen at the anode is coupled with the oxidation/decomposition of water at the cathode, as illustrated by reactions (3.1)–(3.3).[84] These reactions take place in specialized electrochemical cells that often employ different types of electrolytes. To improve the overall performance of electrochemical ammonia synthesis, various electrolytic technologies can be employed, such as Proton Exchange Membrane (PEM), Anion Exchange Membrane (AEM), and Solid Oxide Electrolysis (SOE), while acknowledging that the intrinsic efficiency of the underlying reactions is limited by thermodynamic constraints. In PEM electrolysis, a solid proton-conducting membrane separates the anode and cathode. This technology is known for its high efficiency, low operating temperatures, and suitability for integration with renewable energy sources due to its ability to efficiently transport protons while minimizing energy losses and enabling rapid response to variable power input. The relevant reactions are provided in eqn (3.1)–(3.3).

$$\text{An.: } 2H_2O \rightarrow O_2 + 4H^+ + 4e^- \quad (3.1)$$

$$\text{Cat.: } N_2 + 6e^- + 6H^+ \rightarrow 2NH_3 \quad (3.2)$$

$$\text{Total: } 2N_2 + 6H_2O \rightarrow 4NH_3 + 3O_2 \quad (3.3)$$

PEM technology faces challenges, including the high cost of platinum catalysts and the vulnerability of membranes to contamination and degradation, which can reduce both their efficiency and lifespan. Therefore, continuous research is necessary to develop more cost-effective and durable materials for long-term viability.[85] AEM electrolysis uses an anion-conducting membrane, which allows for the transport of hydroxide ions (OH^-). This technology is considered cost-effective because it uses non-precious materials, offering a potential advantage in terms of material costs. Hydrogen production occurs at the cathode, similar to PEM, but with different ion transport mechanisms. The use of non-precious materials offers advantages for AEM technology, but its lower ionic conductivity and membrane instability under alkaline

conditions limits efficiency and long-term performance, highlighting the need for ongoing research to improve membrane durability and overall system efficiency.[86] Finally, SOE systems operate at high temperatures, using a solid oxide electrolyte. They can be highly efficient when paired with heat from renewable sources (such as solar thermal or waste heat) and can directly utilize the heat for water splitting, reducing electricity consumption. However, high operating temperatures also pose challenges, such as material degradation and increased energy requirements for system maintenance, which can impact the long-term viability of SOE systems.[87] The choice of technology for electrochemical ammonia synthesis depends on multiple factors, with each approach offering unique advantages that must align with the specific process goals and operational conditions. An essential aspect is the coupling with renewable electricity sources, as electrochemical systems can directly operate with intermittent power input. This feature enables the replacement of fossil-based energy supply, thereby reducing CO_2 emissions while supporting the integration of variable renewable energy into the grid.[88]

3.3.2 Challenges. Despite promising advancements, several challenges hinder the commercial realization of electrochemical ammonia synthesis. These include competition with the Hydrogen Evolution Reaction (HER), low N_2 solubility and activation, catalyst and membrane stability as well as energy efficiency issues. The primary challenge is the competition with HER, which is thermodynamically favoured over the NRR due to its lower energy requirement for H_2 formation. This competition limits NRR selectivity and reduces NH_3 yields, making it difficult to reach high production rates.[63] Overcoming this requires advanced catalyst engineering. Various catalysts, such as transition metals, non-metallics and metal–organic compounds (MOCs), have been explored, but they still fall short of the U.S. Department of Energy's (DOE) performance targets of 7×10^{-7} mol cm^{-2} s^{-1} (2520 μmol h^{-1} cm^{-2}) at 90% faradaic efficiency.[46,47,89] Another significant challenge is the low solubility of N_2 in aqueous media and the high activation energy required for its reduction. In PEM and AEM systems, the limited solubility of N_2 restricts its availability at the catalyst surface, while the N_2 triple bond requires substantial energy to break. SOE systems, operating at higher temperatures, improve reaction kinetics but do not fully mitigate this issue. Additionally, the stability of catalysts and membranes is crucial for long-term efficiency. In PEM and AEM systems, catalysts such as Pt and Ir degrade under harsh conditions, while in AEM systems, membrane degradation is exacerbated by chemical corrosion. In SOE systems, high operational temperatures accelerate catalyst degradation. Finally, energy efficiency and system integration remain significant hurdles. In PEM and AEM systems, energy losses arise from membrane resistance and electrode overpotentials, while SOE systems suffer from thermal losses. Overcoming these challenges is vital for the commercialization of electrochemical ammonia production, requiring advancements in catalysts, electrolytes, and system integration.[90–92] To assess the efficiency of electrochemical ammonia production techniques, it is crucial to consider the various technological approaches employed in these processes. Aqueous NRR and SOE NRR are two prominent methods, each with distinct mechanisms and efficiency profiles. Aqueous NRR typically involves mild conditions and utilizes PEM or AEM membranes, which facilitate ion transport and enable the necessary electrochemical reactions.[93] These membranes are especially relevant due to their efficient ion conduction in aqueous environments, enhancing overall reaction efficiency. In contrast, SOE NRR leverages thermal energy to drive the reactions, reducing the required electrical energy input.[94] Fig. 10 highlights the significant energy requirements associated with these processes. The traditional Haber–Bosch process requires less than 30 GJ per ton of NH_3. In comparison, the electrified Haber–Bosch process—where hydrogen is produced *via* water electrolysis using either alkaline (AEL) or proton-exchange membrane (PEMEL) electrolyzers—operates within a similar energy range, between 30–35 GJ per ton of NH_3. This indicates that while H_2 production is electrified, the remaining energy demands of the HB process, such as compression and heating, are similar to the conventional process, positioning the electrified route as a competitive alternative. In contrast, direct electrochemical ammonia synthesis *via* aqueous NRR requires significantly higher energy inputs, approximately 50–70 GJ per ton of NH_3.

This estimate includes energy losses associated with gas purging, product separation, and purification steps such as pressure swing adsorption (PSA), which are necessary to remove unreacted N_2 and H_2 and to isolate the produced NH_3. Despite these elevated energy requirements, NRR using SOE, whether employing water or hydrogen as the reactant, demonstrates comparable energy consumption to the conventional HB process, highlighting the considerable efficiency potential of this technology. Furthermore, smaller energy components, such as heating, distillation, adsorption, O_2 compression, and air separation, contribute to the overall energy demand, underscoring the importance of optimizing energy use across all stages of the ammonia production process to improve overall efficiency.[39]

3.3.3 Lithium-mediated NRR (Li-mNRR). The Li-mNRR has garnered significant attention due to its potential for high ammonia production efficiencies. This process utilizes lithium-based electrolytes to facilitate reaction pathways and enhance the catalytic conversion of N_2 to NH_3.[68] This was first explored by Fichter *et al.* in 1930, achieving yields up to 10% at 10 bar.[95] After a period of stagnation, Tsuneto *et al.*[96] revitalized the field in 1993, optimizing electrolyte compositions with polar aprotic solvents, leading to faradaic efficiencies (FEs) of 8% at 1 bar and 48% at 50 bar.[84] In 2020, Lazouski *et al.* introduced a gas diffusion electrode, addressing transport limitations without requiring increased pressure.[97]

Several strategies have since been developed to improve the process, including (I) operating under mild pressure and temperature conditions, (II) introducing small amounts of O_2, (III) utilizing potential cycling, (IV) using recyclable ionic liquids (ILs) as proton sources, and (V) employing high-surface-area and gas diffusion electrodes.[68] Despite these advancements, the energy input for Li-mNRR remains high, approximately three times higher than that of aqueous electrochemical NRR or SOEL. The NRR electrolyzer is the primary contributor to this energy demand, with additional energy required for

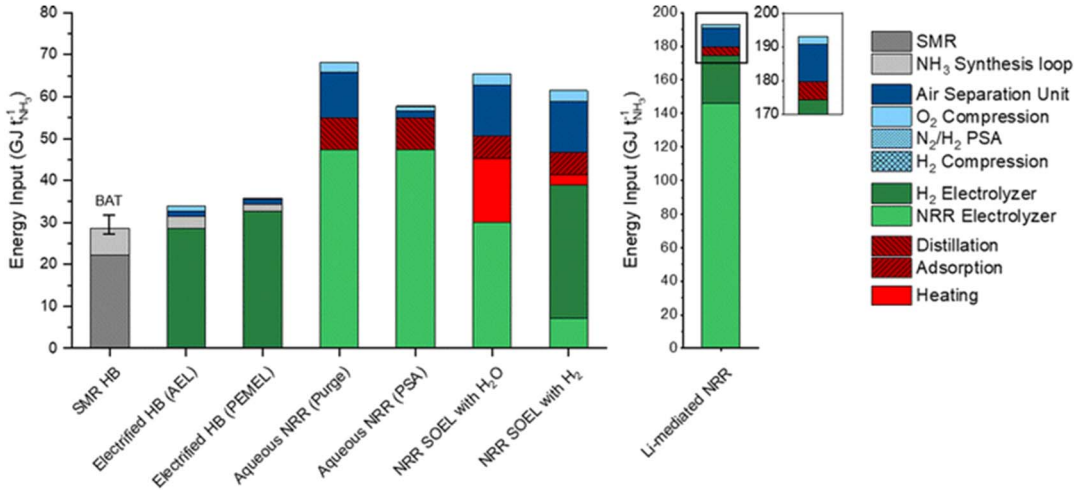

Fig. 10 Comparison of the projected energy requirements for conventional Haber–Bosch, electrified Haber–Bosch, aqueous NRR and SOE ammonia synthesis processes.[39] Reproduced from ref. 39 *via* Creative Commons CC BY 3.0 licence

hydrogen electrolyzers, air separation, and oxygen compression. These factors limit the practicality and economic feasibility of the process.[39] Research efforts are directed toward optimizing Li-based electrolytes to improve electron transport and catalytic NH_3 formation. While other lithium electrolytes, such as $LiPF_6$ and LiTFSI, have been explored for their electrochemical properties, and $LiBF_4$ outperforms them in terms of both faradaic efficiency and overall system stability. Additionally, adjusting electrolyte concentration ratios and utilizing aprotic solvents such as tetrahydrofuran (THF) and ethanol (EtOH) enhance N_2 solubility and accelerate reaction kinetics, leading to increased ammonia yields.[98] However, Li-mNRR shares challenges with other electrochemical techniques, such as high energy input and suppression of side reactions, notably the HER. HER competes for electrons and protons, reducing ammonia yields and increasing energy consumption. To address this, research is focused on catalyst development to facilitate N_2 reduction over HER. Advanced materials like transition metal nitrides, borides, and carbides are promising, providing active sites for N_2 activation while suppressing HER.[46] A detailed overview and comparison of catalytic systems applied to Li-mNRR is provided in Section 4.2.3.1. Optimizing production rates, faradaic efficiency, costs, and catalyst stability is essential for the practical implementation of Li-mNRR. A notable breakthrough in 2023 by Fu *et al.* achieved a faradaic efficiency of 61% at 1 bar and room temperature in a continuous-flow reactor. Nevertheless, even with 100% faradaic efficiency, the maximum thermodynamic energy efficiency of Li-mNRR is limited to 28%, compared to 63% for the Haber–Bosch process.[67] This gap highlights the need for further research to improve energy efficiency and make Li-mNRR viable under ambient conditions.

3.4 Photo(electro)chemical route

3.4.1 Photocatalysis. Another promising technique that has gained considerable attention in recent years is photo(electro)catalysis, which is employed for the synthesis of various chemical compounds, including NH_3, H_2 and CO_2 conversion products (*e.g.* carbon monoxide, *etc*).[99–101] This method offers a promising approach for more sustainable synthesis processes, utilizing semiconductor materials that typically absorb light from energy sources such as UV radiation, and in some cases, visible light. Photon excitation initiates reduction and oxidation processes that drive the production of specific species. This generally occurs in three main steps: 1. Photoexcitation, 2. Electron transfer, and 3. Photoreduction & photooxidation. This process can be applied for NRR, where N_2 is reduced to form NH_3, starting with photoexcitation, where photons interact with the semiconductor material, causing electrons to be excited from the valence band (VB) to the conduction band (CB). This excitation leaves holes in the VB, which act as oxidative species, while the electrons in the CB function as reductive species. In the following step, the electrons and holes are transferred to the active sites of the photocatalyst and finally photooxidation and photoreduction occur. First, solar-driven H_2O splitting occurs, where water is dissociated into oxygen and protons, with hydrogen being reduced in the conduction band (CB). Subsequently, nitrogen fixation takes place, where H_2O molecules are oxidized in the valence band (VB), generating H^+ and oxygen, and NH_3 is synthesized as the final product.[48] Fig. 11 illustrates the photocatalytic process, with a particular emphasis on its application to the NRR. There are several challenges associated with the photocatalytic process, with particular emphasis on the recombination of electrons and holes, which can significantly reduce overall efficiency. Recombination can be mitigated by introducing organic scavengers, like methanol (MeOH) or ethanol (EtOH),[102] which effectively capture intermediate species, preventing their recombination and ensuring a more selective reaction pathway. Well-designed photocatalysts, tailored with specific electronic structures, can also be employed to minimize recombination and enhance efficiency.[103] Before 2017, faradaic efficiencies were reported below 1%. Yet significant and rapid progress in

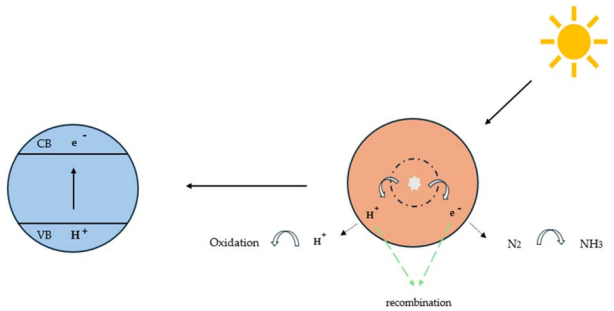

Fig. 11 Reaction mechanism of photocatalytic reduction.

catalyst design has pushed FE into the 10–20% range, with some cases even surpassing 30%. This highlights the remarkable advancements made in the field, underscoring the importance of continued innovation in catalyst development.[104,105]

3.4.2 Photo electrocatalysis (PEC). The key difference between photocatalysis and photo electrocatalysis lies in how the redox reactions are driven. In photocatalysis, the charge carriers are generated through light absorption, while in photo electrocatalysis, external circuits induce these carriers.[105,106] By combining the strengths of both approaches—photocatalysis for its light-driven processes and electrocatalysis for its enhanced efficiency, there is significant potential for improvement in sustainability. Despite their promise, both techniques face challenges that often lead to low yields, including high charge carrier recombination, limited light absorption due to mismatched bandgaps, slow electron transfer, and photodegradation.[106–108] To address these issues, catalyst design plays a pivotal role. Innovations such as doping, cocatalyst deposition, defect integration, and crystal facet tuning can help overcome these barriers.[109] Furthermore, optimizing the electrolyte to control proton transfer rates and increase N_2 solubility remains an active area of research.[110] With continued advancements in catalyst engineering and electrolyte optimization, PEC holds the potential to overcome these current limitations and significantly contribute to more efficient and sustainable ammonia production (Fig. 12).

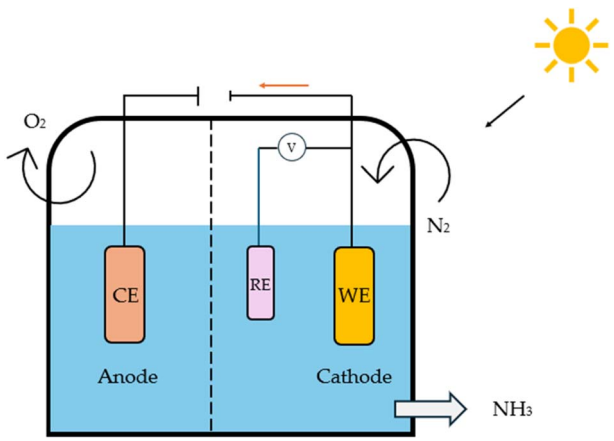

Fig. 12 Setup configuration of a photoelectrochemical cell for N_2 reduction.

4 Catalyst development and analysis

4.1 Towards efficient electrocatalysts for NRR

As highlighted in the previous sections, the demand for efficient electrochemical systems has driven extensive research into effective catalysts, combining theoretical/modelling and experimental efforts. Properties such as crystallinity, morphology, particle size, and the availability of active surface sites are critical for achieving high efficiency and stability. These factors are particularly important under conditions relevant for industrial-scale applications, including extended operation times (>1000 h), moderate temperatures (<100 °C), pressures (~1 atm), and practical current densities (≥10 mA cm^{-2}).[111] Early studies primarily focused on noble and transition metals, but recent efforts have increasingly explored non-metallic catalysts to overcome the kinetic limitations of the NRR and enhance selectivity under moderate conditions.[63,112] Metals are often combined with conductive supports (*e.g.*, carbon sheets, graphene oxide), which play a crucial role in catalyst development, aiming to balance efficiency, stability, and cost-effectiveness. A major challenge remains the suppression of the competing HER to maximize NRR efficiency. Since HER often dominates under electrochemical conditions, identifying catalysts with high N_2 selectivity is essential. Addressing this issue requires a detailed evaluation of catalyst performance based on experimental data or, alternatively, on simulation-based studies based on fundamental principles.[113] This evaluation faces the challenge of inconsistency and incompleteness of available catalyst data. Reported values for key parameters, such as production rates (PR), faradaic efficiency (FE), and catalyst costs (CC), often lack standardization, making direct comparisons difficult. Although review papers attempt to compile these metrics, discrepancies in measurement conditions and reporting standards persist. To address this, we have developed a structured methodology for the evaluation of the available datasets, highlighting emerging trends, promising catalysts, and identifying critical research gaps.

4.2 Methodology for data analysis and graphical representation

To provide a structured and unified approach, a systematic methodology was developed for intuitive data evaluation and visualization. This methodology integrates key metrics, namely PR, FE, and CC, into a cohesive framework for a holistic assessment of catalyst performance and practicality for industrial applications. A major challenge in this analysis was the inconsistency in the reporting of PR, often presented in different units across studies. To standardize the data, production rates were categorized into three units: (1) μmol mg^{-1} h^{-1} (per catalyst mass), (2) μmol cm^{-2} h^{-1} (per electrode area), and (3) μmol h^{-1} L^{-1} g^{-1} (per catalyst mass and reaction medium volume, commonly applied in photocatalytic suspension systems). FE, consistently reported as percentages, were

extracted directly from the literature, although the data was limited, particularly for photocatalysts. Despite these gaps, a general comparison of available data was carried out. CC analysis followed a two-tier approach: commercially available catalysts were sourced from chemical suppliers (*e.g.* Sigma-Aldrich) and expressed as cost per gram. Synthesized catalysts were evaluated based on the cost of their raw materials. Whenever possible, bulk pricing was applied to estimate large-scale synthesis costs. A correction factor was applied to refine the cost estimates by accounting for synthesis complexity, material toxicity, and energy demand. Each of these three parameters was evaluated on a scale from 1 to 5, and the correction factor was defined as their arithmetic mean. In all cases, a higher score corresponds to a less favourable characteristic. Synthesis complexity was assessed by examining the reported preparation route, where a score of 1 indicated a simple synthesis and 5 reflected a highly complex procedure. Material toxicity was determined from the safety data sheets (SDS) of the starting materials, with values ranging from 1 (low toxicity) to 5 (high toxicity). Energy demand was evaluated analogously, where 1 represented low energy consumption and 5 denoted highly energy-intensive synthesis conditions. The resulting average score was then multiplied with the raw material cost, providing a more realistic estimate of the overall catalyst cost by incorporating practical synthesis challenges. To enable direct comparison across heterogeneous studies, a scoring system was developed in this work to normalize PR, FE, and CC onto a common scale of 0.5–10 (eqn (4.1)–(4.4)). The lower bound of 0.5 was chosen to avoid assigning zero scores to catalysts with the lowest performance, ensuring all catalysts contribute to the comparative analysis. Higher scores reflect more favourable outcomes, with a maximum combined score of 30.

$$S_{PR} = 0.5 + \left(\frac{PR - PR_{min}}{PR_{max} - PR_{min}}\right) \times 9.5 \quad (4.1)$$

$$S_{FE} = 0.5 + \left(\frac{FE - FE_{min}}{Fe_{max} - FE_{min}}\right) \times 9.5 \quad (4.2)$$

$$S_{CC} = 10 - \left(\frac{SC - SC_{min}}{SC_{max} - SC_{min}}\right) \times 9.5 \quad (4.3)$$

$$S = S_{PR} + S_{FE} + S_{CC} \quad (4.4)$$

For the CC analysis, normalization was performed in the same manner, using eqn (4.3), as lower costs are desirable and thus represented by a higher point distribution. To ensure comparability, normalization was performed within each dataset (grouped by methodology and units) relative to the highest value. Data points with exceptionally high values were excluded from the normalization process to prevent distortion. These outliers are highlighted separately in the subsequent analysis to preserve their significance. Critical factors influencing catalyst performance—such as electrolytes, pH, pressure, temperature, and applied potential—are essential for comprehensive analysis. While this information is often incomplete in the literature, it was incorporated where available or noted as missing. Catalytic efficiency is ideally assessed through turnover frequency (TOF), which requires knowledge of the active catalytic surface, often determined using techniques such as SEM or others, such as electrochemical techniques. However, TOF values are rarely reported in the studies analyzed here, which highlights the need for standardized evaluation procedures to enable more comprehensive catalyst benchmarking in the future.

4.2.1 Identification of data-reporting gaps and limitations. As shown in Table 2, ammonia PR are reported using fundamentally different units and normalization strategies, which hinders direct comparison between catalysts. For example, Ni-wire electrodes are reported per area (223 nmol cm^{-2} s^{-1}), P-C_3N_4 as an absolute rate (4.9 μmol h^{-1}), and Co_3Fe-MOF per mass (8.79 μg h^{-1} mg_{cat}^{-1}), illustrating how reported differences may reflect normalization rather than intrinsic activity. This inconsistency is pervasive across NH_3 electrocatalysis and photocatalysis, hindering reliable benchmarking. In related fields such as HER and CO_2RR, area-normalized rates (μmol cm^{-2} s^{-1}) are standard, providing a direct measure of intrinsic activity and enabling cross-study comparison. Mass- and BET-normalized values offer complementary insight for heterogeneous and porous catalysts, reflecting material efficiency and surface effects. For future studies and potential scale-up, adopting area normalization as the primary metric, supplemented by mass and BET data, would establish a consistent and informative framework for evaluating catalytic performance. To address the issue of heterogeneous metrics, the PR values of the 215 catalysts collected in our database were normalized and subsequently evaluated using a structured scoring framework as described in Section 4.2 providing a consistent basis for cross-catalyst comparison.

Building on this, Table 2 highlights further gaps in reporting key catalytic parameters. Most notably, TOF is not reported for the selected systems, limiting assessment of intrinsic activity. Surface-area reporting is inconsistent: O-g-C_3N_4 includes BET measurements, P-C_3N_4 and Co_3Fe-MOF report ESCA data, while several systems—including Ni-wire, Mo-foil, Cu, V_2CT_x Mxene, Pt_1/N-MoS_2, and Cs_2O/Os–Au—provide none. Stability assessments vary from extended continuous operation (Ni-wire, 96 h) to short-term cycling (V_2CT_x Mxene, 2 h; Pt_1/N-MoS_2, 5 h), or are entirely omitted (Mo-foil, Cu, Cs_2O/Os–Au). This combination of inconsistent normalization, missing TOF, variable surface-area data, and heterogeneous stability testing complicates benchmarking and can mislead apparent performance comparisons.

Stability and long-term performance are particularly under-reported, yet they are crucial for evaluating catalyst durability and guiding scale-up efforts. Recent Li-mNRR studies have demonstrated that *operando* and *in situ* characterization techniques—such as GI-WAXS,[123] *in situ* ATR-SEIRAS,[124] and flow-cell X-ray scattering[125]—provide time-resolved insights into the evolution of the solid-electrolyte interphase, surface intermediates, and dynamic structural changes under reaction conditions. These approaches allow researchers to directly correlate structural and chemical changes with catalytic performance,

Table 2 Comparison of NH_3 production-rate normalization and reporting of key catalytic parameters across selected catalytic systems

Entry	Catalyst	Production rate (PR)	Turnover frequency (TOF)	Surface area (ECSA, BET)	Stability	References
12	Ni-wire	223 nmol cm^{-2} s^{-1}	Not reported	Not reported	96 h (continuous)	114
14	Mo-foil	0.22 nmol cm^{-2} s^{-1}	Not reported	Not reported	Not reported	115
22	Cu	58 nmol cm^{-2} s^{-1}	Not reported	Not reported	Not reported	116
123	P-C_3N_4	4.9 μmol h^{-1}	Not reported	Reported BET 10 m^2 g^{-1}	Stability test reported (reusable)	117
199	O-g-C_3N_4	118.8 mg L^{-1} h^{-1} g_{cat}^{-1}	Not reported	Reported BET 220.16 m^2 g^{-1}	20 h (continuous)	118
31	V_2CT_x Mxene	12.6 mg h^{-1} mg_{cat}^{-1}	Not reported	Not reported	2 h (cycling); 24 h (continuous)	119
66	Co_3Fe-MOF	8.79 μg h^{-1} mg_{cat}^{-1}	Not reported	Reported (ESCA) 17.74 mF cm^{-2}	2 h (cycling, 4 cycles)	120
155	Pt_1/N-MoS_2	121.2 μmol g_{cat}^{-1} h^{-1}	Not reported	Not reported	5 h (cycling, 4 cycles)	121
159	Cs_2O/Os–Au	2685 μmol h^{-1} g Os^{-1}	Not reported	Not reported	Not reported	122

enabling systematic evaluation of stability, understanding of deactivation mechanisms, and guidance for the design of more robust catalysts.

Adopting a standardized reporting framework, including TOF, surface area, stability, and consistent normalization, would enable more rigorous comparisons and clearer insights into intrinsic catalytic activity.

As indicated by our data analysis of catalytic systems (Tables 6–8), photocatalytic nitrogen reduction remains comparatively underrepresented relative to electrocatalytic and Li-mediated approaches. Many commonly employed materials—such as transition-metal centers (Mo, Ni, Cu), high-surface-area scaffolds (MXenes, MOFs), and defect-engineered heterostructures—are intrinsically photoactive, yet they are predominantly explored under electrochemical bias or in Li-mediated systems. This is exemplified by MXene–metal oxide heterostructures, which are primarily designed to maximize charge transfer kinetics, surface adsorption, and defect-mediated activity under applied potential, rather than optimizing light absorption or photogenerated carrier separation.[126] As highlighted by Ranjith *et al.*, this underrepresentation reflects the intrinsic challenges of photo-driven N_2 activation.[127] Developing efficient heterojunction photocatalysts remains difficult due to low conversion efficiencies and strong material dependence, requiring simultaneous optimization of light absorption, charge separation, band alignment, and redox potential. Rapid recombination of photogenerated carriers, limited visible-light harvesting, competitive hydrogen evolution, and insufficient surface electron density in aqueous media further restrict activity.[128] Consequently, advanced heterostructures rarely achieve measurable ammonia formation under purely photocatalytic conditions, explaining the sparse and heterogeneous representation and the difficulty of generating reproducible, reportable data.

4.2.2 Integration of catalyst cost into performance assessment. To highlight the novel cost-performance evaluation framework developed in this study, an illustrative analysis was conducted prior to the detailed discussion of individual catalytic systems. Ten representative catalysts spanning electrochemical NRR (electrocatalysis), lithium-mediated NRR (Li-mNRR), and photoelectrocatalysis were selected based on their contrasting cost characteristics, categorized as low-cost and high-cost materials. The resulting visualization (Fig. 13) demonstrates how the combined consideration of production rates, faradaic efficiency, and catalyst cost can guide the identification of promising catalyst families for further research and scale-up. Non-noble metals (*e.g.*, Mo-, Ni-, and Cu-based catalysts) generally exhibit a favorable cost-to-performance ratio compared with noble-metal-based materials, while synthesis complexity further modulates the overall cost. This approach underscores the practical relevance of integrating economic considerations alongside performance metrics and provides a clear, actionable overview ahead of the comprehensive analysis of all 215 catalytic systems. Details for the remaining catalysts, including their performance and cost metrics, are provided in the SI (Table S1), with the original literature sources of each catalyst explicitly cited.

4.2.3 Results and interpretation of catalyst performance evaluation. This section presents the results of the catalyst performance evaluation for Li-mNRR and (photo-)electrocatalysis. Based on the metrics of production rates, faradaic efficiency, and catalyst costs, a comparative analysis of the various catalytic systems was conducted to identify performance trends and trade-offs (Fig. 14–19) visualize the point distribution of the assessed catalysts for each technique, as determined

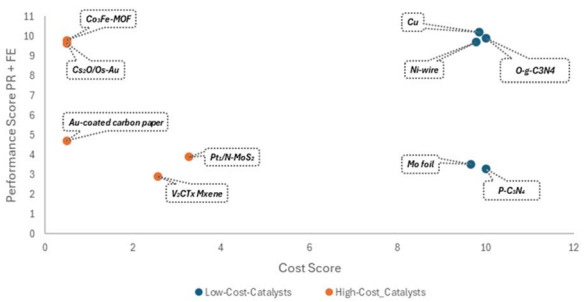

Fig. 13 Cost performance comparison of selected catalysts.

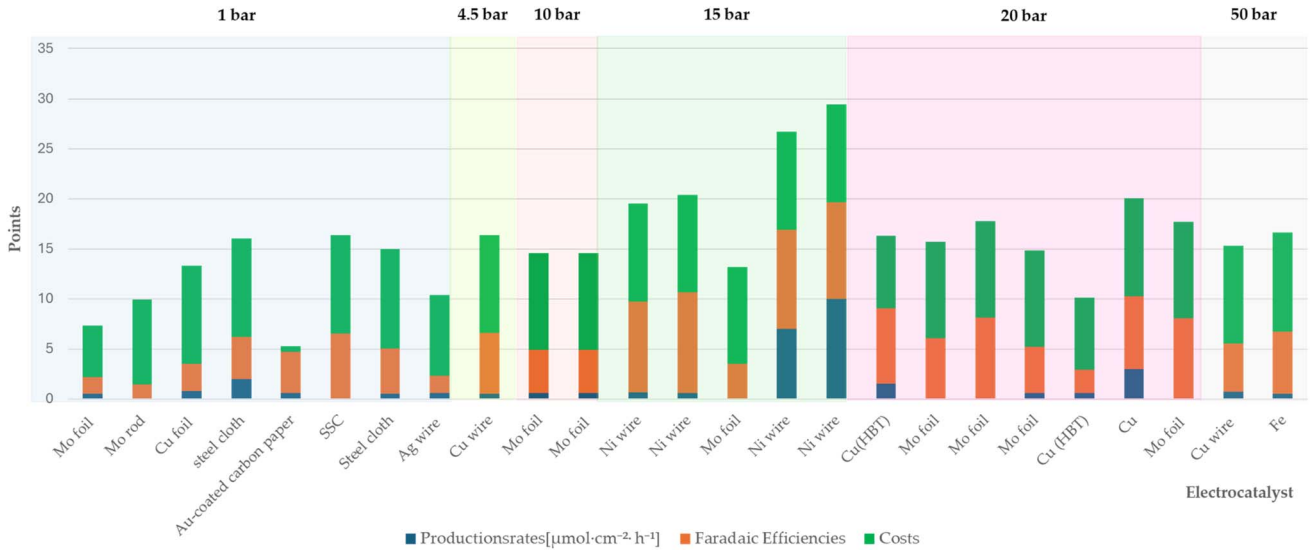

Fig. 14 Comparison of catalysts for the Li-mNRR.

through eqn (4.1)–(4.3). The *x*-axis shows the tested catalysts, while the *y*-axis represents the total score, *S*, signalling the contribution of each criterion in different colours: blue (S_{PR}), orange (S_{FE}), and green (S_{CC}). The background colours in the diagrams provide additional context, regarding the applied pressure for Li-mNRR (Fig. 14) and the electrolytes for (photo-) electrocatalysis (Fig. 15–19). This approach allows for an easy and quantitative comparison of the catalysts' performance across different conditions and media.

Table 3 Evaluation scores of various electrode materials based on NH_3 production rate, faradaic efficiency, and estimated catalyst cost

Entry	Catalyst	Score (points)	References
1	Mo foil	7.3	115
2	Mo rod	9.9	134
3	Cu foil	13.3	135
4	Steel cloth	16.0	136
5	Au-coated carbon paper	5.2	137
6	SSC	16.4	138
7	Steel cloth	15.0	139
8	Ag wire	10.4	140
9	Cu wire	16.4	141
10	Mo foil	14.6	142
11	Mo foil	14.6	143
12	Ni-wire	19.5	114
13	Ni-wire	20.4	114
14	Mo-foil	13.2	144
15	Ni wire	26.7	145
16	Ni wire	29.4	145
17	Cu(HBT)	16.3	146
18	Mo-foil	15.7	144
19	Mo-foil	17.8	144
20	Mo-foil	14.8	144
21	Cu(HBT)	10.1	147
22	Cu	20.1	148
23	Mo-foil	17.7	144
24	Cu wire	15.3	149
25	Fe	16.6	96

4.2.3.1 Li-mediated nitrogen reduction reaction (Li-mNRR). The literature data showed that nickel, molybdenum and copper are widely used catalysts, although other species have also been studied (*e.g.* steel, Ag, Fe), as summarized in Table 3. Nickel wire under elevated pressure (15 bar) showed the highest performance ($S = 29.4$), as shown in Fig. 14. This is likely due to nickel's electronic properties, which facilitate efficient electron transfer, and its strong interaction with N_2, as indicated by the high binding energy of the $Ni(N_2)_4$ complex (120 kJ mol^{-1}). Both aspects contribute to effective nitrogen activation.[129] Molybdenum exhibits modest ammonia production rates at atmospheric pressure (1 atm) and lacks comprehensive data for elevated pressures (15 and 20 bar), molybdenum remains a compelling candidate due to its strong affinity for nitrogen binding and its versatile oxidation states.[130,131] Notably, molybdenum is a key component in the active sites of different enzymes, such as nitrogenase, found in nature, in the pathway of nitrogen fixation, which efficiently catalyse nitrogen-based molecules reduction. These properties contribute to moderate the high faradaic efficiencies in molybdenum-based catalysts, particularly under increased pressure. Furthermore, molybdenum's relative abundance and cost-effectiveness enhance its appeal for industrial applications. As of early 2025, the price of high-purity molybdenum ranges between €25 and €90 per kilogram, depending on form and purity levels.[132] Copper has shown considerable promise, particularly at atmospheric pressure, where its ammonia production rates are comparable to those of molybdenum, with further improvements observed under elevated pressure conditions. The copper-based compound Cu(HBT) demonstrates high faradaic efficiency, elevated production rates, and moderate costs, highlighting the influence of ligands on enhancing copper's catalytic performance. Copper's high faradaic efficiencies are largely attributed to its excellent electrical conductivity (~5.96×10^7 S m^{-1} at 20 °

C) which boosts catalytic performance.[133] As of early 2025, the price of high-purity copper ranges between €6 and €9 per kilogram, depending on form and purity levels, making it an economically attractive starting material for industrial applications. Alternative materials, such as Au-coated carbon paper, Ag, Fe, and stainless-steel cloth (SSC), have been investigated for their catalytic potential in Li-mNRR, but their overall performance generally falls short in comparison with Ni, Mo and Cu. Nevertheless, SSC stands out within this group due to its favourable combination of moderate ammonia production rates, appreciable faradaic efficiencies, and low material costs, making it a potentially scalable option for industrial applications. Beyond catalyst composition, the choice of electrolyte exerts a substantial influence on reaction kinetics and overall NRR efficiency. Among the lithium-based electrolytes, $LiBF_4$ has demonstrated superior performance, with reported FE's reaching up to 61%.[98] In particular, synergistic effects have been observed when $LiBF_4$ is paired with copper-based catalysts, where electrolyte-catalyst interactions appear to enhance N_2 activation and electron transfer efficiency. These findings highlight the critical importance of electrolyte-catalyst coupling in optimizing Li-mNRR systems. Continued refinement of catalyst materials—especially Ni, Mo, and Cu—when used in conjunction with high-performance electrolytes such as $LiBF_4$, could lead to substantial improvements in efficiency, scalability, and cost-effectiveness. This approach holds significant promise for the development of viable technologies for sustainable, industrial-scale ammonia synthesis.

4.2.3.2 Electrocatalysis

4.2.3.2.1 Production rates per mass of catalyst ([μmol mg^{-1} h^{-1}]). The evaluated data, reported in Fig. 15 and summarized in Table 4, reveal that molybdenum-based compounds—such as Mo_2N nanorods, MoS_2, and Mo_3Fe_3C—consistently achieve high FEs and notable ammonia PR, while maintaining moderate material costs. In addition to these intrinsic properties, the choice of electrolyte—ranging from acidic to basic—also contributes to the observed catalytic performance and selectivity. Building on the favourable properties discussed previously, their catalytic performance is further enhanced when molybdenum is combined with elements such as carbon, nitrogen, or sulphur.[131,150–152] These heteroelemental combinations introduce electronic modifications, alter the d-band structure, and promote the formation of vacancy-rich or defect-engineered sites, which collectively improve N_2 activation and facilitate multi-electron transfer processes. The synergy between intrinsic material properties and structural tunability makes molybdenum-based systems highly adaptable for nitrogen reduction applications and supports their growing prominence in the field. MOFs, TCPP-based ligands, and MXenes demonstrate outstanding catalytic performance in electrochemical NRR, characterized by high faradaic efficiencies and moderate to high ammonia production rates. Their superior activity is primarily attributed to their intrinsic porosity, which provides a high density of accessible active sites and promotes efficient mass and charge transport.[153] Furthermore, the tuneable chemical composition and structural flexibility of these materials allow for precise modulation of their electronic and catalytic properties. Despite their promising performance, the relatively high synthesis costs and limited scalability of these materials currently hinder their widespread application.[154,155] To address these challenges, defect engineering has emerged as a complementary strategy to enhance catalytic activity. By introducing vacancy sites or structural irregularities, materials such as defective UiO-66-NH_2 and defect-rich MoS_2 nanoflowers exhibit improved N_2 adsorption and activation, thereby lowering the energy barrier for ammonia synthesis.[156] The combined benefits of structural tunability and defect engineering underscore the potential of these advanced

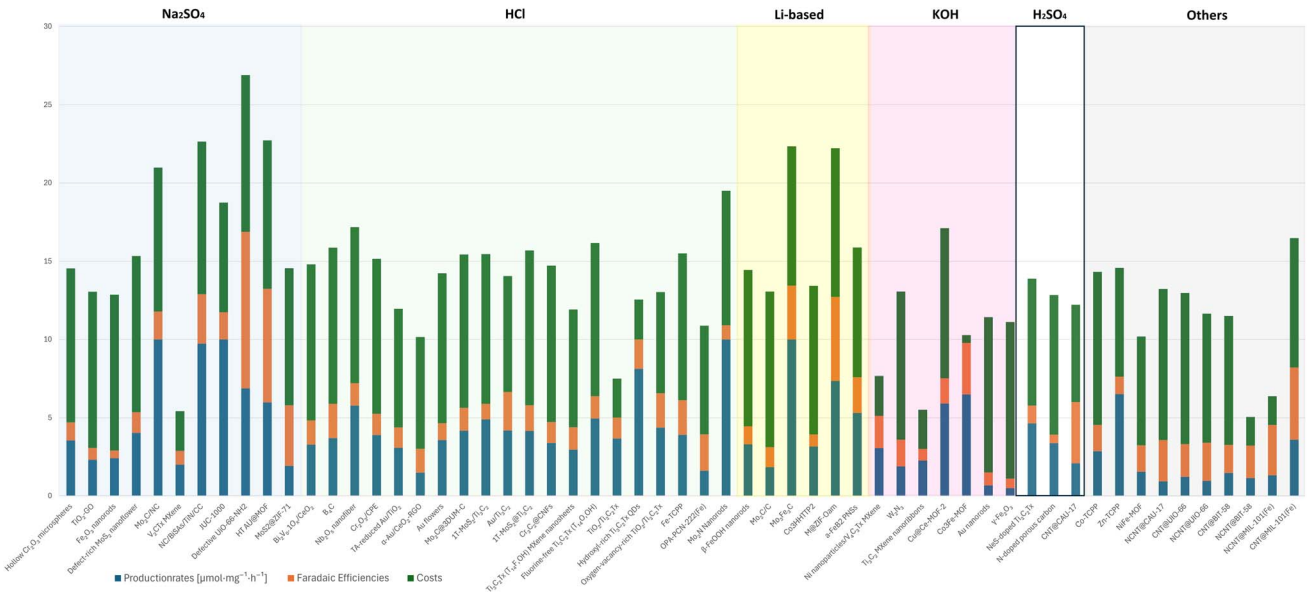

Fig. 15 Comparative analysis of diverse electrocatalysts in varied electrolyte compositions.

Table 4 Evaluation scores of various electrode materials based on NH_3 production rate, faradaic efficiency, and estimated catalyst cost

Entry	Catalyst	Score (points)	References
26	Hollow Cr_2O_3 microspheres	14.6	157
27	TiO_2-GO	13.1	158
28	Fe_2O_3 nanorods	12.9	159
29	Defect-rich MoS_2 nanoflower	15.3	160
30	Mo_2C/NC	21.0	161
31	V_2CT_x MXene	5.4	162
32	NC/BiSAs/TiN/CC	22.6	163
33	JUC-1000	18.7	164
34	Defective UiO-66-NH_2	26.9	165
35	HT-Au@MOF	22.7	166
36	MoS2@ZIF-71	14.6	167
37	$Bi_2V_0.1O_x/CeO_2$	14.8	168
38	B_4C	15.9	169
39	Nb_2O_5 nanofiber	17.2	170
40	Cr_2O_3/CPE	15.2	171
41	TA-reduced Au/TiO_2	12.0	172
42	α-Au/CeO_2-RGO	10.2	173
43	Au flowers	14.2	174
44	Mo_2C@3DUM-C	15.4	175
45	Au/Ti_3C_2	14.1	176
46	1T-MoS_2/Ti_3C_2	15.5	177
47	Cr_3C_2@CNFs	14.7	178
48	$Ti_3C_2T_x$ (T_{14}F,OH) MXene nanosheets	11.9	179
49	Fluorine-free $Ti_3C_2T_x$ (T_{14}O,OH)	16.2	180
50	$TiO_2/Ti_3C_2T_x$	7.5	181
51	Hydroxyl-rich $Ti_3C_2T_x$ QDs	12.6	182
52	Oxygen-vacancy-rich $TiO_2/Ti_3C_2T_x$	13.0	183
53	Fe-TCPP	15.5	184
54	OPA-PCN-222 (Fe)	10.9	185
55	Mo_2N nanorods	19.5	186
56	β-FeOOH nanorods	14.5	187
57	Mo_2C/C	13.1	188
58	Mo_3Fe_3C	22.3	188
59	Co3HHTTP2	13.4	189
60	M@ZIF-Oam	22.2	190
61	a-FeB_2 PNSs	15.9	191
62	Ni nanoparticles/$V_4C_3T_x$ MXene	7.7	192
63	W_2N_3	13.1	193
64	Ti_3C_2 MXene nanoribbons	5.5	194
65	Cu@Ce-MOF-2	17.1	195
66	Co3Fe-MOF	10.3	120
67	Au nanorods	11.4	196
68	γ-Fe_2O_3	11.1	197
69	NeS-doped $Ti_3C_2T_x$	13.9	198
70	N-doped porous carbon	12.8	199
71	CNT@CAU-17	12.2	200
72	Co-TCPP	14.3	201
73	Zn-TCPP	14.6	201
74	NiFe-MOF	10.2	202
75	NCNT@CAU-17	13.2	203
76	CNT@UIO-66	13.0	204
77	NCNT@UiO-66	11.7	204
78	CNT@BIT-58	11.5	205
79	NCNT@BIT-58	5.1	205
80	NCNT@MIL-101(Fe)	6.6	206
81	CNT@MIL-101(Fe)	16.5	206

materials for high-performance nitrogen reduction. These findings are summarized in Fig. 15, which highlights the correlation between material class, structural characteristics, and catalytic performance.

4.2.3.2.2 Production rates per unit area of catalyst [μmol cm^{-2} h^{-1}]. Further analysis of the evaluated systems confirms the recurrent effectiveness of molybdenum-based materials (Table 5). Beyond the previously discussed compounds, MoO_3

Table 5 Evaluation scores of various electrode materials based on NH_3 production rate, faradaic efficiency, and estimated catalyst cost

Entry	Catalyst	Score (points)	References
82	TiO_2/Ti	14.6	207
83	MoS_2/CC	13.1	208
84	MnO/TM	12.9	187
85	Fe_3O_4/Ti	15.3	209
86	a-Mo_2C	**21.0**	210
87	TiN-PE	5.4	211
88	ZIF-67@Ti_3C_2	22.6	212
89	In-MOF	18.7	213
90	H-KUST	26.9	214
91	MoO_3 nanosheet	22.7	215
92	Mo nanofilm	14.6	216
93	Ru/C	14.	217
94	VN/TM	15.9	218
95	Ag nanosheet	17.2	219
96	MoN	15.2	220
97	MoN NA/CC	12.0	221
98	TiB2	10.2	222
99	VN/CC	14.2	223
100	MV-MoN@NC	15.4	224
101	Mo_2N	14.1	47
102	PEBCD/C	15.5	225
103	AuHNCs	14.7	226
104	Surface-engineered Ti_3C_2	11.9	46
105	NH_2-MIL-88B-Fe	16.2	227
106	Au-nanorod	7.5	228
107	Ru/Ti	12.6	229
108	VN	13.0	230
109	Cu/$Ti_3C_2T_x$ MXene	15.5	231
110	Ag–Au@ZIF	10.9	232
111	$CrO_{0.66}N_{0.56}$	19.5	233
112	Au@ZIF-8	14.5	234
113	Fe_2O_3-CNT	13.1	47
114	CP_2TiCl_2	22.3	235

nanosheets and Mo_2C@3DUM-C have demonstrated substantial activity toward nitrogen reduction, reinforcing molybdenum's relevance across various structural forms. In parallel, composite and hybrid materials such as MXene/ZIF systems—including Cu/$Ti_3C_2T_x$, ZIF-67@Ti_3C_2, Ag–Au@ZIF, and Au@ZIF-8—as well as MOFs like In-MOF and HKUST-1, exhibit high faradaic efficiencies and significant ammonia production rates, as summarized in Fig. 16. These results underscore the potential of framework-based and two-dimensional materials for NRR applications. A noteworthy organometallic compound in this context is Cp_2TiCl_2 (ferrocene analogue), which achieves high ammonia production rates despites its relatively low FE. This discrepancy suggests that while the compound exhibits intrinsic N_2 reduction activity, its electron transfer efficiency may be insufficient. A potential pathway to improve its performance lies in the integration with highly conductive materials—such as carbon-based nanostructures or MXenes—which may enhance charge transport and stabilize intermediate species. Surface-engineered titanium-based materials also show promise. In particular, Ti_3C_2 MXenes containing engineered surface defects demonstrate enhanced activity, likely due to the formation of additional catalytically active sites. Titanium's widespread use is further justified by its corrosion resistance, structural stability, and capacity to form synergistic composites. However, as illustrated in Fig. 16, the performance of Ti-based catalysts varies significantly. While some systems yield promising results, others remain less effective, indicating that the catalytic behaviour is highly sensitive to structural and compositional factors. Furthermore, current data on Ru/Ti systems remain incomplete—particularly with respect to faradaic efficiency—which hinders full performance evaluation and comparison. Finally, no clear correlation has yet emerged

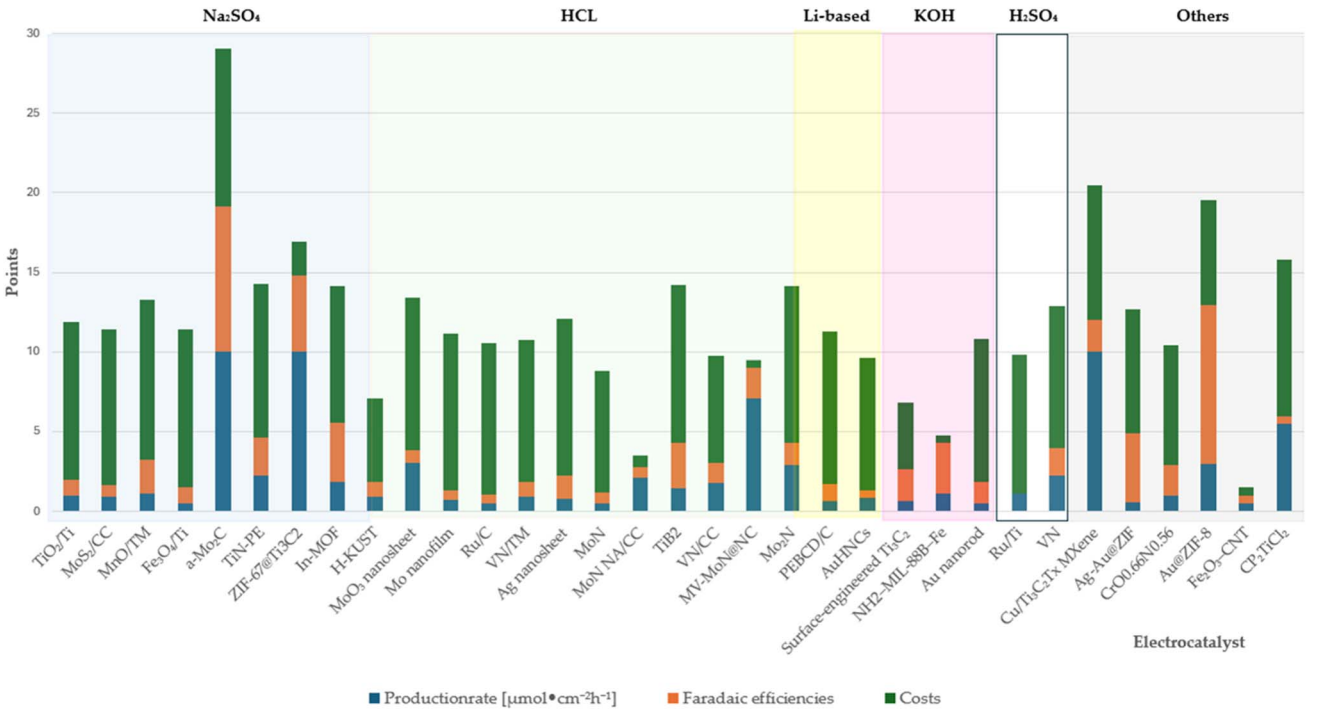

Fig. 16 Comparative analysis of electrocatalysts in varied electrolyte compositions.

between the choice of electrolyte and catalytic output, highlighting a knowledge gap requiring systematic investigation in future studies.

4.2.3.2.3 Photocatalysis. The comparison of various photocatalysts is based on reported experiments conducted under moderate temperatures, as summarized in Tables 6 and 7. In many cases, the authors specified temperatures within the range of 15–30 °C, which in this work is generalized as room temperature. For clarity, the graphical representation is divided into two figures: Fig. 17 summarizes systems for which both production rates and faradaic efficiencies were reported, whereas Fig. 18 presents data from studies in which faradaic efficiencies were not available. Although the results for photocatalysts exhibit limited variability overall, a few systems clearly stand out—most notably Ru/MOF/C_3N_4, P-C_3N_4, and Bi_5O_7Br nanotubes. While these materials demonstrate superior performance, the majority of photocatalysts show rather uniform behavior in terms of production rates, faradaic efficiencies, and costs. A particularly interesting observation is that the most efficient catalysts often share structural and electronic characteristics, including optimized bandgaps and enhanced charge carrier separation. A consistent trend emerges with graphitic carbon nitride (g-C_3N_4): its high photocatalytic activity is commonly attributed to its narrow bandgap (~2.7 eV), enabling visible light absorption, and to its excellent thermal and chemical stability under harsh conditions. Furthermore, its layered structure provides a high specific surface area, facilitating effective adsorption of reactants and improving reaction kinetics.[236] As a result, g-C_3N_4 is frequently modified or combined with other materials—such as molybdenum compounds (*e.g.*, MoO_2), gold (Au), MOFs, or ruthenium (Ru)—to enhance its photocatalytic performance. Notably, the integration of noble metals or the construction of heterojunctions has been shown to improve charge carrier dynamics by promoting charge separation and reducing recombination losses. These effects are often realized through the formation of internal electric fields or Schottky junctions at the material interfaces, both of which facilitate unidirectional charge flow and enhance photocatalytic efficiency. As is well-documented in the literature, doping and defect engineering are additional effective strategies to modulate the electronic structure and surface reactivity. These modifications allow for fine-tuning of band positions, increased density of active sites, and improved kinetics of key reaction steps, such as N_2 adsorption and activation. Bismuth-based materials also show strong potential, with compounds like Bi_5O_7Br demonstrating higher faradaic efficiencies and production rates compared to many alternatives. Their favorable bandgaps (typically 1.8–2.8 eV) support efficient visible light absorption, while their chemical flexibility and stability in aqueous environments make them suitable for surface and structural tailoring, such as through doping or nanoscale morphology control, to further optimize their catalytic behavior.[237,238] Moreover, materials previously studied as electrocatalysts, including molybdenum compounds, TiO_2, Ti_3C_2 MXenes, MOF, and other porous structures, are increasingly utilized in photocatalysis, owing to their high surface areas, stability, and intrinsic catalytic activity.[239] While Fig. 16 provides a comparative overview of photocatalyst performance, it does not conclusively indicate whether variations in electrolytes significantly impact the reaction mechanism and further studies are needed to shed light on this aspect. Fig. 17 presents ammonia production rates for selected materials under mild conditions (15–30 °C) along with their electrolyte compositions. Even though faradaic efficiency data are not available for these experiments, production rates alone offer valuable insights. Materials such as C_3N_4, bismuth-based compounds, MOFs, and TiO_2 demonstrate notably high ammonia yields, highlighting their potential for nitrogen reduction under ambient conditions. Their favorable structural and electronic properties, such as optimized bandgaps and high surface areas, facilitate efficient N_2 activation upon light exposure, enhancing overall photocatalytic performance. No clear correlation between electrolyte composition and catalytic output was observed, and variations within the tested temperature range appear minimal, suggesting that neither factor strongly dominates under these conditions.

Table 6 Evaluation scores of various electrode materials based on NH_3 production rate, faradaic efficiency, and estimated catalyst cost

Entry	Catalyst	Score (points)	References
115	Fe-BiOBr nanosheet (1)	16.8	240
116	Fe-BiOCl nanosheet (2)	21.1	241
117	Bi_5O_7Br nanotube	21.4	242
118	Bi_2MoO_6 sphere	19.5	243
119	CuCr-LDH nanosheet	13.4	244
120	MoO_{3-x} nanosheet	16.4	245
121	$Ti_3C_2T_x/TiO_2$	16.6	246
122	WO_3	14.7	247
123	P-C_3N_4	13.3	248
124	Au–$Ru_{0.31}$ nanokristalle	12.0	249
125	Mo-$W_{18}O_{49}$ ultrathin nanowires	16.0	250
126	Au/TiO_2-OV	15.7	251
127	CuCr-LDH nanosheets	13.3	252
128	SAFe-porous g-C_3N_4	13.0	253
129	Co-doped Bi_2MoO_6	14.4	254
130	Fe/Zr-MOFs	12.8	255
131	COFX Au	16.8	256
132	Ru/MOF/C_3N_4	28.4	257
133	PCN-V	12.5	258
134	IN_2S_3-X@ZnS	12.7	259
135	Ag–Pt/TiO_2	12.2	260
136	POM($PMo_{10}V_2$) and MOF(MIL-88-A)	13.0	261
137	$CEF_3/LiNbO_3$	13.4	262
138	Ru-$KzTa_2O_{6-x}$	11.1	263
139	$C_3N_4/MoS_2/Mn_3O_4$ SVs	16.7	264
140	B-C_3N_4 (MoO_2)	19.4	265
141	Au/TiO_2	14.1	266
142	Au/g-C_3N_4 hollow sphere	17.3	267
143	Ru-CoS/g-C_3N_4 SVs	18.1	268

4.2.3.2.4 PEC performance [μmol mg^{-1} L^{-1} h^{-1}]. A comparative overview of photocatalyst performance in flow systems, expressed in μmol mg^{-1} L^{-1} h^{-1}, is provided in Fig. 19, while the corresponding data are summarized in Table 8. Although

Table 7 Evaluation scores of photocatalysts based on NH_3 production rate, faradaic efficiency, and estimated catalyst cost

Entry	Catalyst	Score (points)	References
144	BiOBr nanosheet (1)	12.4	269
145	Bi_5O_7Br nanostructure	20.0	270
146	Bi_2MoO_6/BiOBr	13.3	271
147	H-Bi_5O_7I	15.5	272
148	$Cu\delta^+$-ZnAl-LDH nanosheet	13.4	273
149	FeS_2-FeP-CeO_2	19.6	274
150	In_2O_3/In_2S_3 microsphere	11.6	275
151	GaN (Ru) NVs	15.0	276
152	Ultrathin MoS_2 SVs	16.0	277
153	FeN-CDs/TiO_2@CN	16.3	278
154	Al-PMOF(Fe)	10.5	279
155	Pt_1/N-MoS_2	7.1	280
156	Fe-BiOCl nanosheets	18.4	281
157	Au/$(BiO)_2CO_3$	11.7	282
158	5%Ru@n-GaN NWs	12.2	283
159	Cs_2O/Os–Au	10.1	284
160	UiO-66(–NH_2)/$CuInS_2$	13.1	285
161	$FeIN_2S_4$/Fe-Pal	17.1	286
162	Bi_2S_3/OV-Bi_2MoO_6	13.9	287
163	Cu–Cu_2O/CMOH	15.3	288
164	Co-doped Bi_2MoO_6 (1)	13.9	289
165	Cu-doped Bi_2MoO_6 (2)	15.0	290
166	Bi-MOF/g-C_3N_4	15.4	291
167	Cu_2O clusters/MIL-100(Fe)	12.3	292
168	BiOBr/OV-TiO_2-Cu	15.0	293
169	S-doped-g-C_3N_4	19.9	294
170	Carbon-$WO_3 \cdot H_2O$	15.5	295
171	ZnO/$ZnSnO_3$/carbon dots	19.7	296
172	TiO_2/BiOBr	18.1	297
173	$Bi_2SN_2O_7$/BiOBr	16.6	298
174	Boron-doped graphene quantum dots/Bi_2MoO_6	14.8	299
175	2D/2D $Bi_{12}O_{17}Br_2$/ZnCr-LDH	7.0	300
176	N-graphyne/Bi/BiOBr	11.5	301
177	p-TiO_2	12.6	302
178	Bi_2S_3@PCN	11.1	303
179	NanoMIL-125(Ti)	15.5	304
180	COF/g-C_3N_4/CNT	14.7	305
181	$NiSnO_3$-g-C_3N_4	17.4	306
182	Sb/TiO_2	11.3	307
183	Few-layer g-C_3N_4 NVs	20.0	308
184	NC-g-C_3N_4	18.2	309
185	MOF-74(Zn)@DF-C_3N_4	18.3	310
186	S-g-C_3N_4 nanosheet CVs	19.9	311
187	WS_2@TiO_2 film	18.1	312
188	B-g-C_3N_4 nanosheet	16.3	313
189	B-g-C_3N_4	16.5	314
190	YF3+/ATP nanocomposite	11.8	315
191	$In(OH)_3$/g-C_3N_4	19.2	316
192	Fe-$SrMoO_4$	13.3	317
193	Cyano group/g-C_3N_4	19.5	318
194	In_2S_3 nanotube SVs	11.8	319
195	Pr^{3+}:CeF_3/ATP (attapulgite)	17.4	320
196	AuRuNPs	10.4	321

quantum efficiency values are not reported in the dataset, the catalytic systems are represented by their production rates and estimated costs. Among the evaluated systems, the most active materials include O-g-C_3N_4 NVs, C_3N_4-MoS_2-$PbTiO_3$, and TiO_2 modified with $Bi_2O_3/NaBiS_2$ as well TiO_2 QDs/FeS_4. A recurring pattern is observed across the most efficient systems: many incorporate elements such as molybdenum, TiO_2, g-C_3N_4, or bismuth, either as individual phases or within composite structures. These components appear to play a central role in enhancing light absorption, improving charge separation, and promoting N_2 activation, thereby driving photocatalytic performance. Although the subsequent data section does not include faradaic efficiency values, the observed production rate trends remain consistent with previous findings. Regarding solvent

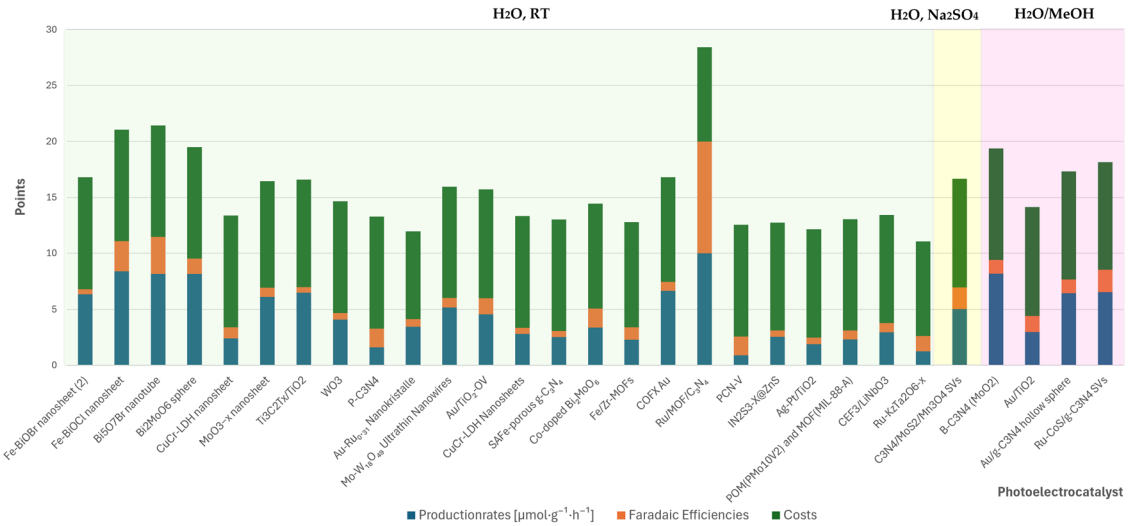

Fig. 17 Performance comparison of different photocatalytic systems.

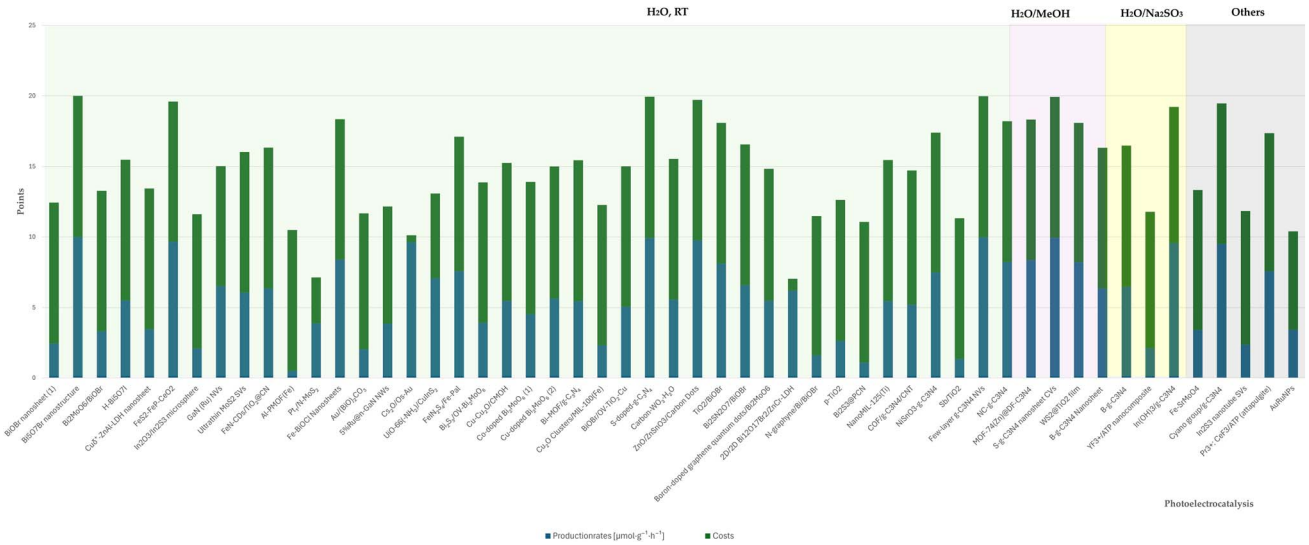

Fig. 18 Performance comparison of different photocatalytic systems.

effects, mixed solvent systems such as H_2O/MeOH or H_2O/EtOH do not reveal a clear trend, suggesting that solvent influence is likely system-specific and should be addressed in more targeted investigations.

4.3 Machine learning (*k*-means clustering) catalyst analysis for eNRR

Machine learning (ML) emerges as a powerful tool in several areas of activity. Recently it has been explored with focus on catalyst discovery and optimization, offering the potential to significantly accelerate research in electrochemical ammonia synthesis.[340,341] Traditional experimental and computational approaches require extensive screening of catalytic materials, often involving high economic and time costs. ML-based methods can help overcome these limitations by efficiently analyzing large datasets, identifying key performance trends, and predicting promising catalyst candidates with reduced experimental effort. Among ML approaches, unsupervised learning techniques such as clustering are particularly valuable, as they provide a structured way to analyze heterogeneous catalyst datasets.[342] Given the complexity of electrochemical NRR, where the interplay of CC, FE, and PR, already highlighted in the previous sections, creates nontrivial trade-offs, clustering offers a holistic means of comparison that complements conventional analysis. To address the challenge of inconsistent reporting across studies, production rates were normalized within each experimental methodology and converted into a point-based system, enabling relative ranking of catalysts on a unified scale. Building on this framework, clustering was applied to identify groups of catalysts with comparable performance, based on normalized PR, FE, and CC. It should be emphasized that this approach constitutes a qualitative,

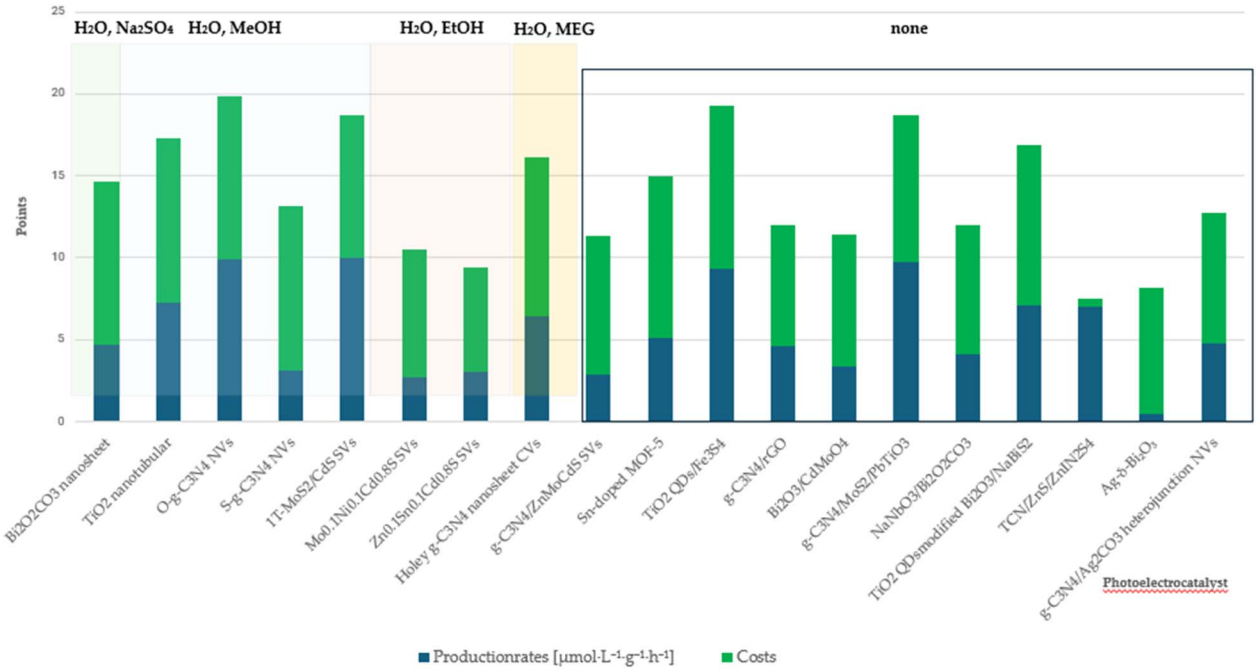

Fig. 19 Comparison of photo electrocatalysts.

exploratory analysis—designed to reveal relative trends and recurring patterns, rather than to provide quantitatively comparable benchmarks across all methods.[343,344]

4.3.1 Clustering technique. *k*-Means clustering is one of the most widely used algorithms in unsupervised machine learning due to its simplicity and efficiency.[345] Its core principle is to partition a dataset into *k* clusters by minimizing the distance between data points and their respective cluster centroids. The algorithm iteratively updates the position of each centroid until the optimal grouping of data points is achieved. In this way, catalysts with similar performance profiles can be grouped together, enabling a structured comparison across heterogeneous datasets. A critical step in applying *k*-means is the selection of the number of clusters (k). To evaluate clustering quality and determine the most suitable cluster count, the silhouette coefficient is frequently employed. These metric balances two aspects: (i) the average intra-cluster distance $a(i)$, which measures how closely an object is grouped with others in its cluster, and (ii) the nearest inter-cluster distance $b(i)$, which measures how far the object is from members of the closest neighboring cluster. The silhouette coefficient for an object i is defined as:

$$s(i) = \frac{b(i) - a(i)}{\max(a(i),\ \ b(i))} \tag{4.5}$$

The value of $s(i)$ ranges from −1 to 1. If $s(i)$ approaches 1, the object is well-clustered and clearly separated from other groups. Values near 0 indicate overlapping clusters or ambiguous assignments, while negative values suggest misclassification. For visual interpretation, silhouette plots can be constructed (Fig. S1, SI), showing the distribution of $s(i)$ across all clusters. Wide and clearly separated silhouettes indicate robust clustering, whereas narrow silhouettes reveal weak separation. By comparing silhouette coefficients across different values of k, the optimal cluster number can be identified. In addition, elbow plots (Fig. S2, SI) were generated to visually identify the point of diminishing returns in explained variance as k increases. In the context of eNRR catalyst analysis, clustering supported by silhouette evaluation provides a practical and

Table 8 Evaluation scores of photo electrocatalysts based on NH_3 production rate, faradaic efficiency, and estimated catalyst cost

Entry	Catalyst	Score (points)	References
197	$Bi_2O_2CO_3$ nanosheet	14.6	322
198	TiO_2 nanotubular	17.3	323
199	O-g-C_3N_4 NVs	19.9	324
200	S-g-C_3N_4 NVs	13.1	324
201	1T-MoS_2/CdS SVs	18.7	325
202	$Mo_{0.1}Ni_{0.1}Cd_{0.8}S$ SVs	10.5	326
203	$Zn_{0.1}Sn_{0.1}Cd_{0.8}S$ SVs	9.4	327
204	Holey g-C_3N_4 nanosheet CVs	16.2	328
205	g-C_3N_4/ZnMoCdS SVs	11.3	329
206	Sn-doped MOF-5	14.9	330
207	TiO_2 QDs/Fe_3S_4	19.3	331
208	g-C_3N_4/rGO	12.0	332
209	Bi_2O_3/$CdMoO_4$	11.4	333
210	g-C_3N_4/MoS_2/$PbTiO_3$	18.7	334
211	$NaNbO_3$/$Bi_2O_2CO_3$	12.0	335
212	TiO_2 QDsmodified Bi_2O_3/$NaBiS_2$	16.9	336
213	TCN/ZnS/$ZnIN_2S_4$	7.5	337
214	Ag-δ-Bi_2O_3	8.2	338
215	g-C_3N_4/Ag_2CO_3 heterojunction NVs	12.8	339

interpretable means of detecting patterns, such as the recurrent grouping of certain metals or catalyst families in high-performing clusters. This approach complements conventional method-specific analysis and highlights trends that may guide future catalyst design efforts.[342,346] Following the establishment of the clustering methodology, analysis was applied to the catalyst dataset to quantitatively elucidate underlying performance trends. The resulting 3D scatter plot (Fig. 20) depicts the clustering of the evaluated eNRR catalysts based on normalized PR, FE, and CC. Catalytic systems highlighted and labeled in red correspond to those achieving a total score exceeding 20 points, thereby defining the top-performing catalysts within the dataset (Fig. 21). Crucially, this normalization step solved one of the key challenges in catalyst comparison: the inconsistent reporting of performance metrics across studies. By converting absolute values into relative, unit-independent scores, heterogeneous datasets could be merged into a unified framework, enabling meaningful clustering and ensuring that observed trends truly reflect intrinsic catalyst performance rather than methodological bias. Importantly, the scoring procedure is fully unit-independent, as all input parameters were normalized prior to clustering. This normalization eliminates potential bias arising from differences in the absolute magnitudes of production rates, efficiencies, or costs, ensuring a consistent and objective ranking of catalysts.

The top-scoring catalysts identified through this data-driven approach closely match those previously highlighted in the qualitative analysis, independently confirming their superior performance. For direct comparison, these catalysts are summarized in Table 9, including their calculated scores, key performance metrics, and qualitative classification. This overview provides a clear framework for assessing the correspondence between quantitative and qualitative evaluations and for prioritizing candidates for further experimental validation. Notably, the strong correspondence between the ML-based clustering results and the qualitative selection confirms that this unit-independent scoring approach can reliably highlight promising candidates, suggesting that similar ML-assisted strategies may accelerate catalyst screening in future studies.

While machine-learning approaches hold significant potential for accelerating the discovery of catalytic systems, their effectiveness critically depends on the availability of high-quality, standardized data. To this end, we propose a minimal set of reporting requirements for NRR publications, including: (i) ammonia production rates reported in a unified metric (μmol cm^{-2} s^{-1}) to enable direct cross-catalyst comparison, (ii) faradaic efficiency, (iii) turnover frequency (TOF), (iv) electrochemically active surface area (ECSA), and, where available, complementary physical surface area metrics (*e.g.*, BET) (v) stability metrics expressed in hours of continuous or cycling operation, and, where feasible, (vi) catalyst cost. Collecting these data systematically as SI would allow the establishment of an open-access database, enabling machine-learning algorithms to directly exploit the dataset. Such a resource could accelerate the rational design and discovery of catalysts not only for NRR, but also for related reactions such as HER and CO_2RR, bridging the gap between experimental reporting and computational screening.

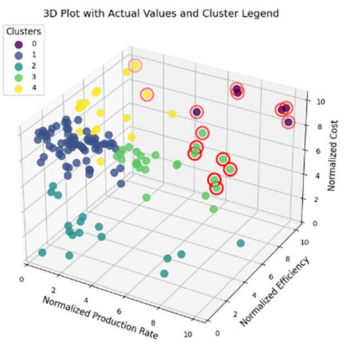

Fig. 20 Clustering results obtained by applying *k*-means method to the catalyst data collection.

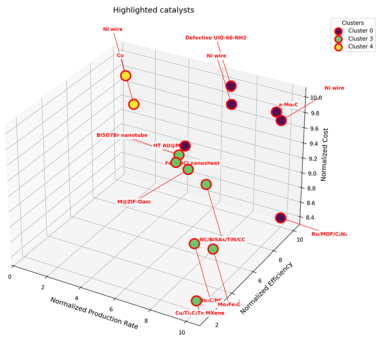

Fig. 21 Detailed view of the relevant range of catalysts identified through the *k*-means method.

4.4 Rational catalyst design guidelines

Based on the combined quantitative evaluation and ML-assisted analysis, this section distills the key insights into practical design guidelines for NRR catalysts. To provide a concise overview, 140 representative catalytic systems were grouped into five major material classes: Mo-based catalysts, MOF-based hybrids, MXenes and their composites, transition-metal nitrides/carbides, and noble-metal-based materials. To

Table 9 Overview of catalytic systems achieving the highest performance scores among the evaluated datasets

Entry	Catalyst	Method	Score (points)
16	Ni wire	LimNRR	29.4
22	Cu	LimNRR	20.1
30	Mo_2C/NC	Electrocatalysis	21.0
32	NC/BiSAs/TiN/CC	Electrocatalysis	22.6
34	Defective UiO-66NH_2	Electrocatalysis	26.9
35	HT-Au@MOF	Electrocatalysis	22.7
58	Mo_3Fe_3C	Electrocatalysis	22.3
60	M@ZIF-OAM	Electrocatalysis	22.2
86	a-Mo_2C	Electrocatalysis	29.1
109	Cu/Ti_3CT_x Mxene	Electrocatalysis	20.5
116	Fe-BiOCl-nanosheet	Photocatalysis	21.1
117	Bi_5O_7Br-nanotube	Photocatalysis	21.4
132	Ru/MOF/C_3N_4	Photocatalysis	28.4

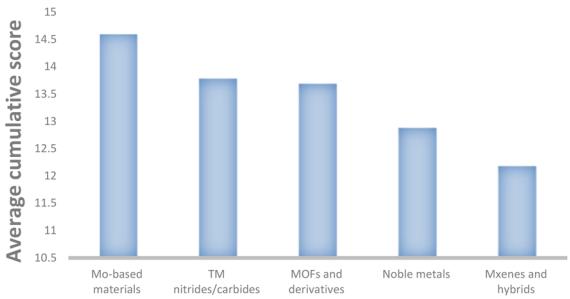

Fig. 22 Average cumulative scores of representative catalyst classes for electro-chemical NRR.

provide an insightful overview of the evaluated catalytic systems, Fig. 22 summarizes the average cumulative performance scores of the different catalyst classes, highlighting recurring features associated with high activity and favorable cost–performance. Mo-based catalysts, transition-metal nitrides/carbides, as well as MOF-based systems and their derivatives consistently populate the top-performing range, reflecting their balanced activity, elemental abundance, and tunable coordination environments. These characteristics render them particularly suitable as foundational platforms for electrocatalytic NRR. In contrast, MXenes and MXene-based hybrids, as well as noble-metal-based catalysts, generally exhibit less favorable overall performance, predominantly due to their limited abundance and higher material costs. This class-based comparison confirms that future catalyst development must carefully balance catalytic performance, faradaic efficiency, and material cost to enable realistic scale-up and practical implementation.

5 Conclusion and outlook

This review provides a comprehensive overview of the current state-of-the-art methods for NRR, with particular emphasis on the electrochemical pathway. Special attention is devoted to catalytic materials and systems, since catalysis remains a crucial factor for enabling efficient scale-up toward practical NH_3 production. To systematically explore trends in catalyst design, a dataset of 215 catalytic systems was compiled and analyzed. A key insight from this effort was the inconsistency of reported data, particularly the frequent omission of values such as TOF or stability, and the lack of uniformity in the units used for production rates. To address these issues, a normalization procedure was applied, enabling unit-independent comparison across catalytic systems. The resulting dataset was subsequently evaluated through a combined approach of qualitative/quantitative manual assessment and quantitative analysis employing machine learning techniques. These analyses enabled the identification of key trends in catalyst design, highlighting the critical role of transition-metal centers (*e.g.*, Mo, Ni, Cu), conductive high-surface-area supports, including materials such as MOFs and MXenes, and structural tailoring through porosity, defect engineering, and heteroatom doping. Such characteristics consistently correlate with enhanced performance, providing a clear framework to guide the rational development of catalysts for both fundamental research and industrial applications. In line with this framework, Mo-based catalysts, transition-metal nitrides and carbides, as well as MOFs and their derivatives emerge as particularly promising material classes, as they combine high intrinsic activity with material abundance, structural tunability, and favorable cost–performance characteristics. These systems therefore represent a strong basis for future electrocatalyst development in electrochemical NRR. To accelerate catalyst development for the NRR, improvements in the standardization of data reporting are essential. It is emphasized that a fundamental, consistent unit should be adopted to represent catalytic activity in terms of ammonia production. We propose using a molecular unit per time and catalyst surface area, such as μmol cm^{-2} s^{-1}. In addition, TOF should be included as an intrinsic descriptor, as it reflects the activity per active site and provides complementary information on catalyst performance. Furthermore, we propose systematic reporting of key parameters, particularly when evaluating catalysts or catalytic systems. In this context, the electrochemically active surface area (ECSA), complemented by physical surface area measurements (BET) when available, along with TOF and stability expressed in hours, are essential descriptors for adequately characterizing a catalytic system. The absence of such standardized and comprehensive data not only hampers direct comparison between catalysts but also limits the application of advanced computational approaches. Machine learning, in particular, has the potential to significantly accelerate catalyst screening and identify key trends in design parameters. Its effectiveness, however, depends on the availability of high-quality, well-curated datasets. As highlighted by this review, current data fragmentation can severely restrict the generalization of the obtained conclusions. Nevertheless, the potential of ML methods is enormous, and, with consistent and standardized reporting, they fully realize their capabilities, enabling the targeted development and optimization of NRR catalysts.

Conflicts of interest

The authors declare no conflict of interest.

Abbreviations

ADP	Adenosine diphosphate
AEL	Alkaline electrolysis
AEM	Anion exchange membrane
ATP	Adenosine triphosphate
BET	Brunauer–Emmett–Teller
CB	Conduction band
CC	Catalyst cost
CCS	Carbon capture and storage
Cp_2TiCl_2	Titanocen-dichlorid
DFT	Density functional theory
DOE	Department of energy
E_a	Activation energy
ECSA	Electrochemically active surface area

EtOH	Ethanol
FE	Faradaic efficiency
GJ	Gigajoule
HB	Haber–Bosch
HER	Hydrogen evolution reaction
ILs	Ionic liquids
kWh	Kilowatt-hour
$LiBF_4$	Lithiumtetrafluoroborat
Li-mNRR	Lithium-mediated nitrogen reduction reaction
$LiPF_6$	Lithiumhexafluorophosphat
LiTFSI	Lithiumbis(trifluormethylsulfonyl)imid
LH_2	Liquefied hydrogen
LMeOH	Liquefied methanol
LNH_3	Liquefied ammonia
MOC	Metal–organic compound
MOF	Metal–organic framework
MPa	Megapascal
NRR	Nitrogen reduction reaction
NTP	Non-thermal plasma
P/Pi	Phosphate/inorganic phosphate
PEC	Photoelectrocatalysis
PEM	Proton exchange membrane
PEMEL	Proton exchange membrane electrolyzer
PR	Production rate
PSA	Pressure swing adsorption
PV	Photovoltaic
QDs	Quantum dots
SEM	Scanning electron microscopy
SMR	Steam methane reforming
SOE	Solid oxide electrolysis
SSC	Stainless steel cloth
TCPP	Tetrakis(4-carboxyphenyl)porphyrin
THF	Tetrahydrofuran
t	metric ton
TOF	Turnover frequency
TRL	Technology readiness level
VB	Valence band
ΔG	Free energy difference

Data availability

All data analysed in this review are taken from previously published studies and are available in the cited literature. The compiled dataset used for comparison is provided in the manuscript and in the supplementary information (SI). Supplementary information is available. See DOI: https://doi.org/10.1039/d5na01170a.

Acknowledgements

This work was financed by national funds from FCT – Fundação para a Ciência e a Tecnologia, I.P., under the scope of the project UID/50006/2025 of the Associate Laboratory for Green Chemistry – LAQV REQUIMTE. More details can be found here: https://laqv.requimte.pt/a/74-funding. HyLab's authors acknowledge the Base Funding Project of the Collaborative Laboratory, managed by ANI – Agência Nacional de Inovação and funded through the call RE-C05-i02-Missão Interface No. 01/C05-i02/2022 of the Portuguese Recovery and Resilience Plan (PRR).

References

1 D. E. Canfield, A. N. Glazer and P. G. Falkowski, The Evolution and Future of Earth's Nitrogen Cycle, *Science*, 2010, **330**(6001), 192–196, DOI: 10.1126/science.1186120.
2 O. Elishav, L. B. Mosevitzky, E. M. Miller, *et al.*, Progress and Prospective of Nitrogen-Based Alternative Fuels, *Chem. Rev.*, 2020, **120**(12), 5352–5436, DOI: 10.1021/acs.chemrev.9b00538.
3 V. Smil, Nitrogen and Food Production: Proteins for Human Diets, *Ambio*, 2002, **31**(2), 126–131, DOI: 10.1579/0044-7447-31.2.126.
4 J. W. Erisman, M. A. Sutton, J. Galloway, Z. Klimont and W. Winiwarter, How a century of ammonia synthesis changed the world, *Nat. Geosci.*, 2008, **1**(10), 636–639, DOI: 10.1038/ngeo325.
5 https://www.un.org/en/desa/world-population-projected-reach-98-billion-2050-and-112-billion-2100.
6 N. H. A. Bahar, M. Lo, M. Sanjaya, *et al.*, Meeting the food security challenge for nine billion people in 2050: What impact on forests?, *Global Environ. Change*, 2020, **62**, 102056, DOI: 10.1016/j.gloenvcha.2020.102056.
7 A. Klerke, C. H. Christensen, J. K. Nørskov and T. Vegge, Ammonia for hydrogen storage: challenges and opportunities, *J. Mater. Chem.*, 2008, **18**(20), 2304, DOI: 10.1039/b720020j.
8 Institute for Sustainable Process Technology, https://ispt.eu/news/launch-of-the-green-ammonia-innovation-platform/, accessed August 29, 2024.
9 D. K. Madheswaran, S. Vengatesan, S. Jegadheeswaran, *et al.*, Ammonia as a hydrogen carrier: A comprehensive analysis of electrolysis efficiency and its potential in sustainable energy systems, *Renewable Sustainable Energy Rev.*, 2025, **221**, 115915, DOI: 10.1016/j.rser.2025.115915.
10 M. Alnajideen, H. Shi, W. Northrop, *et al.*, Ammonia combustion and emissions in practical applications: a review, *Carbon Neutrality*, 2024, **3**(1), 13, DOI: 10.1007/s43979-024-00088-6.
11 The Royal Society, *Ammonia: Zero-Carbon Fertiliser, Fuel and Energy Store*, 2020.
12 S. Z. S. Al Ghafri, S. Munro, U. Cardella, *et al.*, Hydrogen liquefaction: a review of the fundamental physics, engineering practice and future opportunities, *Energy Environ. Sci.*, 2022, **15**(7), 2690–2731, DOI: 10.1039/D2EE00099G.
13 P. Mayer, A. Ramirez, G. Pezzella, *et al.*, Blue vs. Green Ammonia Production: A Techno-Economic and Life Cycle Assessment Perspective, *SSRN Electron. J.*, 2022, DOI: 10.2139/ssrn.4309114.
14 R. Kevin and C. Gabriel, *Innovation Outlook : Renewable Ammonia*, International Renewable Energy Agency ; Ammonia Energy Association, 2022.

15 https://www.iea.org/reports/ammonia-technology-roadmap/executive-summary.
16 M. R. Moghadam, A. Bazmandegan-Shamili and H. Bagheri, The current methods of ammonia synthesis by Haber-Bosch process, in *Progresses in Ammonia: Science, Technology and Membranes*, Elsevier, 2024, pp. 1–32, DOI: 10.1016/B978-0-323-88516-4.00002-0.
17 H. Liu, Ammonia synthesis catalyst 100 years: Practice, enlightenment and challenge, *Chin. J. Catal.*, 2014, **35**(10), 1619–1640, DOI: 10.1016/S1872-2067(14)60118-2.
18 B. Elvers, S. Hawkins, G. Schulz, *Ullmann's Encyclopedia of Industrial Chemistry*, Wiley-VCH, 2000, DOI: 10.1002/14356007.
19 S. M. Horrocks, Enriching the Earth: Fritz Haber, Carl Bosch, and the Transformation of World Food (review), *Technol Cult.*, 2002, **43**(3), 622–623, DOI: 10.1353/tech.2002.0114.
20 H. Liu, Ammonia synthesis catalyst 100 years: Practice, enlightenment and challenge, *Chin. J. Catal.*, 2014, **35**(10), 1619–1640, DOI: 10.1016/S1872-2067(14)60118-2.
21 T. Kandemir, M. E. Schuster, A. Senyshyn, M. Behrens and R. Schlögl, The Haber–Bosch Process Revisited: On the Real Structure and Stability of "Ammonia Iron" under Working Conditions, *Angew. Chem., Int. Ed.*, 2013, **52**(48), 12723–12726, DOI: 10.1002/anie.201305812.
22 F. Haber and G. van Oordt, Über die Bildung von Ammoniak den Elementen, *Z. Anorg. Chem.*, 1905, **44**(1), 341–378, DOI: 10.1002/zaac.19050440122.
23 H. Liu, *Ammonia Synthesis Catalysts*, World Scientific/Chemical Industry Press, China, 2013, DOI: 10.1142/8199.
24 *Catalytic Ammonia Synthesis*, ed. J. R. Jennings, Springer US, 1991, DOI: 10.1007/978-1-4757-9592-9.
25 A. Hellman, K. Honkala, S. Dahl, C. H. Christensen and J. K. Nørskov, Ammonia Synthesis: State of the Bellwether Reaction, in *Comprehensive Inorganic Chemistry II*, Elsevier, 2013, pp. 459–474, DOI: 10.1016/B978-0-08-097774-4.00725-7.
26 A. Hellman, K. Honkala, S. Dahl, C. H. Christensen and J. K. Nørskov, Ammonia Synthesis: State of the Bellwether Reaction, in *Comprehensive Inorganic Chemistry II*, Elsevier, 2013, pp. 459–474, DOI: 10.1016/B978-0-08-097774-4.00725-7.
27 V. Kyriakou, I. Garagounis, E. Vasileiou, A. Vourros and M. Stoukides, Progress in the Electrochemical Synthesis of Ammonia, *Catal. Today*, 2017, **286**, 2–13, DOI: 10.1016/j.cattod.2016.06.014.
28 Global price of Nickel and Iron, https://fred.stlouisfed.org/series, accessed August 29, 2024.
29 Global Ruthenium price, https://www.dailymetalprice.com/metalpricecharts.php?c=ru%26u=kg%26d=480, accessed August 29, 2024.
30 C. J. M. van der Ham, M. T. M. Koper and D. G. H. Hetterscheid, Challenges in reduction of dinitrogen by proton and electron transfer, *Chem. Soc. Rev.*, 2014, **43**(15), 5183–5191, DOI: 10.1039/C4CS00085D.
31 J. H. Kim, T. Y. Dai, M. Yang, *et al.*, Achieving volatile potassium promoted ammonia synthesis via mechanochemistry, *Nat. Commun.*, 2023, **14**(1), 2319, DOI: 10.1038/s41467-023-38050-2.
32 H. Liu and W. Han, Wüstite-based catalyst for ammonia synthesis: Structure, property and performance, *Catal. Today*, 2017, **297**, 276–291, DOI: 10.1016/j.cattod.2017.04.062.
33 C. Smith, A. K. Hill and L. Torrente-Murciano, Current and future role of Haber–Bosch ammonia in a carbon-free energy landscape, *Energy Environ. Sci.*, 2020, **13**(2), 331–344, DOI: 10.1039/C9EE02873K.
34 Natural Gas Prices, Accessed August 30, 2024, (A) Natural Gas Price Per Million Btu - Natural Gas Prices Today (oilcrudeprice.com) (30.08.2024).
35 Agentur für Erneuerbare Energien I, *Kosten Der Stromerzeugung Aus Erneuerbaren Energien 2022: Kurzfassung*, 2023, https://www.irena.org.
36 A. K. Hill, C. Smith and L. Torrente-Murciano, Current and future role of Haber–Bosch ammonia in a carbon-free energy landscape, *Energy Environ. Sci.*, 2019, **12**, 318–330, DOI: 10.1039/C8EE02873K.
37 C. Wu, X. P. Zhang and M. Sterling, Solar power generation intermittency and aggregation, *Sci. Rep.*, 2022, **12**(1), 1363, DOI: 10.1038/s41598-022-05247-2.
38 X. Cai, C. Fu, H. Iriawan, *et al.*, Lithium-mediated electrochemical nitrogen reduction: Mechanistic insights to enhance performance, *iScience*, 2021, **24**(10), DOI: 10.1016/j.isci.2021.103105.
39 B. Izelaar, M. Ramdin, A. Vlierboom, *et al.*, Techno-economic assessment of different small-scale electrochemical NH_3 production plants, *Energy Environ. Sci.*, 2024, **17**(21), 7983–7998, DOI: 10.1039/D4EE03299C.
40 G. Oloveichik, The future of ammonia: Improvement of Haber-Bosch … or electrochemical synthesis? Ammonia Energy, 2017, https://ammoniaenergy.org/articles/the-future-of-ammonia-improvement-of-haber-bosch-or-electrochemical-synthesis/, accessed August 25, 2025.
41 O. Westhead, R. Tort, M. Spry, *et al.*, The origin of overpotential in lithium-mediated nitrogen reduction, *Faraday Discuss.*, 2023, **243**, 321–338, DOI: 10.1039/D2FD00156J.
42 L. Tan, N. Yang, X. Huang, *et al.*, Synthesis of ammonia *via* electrochemical nitrogen reduction on high-index faceted Au nanoparticles with a high faradaic efficiency, *Chem. Commun.*, 2019, **55**(96), 14482–14485, DOI: 10.1039/C9CC06132K.
43 T. Li, H. Li, J. Wang, *et al.*, Achieving 78.2 % Faraday Efficiency for Electrochemical Ammonia Production Via Covalent Modification of CNTs with B_4C, *ChemCatChem*, 2024, **16**(15), DOI: 10.1002/cctc.202400115.
44 M. I. Ahmed, A. Assafiri, D. B. Hibbert and C. Zhao, Li-Mediated Electrochemical Nitrogen Fixation: Key Advances and Future Perspectives, *Small*, 2023, **19**(52), 2305616, DOI: 10.1002/smll.202305616.
45 A. Mangini, L. Fagiolari, A. Sacchetti, A. Garbujo, P. Biasi and F. Bella, Lithium-Mediated Nitrogen Reduction for Ammonia Synthesis: Reviewing the Gap between Continuous Electrolytic Cells and Stepwise Processes

through Galvanic Li–N $_2$ Cells, *Adv. Energy Mater.*, 2024, **14**(25), 2400076, DOI: 10.1002/aenm.202400076.

46 A. Biswas, S. Bhardwaj, T. Boruah and R. S. Dey, Electrochemical ammonia synthesis: fundamental practices and recent developments in transition metal boride, carbide and nitride-class of catalysts, *Mater. Adv.*, 2022, **3**(13), 5207–5233, DOI: 10.1039/D2MA00279E.

47 S. Mahmood, S. Iqbal, Z. Wang, *et al.*, Emerging electrocatalysts for green ammonia production: Recent progress and future outlook, *Arabian J. Chem.*, 2024, **17**(10), 105950, DOI: 10.1016/j.arabjc.2024.105950.

48 D. Ješić, B. Pomeroy, K. M. Kamal, Ž. Kovačič, M. Huš and B. Likozar, Photo- and Photoelectrocatalysis in Nitrogen Reduction Reactions to Ammonia: Interfaces, Mechanisms, and Modeling Simulations, *Adv. Energy Sustainability Res.*, 2024, 202400083, DOI: 10.1002/aesr.202400083.

49 H. Shen, M. Yang, L. Hao, J. Wang, J. Strunk and Z. Sun, Photocatalytic nitrogen reduction to ammonia: Insights into the role of defect engineering in photocatalysts, *Nano Res.*, 2022, **15**(4), 2773–2809, DOI: 10.1007/s12274-021-3725-0.

50 E. Castillejos and E. García-Bordejé, Innovative Approaches to Sustainable Ammonia Synthesis under Mild Conditions, *ChemCatChem*, 2024, **16**(13), e202301603, DOI: 10.1002/cctc.202301603.

51 O. Westhead, J. Barrio, A. Bagger, *et al.*, Near ambient N2 fixation on solid electrodes versus enzymes and homogeneous catalysts, *Nat. Rev. Chem.*, 2023, **7**(3), 184–201, DOI: 10.1038/s41570-023-00462-5.

52 J. Xuan, L. He, W. Wen and Y. Feng, Hydrogenase and Nitrogenase: Key Catalysts in Biohydrogen Production, *Molecules*, 2023, **28**(3), 1392, DOI: 10.3390/molecules28031392.

53 C. J. M. van der Ham, M. T. M. Koper and D. G. H. Hetterscheid, Challenges in reduction of dinitrogen by proton and electron transfer, *Chem. Soc. Rev.*, 2014, **43**(15), 5183–5191, DOI: 10.1039/C4CS00085D.

54 Z. Y. Yang, E. Jimenez-Vicente, H. Kallas, *et al.*, The electronic structure of FeV-cofactor in vanadium-dependent nitrogenase, *Chem. Sci.*, 2021, **12**(20), 6913–6922, DOI: 10.1039/D0SC06561G.

55 B. Hinnemann and J. K. Nørskov, Catalysis by Enzymes: The Biological Ammonia Synthesis, *Top. Catal.*, 2006, **37**(1), 55–70, DOI: 10.1007/s11244-006-0002-0.

56 J. Sgrignani, D. Franco and A. Magistrato, Theoretical Studies of Homogeneous Catalysts Mimicking Nitrogenase, *Molecules*, 2011, **16**(1), 442–465, DOI: 10.3390/molecules16010442.

57 X. Wang, S. Nie, H. Yao, *et al.*, Machine Learning-Assisted DFT Screening of Nitrogen-Doped Graphene Diatomic Catalysts for Nitrogen Reduction Reaction, *Molecules*, 2025, **30**(20), 4131, DOI: 10.3390/molecules30204131.

58 J. Zhao and Z. Chen, Single Mo Atom Supported on Defective Boron Nitride Monolayer as an Efficient Electrocatalyst for Nitrogen Fixation: A Computational Study, *J. Am. Chem. Soc.*, 2017, **139**(36), 12480–12487, DOI: 10.1021/jacs.7b05213.

59 B. K. Burgess, S. Wherland, W. E. Newton and E. I. Stiefel, Nitrogenase reactivity: insight into the nitrogen-fixing process through hydrogen-inhibition and HD-forming reactions, *Biochemistry*, 1981, **20**(18), 5140–5146, DOI: 10.1021/bi00521a007.

60 M. A. Shipman and M. D. Symes, Recent progress towards the electrosynthesis of ammonia from sustainable resources, *Catal. Today*, 2017, **286**, 57–68, DOI: 10.1016/j.cattod.2016.05.008.

61 E. Skúlason, T. Bligaard, S. Gudmundsdóttir, *et al.*, A theoretical evaluation of possible transition metal electro-catalysts for N $_2$ reduction, *Phys. Chem. Chem. Phys.*, 2012, **14**(3), 1235–1245, DOI: 10.1039/C1CP22271F.

62 E. Spatolisano, L. A. Pellegrini, A. R. de Angelis, S. Cattaneo and E. Roccaro, Ammonia as a Carbon-Free Energy Carrier: NH3 Cracking to H2, *Ind. Eng. Chem. Res.*, 2023, **62**(28), 10813–10827, DOI: 10.1021/acs.iecr.3c01419.

63 E. Skúlason, T. Bligaard, S. Gudmundsdóttir, *et al.*, A theoretical evaluation of possible transition metal electro-catalysts for N $_2$ reduction, *Phys. Chem. Chem. Phys.*, 2012, **14**(3), 1235–1245, DOI: 10.1039/C1CP22271F.

64 E. A. Moore and R. Janes, *Metal-Ligand Bonding*, The Royal Society of Chemistry, 2004, DOI: 10.1039/9781847559456.

65 G. Frenking and N. Fröhlich, The Nature of the Bonding in Transition-Metal Compounds, *Chem. Rev.*, 2000, **100**(2), 717–774, DOI: 10.1021/cr980401l.

66 Q. Chen, X. Zhang, Y. Jin, X. Zhou, Z. Yang and H. Nie, An Overview on Noble Metal (Group VIII)-based Heterogeneous Electrocatalysts for Nitrogen Reduction Reaction, *Chem.–Asian J.*, 2020, **15**(24), 4131–4152, DOI: 10.1002/asia.202000969.

67 X. Fu, J. B. Pedersen, Y. Zhou, *et al.*, Continuous-flow electrosynthesis of ammonia by nitrogen reduction and hydrogen oxidation, *Science*, 2023, **379**(6633), 707–712, DOI: 10.1126/science.adf4403.

68 X. Fu, Lithium-mediated nitrogen reduction for electrochemical ammonia synthesis: From batch to flow reactor, *Mater. Today Catal.*, 2023, **3**, 100031, DOI: 10.1016/j.mtcata.2023.100031.

69 W. Zheng and L. Y. S. Lee, Metal–Organic Frameworks for Electrocatalysis: Catalyst or Precatalyst?, *ACS Energy Lett.*, 2021, **6**(8), 2838–2843, DOI: 10.1021/acsenergylett.1c01350.

70 R. Li, Z. Feng, Y. Li, X. Dai, Y. Ma and Y. Tang, Bioinspired Mo tape-porphyrin as an efficient and selective electrocatalyst for ammonia synthesis, *Appl. Surf. Sci.*, 2020, **520**, 146202, DOI: 10.1016/j.apsusc.2020.146202.

71 J. Buddrus, Metallorganische Verbindungen, in *Grundlagen der Organischen Chemie*, De Gruyter, 1980, pp. 353–382, DOI: 10.1515/9783111586311-016.

72 S. Kim, F. Loose and P. J. Chirik, Beyond Ammonia: Nitrogen–Element Bond Forming Reactions with Coordinated Dinitrogen, *Chem. Rev.*, 2020, **120**(12), 5637–5681, DOI: 10.1021/acs.chemrev.9b00705.

73 D. Tsamos, A. Krestou, M. Papagiannaki and S. Maropoulos, An Overview of the Production of

Magnetic Core-Shell Nanoparticles and Their Biomedical Applications, *Metals*, 2022, **12**(4), 605, DOI: 10.3390/met12040605.

74 G. F. Han, F. Li, Z. W. Chen, *et al.*, Mechanochemistry for ammonia synthesis under mild conditions, *Nat. Nanotechnol.*, 2021, **16**(3), 325–330, DOI: 10.1038/s41565-020-00809-9.

75 S. Reichle, L. Kang, D. Demirbas, *et al.*, Mechanocatalytic Synthesis of Ammonia: State of the Catalyst During Reaction and Deactivation Pathway, *Angew. Chem., Int. Ed.*, 2024, **63**(14), e202317038, DOI: 10.1002/anie.202317038.

76 F. Cuccu, D. L. Browne and A. Porcheddu, Ammonia Synthesis by Mechanochemistry, *ChemCatChem*, 2023, **15**(19), e202300762, DOI: 10.1002/cctc.202300762.

77 A. Bogaerts and E. C. Neyts, Plasma Technology: An Emerging Technology for Energy Storage, *ACS Energy Lett.*, 2018, **3**(4), 1013–1027, DOI: 10.1021/acsenergylett.8b00184.

78 T. Zhang, R. Zhou, S. Zhang, *et al.*, Sustainable Ammonia Synthesis from Nitrogen and Water by One-Step Plasma Catalysis, *Energy Environ. Mater.*, 2023, **6**(2), e12344, DOI: 10.1002/eem2.12344.

79 K. H. R. Rouwenhorst, H. H. Kim and L. Lefferts, Vibrationally Excited Activation of N2 in Plasma-Enhanced Catalytic Ammonia Synthesis: A Kinetic Analysis, *ACS Sustain. Chem. Eng.*, 2019, **7**(20), 17515–17522, DOI: 10.1021/acssuschemeng.9b04997.

80 H. M. Nguyen, F. Gorky, S. Guthrie and M. L. Carreon, Sustainable ammonia synthesis from nitrogen wet with sea water by single-step plasma catalysis, *Catal. Today*, 2023, **418**, 114141, DOI: 10.1016/j.cattod.2023.114141.

81 K. H. R. Rouwenhorst, Y. Engelmann, K. van't Veer, R. S. Postma, A. Bogaerts and L. Lefferts, Plasma-driven catalysis: green ammonia synthesis with intermittent electricity, *Green Chem.*, 2020, **22**(19), 6258–6287, DOI: 10.1039/D0GC02058C.

82 H. Jin, S. S. Kim, S. Venkateshalu, J. Lee, K. Lee and K. Jin, Electrochemical Nitrogen Fixation for Green Ammonia: Recent Progress and Challenges, *Advanced Science*, 2023, **10**(23), e202300951, DOI: 10.1002/advs.202300951.

83 IRENA (International Renewable Energy Agency), *Renewable Power Generation Costs in 2024*, International Renewable Energy Agency, Abu Dhabi, 2025, available online accessed on 1 September 2025.

84 J. Mu, X. Gao, T. Yu, *et al.*, Ambient Electrochemical Ammonia Synthesis: From Theoretical Guidance to Catalyst Design, *Advanced Science*, 2024, **11**(15), e202308979, DOI: 10.1002/advs.202308979.

85 M. Carmo, D. L. Fritz, J. Mergel and D. Stolten, A comprehensive review on PEM water electrolysis, *Int. J. Hydrogen Energy*, 2013, **38**(12), 4901–4934, DOI: 10.1016/j.ijhydene.2013.01.151.

86 Q. Li, A. Molina Villarino, C. R. Peltier, *et al.*, Anion Exchange Membrane Water Electrolysis: The Future of Green Hydrogen, *J. Phys. Chem. C*, 2023, **127**(17), 7901–7912, DOI: 10.1021/acs.jpcc.3c00319.

87 Y. Zheng, J. Wang, B. Yu, *et al.*, A review of high temperature co-electrolysis of H_2O and CO_2 to produce sustainable fuels using solid oxide electrolysis cells (SOECs): advanced materials and technology, *Chem. Soc. Rev.*, 2017, **46**(5), 1427–1463, DOI: 10.1039/C6CS00403B.

88 R. F. Service, Liquid sunshine, *Science*, 2018, **361**(6398), 120–123, DOI: 10.1126/science.361.6398.120.

89 G. Kaur, H. Zhu, D. S. Dhawale, *et al.*, A review on intermediate temperature electrochemical synthesis of ammonia, *Appl. Energy*, 2025, **393**, 126092, DOI: 10.1016/j.apenergy.2025.126092.

90 B. H. R. Suryanto, H. L. Du, D. Wang, J. Chen, A. N. Simonov and D. R. MacFarlane, Challenges and prospects in the catalysis of electroreduction of nitrogen to ammonia, *Nat. Catal.*, 2019, **2**(4), 290–296, DOI: 10.1038/s41929-019-0252-4.

91 D. Ripepi, R. Zaffaroni, H. Schreuders, B. Boshuizen and F. M. Mulder, Ammonia Synthesis at Ambient Conditions via Electrochemical Atomic Hydrogen Permeation, *ACS Energy Lett.*, 2021, **6**(11), 3817–3823, DOI: 10.1021/acsenergylett.1c01568.

92 Y. Zhou, X. Fu, I. Chorkendorff and J. K. Nørskov, Electrochemical Ammonia Synthesis: The Energy Efficiency Challenge, *ACS Energy Lett.*, 2025, **10**(1), 128–132, DOI: 10.1021/acsenergylett.4c02954.

93 L. Liu, H. Ma, M. Khan and B. S. Hsiao, Recent Advances and Challenges in Anion Exchange Membranes Development/Application for Water Electrolysis: A Review, *Membranes*, 2024, **14**(4), 85, DOI: 10.3390/membranes14040085.

94 R. Li, T. Li, X. Liu, *et al.*, Green synthesis of ammonia from steam and air using solid oxide electrolysis cells composed of ruthenium-modified perovskite catalyst, *Energy Sci. Eng.*, 2023, **11**(7), 2293–2301, DOI: 10.1002/ese3.1452.

95 F. Fichter, P. Girard and H. Erlenmeyer, Elektrolytische Bindung von komprimiertem Stickstoff bei gewöhnlicher Temperatur, *Helv. Chim. Acta*, 1930, **13**(6), 1228–1236, DOI: 10.1002/hlca.19300130604.

96 A. Tsuneto, A. Kudo and T. Sakata, Efficient Electrochemical Reduction of N2 to NH3 Catalyzed by Lithium, *Chem. Lett.*, 1993, **22**(5), 851–854, DOI: 10.1246/cl.1993.851.

97 N. Lazouski, M. Chung, K. Williams, M. L. Gala and K. Manthiram, Non-aqueous gas diffusion electrodes for rapid ammonia synthesis from nitrogen and water-splitting-derived hydrogen, *Nat. Catal.*, 2020, **3**(5), 463–469, DOI: 10.1038/s41929-020-0455-8.

98 X. Fu, S. Li, N. H. Deissler, J. B. V. Mygind, J. Kibsgaard and I. Chorkendorff, Effect of Lithium Salt on Lithium-Mediated Ammonia Synthesis, *ACS Energy Lett.*, 2024, **9**(8), 3790–3795, DOI: 10.1021/acsenergylett.4c01655.

99 Y. Shi, Z. Zhao, D. Yang, *et al.*, Engineering photocatalytic ammonia synthesis, *Chem. Soc. Rev.*, 2023, **52**(20), 6938–6956, DOI: 10.1039/D2CS00797E.

100 M. J. Molaei, Recent advances in hydrogen production through photocatalytic water splitting: A review, *Fuel*, 2024, **365**, 131159, DOI: 10.1016/j.fuel.2024.131159.

101 Z. Fu, Q. Yang, Z. Liu, *et al.*, Photocatalytic conversion of carbon dioxide: From products to design the catalysts, *J. CO_2 Util.*, 2019, **34**, 63–73, DOI: 10.1016/j.jcou.2019.05.032.
102 A. Cavicchioli and I. G. R. Gutz, Effect of scavengers on the photocatalytic digestion of organic matter in water samples assisted by TiO2 in suspension for the voltammetric determination of heavy metals, *J. Braz. Chem. Soc.*, 2002, **13**(4), 757–763, DOI: 10.1590/S0103-50532002000400006.
103 S. He, Y. Chen, J. Fang, Y. Liu and Z. Lin, Optimizing photocatalysis *via* electron spin control, *Chem. Soc. Rev.*, 2025, **54**, D4CS00317A, DOI: 10.1039/D4CS00317A.
104 L. Niu, Z. Liu, G. Liu, *et al.*, Surface hydrophobic modification enhanced catalytic performance of electrochemical nitrogen reduction reaction, *Nano Res.*, 2022, **15**(5), 3886–3893, DOI: 10.1007/s12274-021-4015-6.
105 M. Nazemi, S. R. Panikkanvalappil and M. A. El-Sayed, Enhancing the rate of electrochemical nitrogen reduction reaction for ammonia synthesis under ambient conditions using hollow gold nanocages, *Nano Energy*, 2018, **49**, 316–323, DOI: 10.1016/j.nanoen.2018.04.039.
106 M. Coha, G. Farinelli, A. Tiraferri, M. Minella and D. Vione, Advanced oxidation processes in the removal of organic substances from produced water: Potential, configurations, and research needs, *Chem. Eng. J.*, 2021, **414**, 128668, DOI: 10.1016/j.cej.2021.128668.
107 HyMAP-CORDIS. *Hybrid Materials for Artificial Photosynthesis*, preprint posted online July 1, 2015, DOI: 10.3030/648319.
108 T. Mao, J. Zha, Y. Hu, Q. Chen, J. Zhang and X. Luo, Research Progress of TiO2 Modification and Photodegradation of Organic Pollutants, *Inorganics*, 2024, **12**(7), 178, DOI: 10.3390/inorganics12070178.
109 U. Abdikarimova, M. Bissenova, N. Matsko, *et al.*, Visible Light-Driven Photocatalysis of Al-Doped SrTiO3: Experimental and DFT Study, *Molecules*, 2024, **29**(22), 5326, DOI: 10.3390/molecules29225326.
110 L. Jiang, X. Bai, X. Zhi, K. Davey and Y. Jiao, Advancing electrochemical N_2 reduction: interfacial electrolyte effects and *operando* computational approaches, *EES Catal.*, 2025, **3**(1), 57–79, DOI: 10.1039/D4EY00197D.
111 M. Zhang, Z. Guan, Y. Qiao, *et al.*, The impact of catalyst structure and morphology on the catalytic performance in NH3-SCR reaction: A review, *Fuel*, 2024, **361**, 130541, DOI: 10.1016/j.fuel.2023.130541.
112 S. Y. Park, Y. J. Jang and D. H. Youn, A Review of Transition Metal Nitride-Based Catalysts for Electrochemical Nitrogen Reduction to Ammonia, *Catalysts*, 2023, **13**(3), 639, DOI: 10.3390/catal13030639.
113 C. Choi, G. H. Gu, J. Noh, H. S. Park and Y. Jung, Understanding potential-dependent competition between electrocatalytic dinitrogen and proton reduction reactions, *Nat. Commun.*, 2021, **12**(1), 4353, DOI: 10.1038/s41467-021-24539-1.
114 H. L. Du, M. Chatti, R. Y. Hodgetts, *et al.*, Electroreduction of nitrogen with almost 100% current-to-ammonia efficiency, *Nature*, 2022, **609**(7928), 722–727, DOI: 10.1038/s41586-022-05108-y.
115 S. Z. Andersen, V. Čolić, S. Yang, *et al.*, A rigorous electrochemical ammonia synthesis protocol with quantitative isotope measurements, *Nature*, 2019, **570**(7762), 504–508, DOI: 10.1038/s41586-019-1260-x.
116 B. H. R. Suryanto, K. Matuszek, J. Choi, *et al.*, Nitrogen reduction to ammonia at high efficiency and rates based on a phosphonium proton shuttle, *Science*, 2021, **372**(6547), 1187–1191, DOI: 10.1126/science.abg2371.
117 Y. Shiraishi, S. Shiota, Y. Kofuji, *et al.*, Nitrogen Fixation with Water on Carbon-Nitride-Based Metal-Free Photocatalysts with 0.1% Solar-to-Ammonia Energy Conversion Efficiency, *ACS Appl. Energy Mater.*, 2018, **1**(8), 4169–4177, DOI: 10.1021/acsaem.8b00829.
118 T. Huang, S. Pan, L. Shi, A. Yu, X. Wang and Y. Fu, Hollow porous prismatic graphitic carbon nitride with nitrogen vacancies and oxygen doping: a high-performance visible light-driven catalyst for nitrogen fixation, *Nanoscale*, 2020, **12**(3), 1833–1841, DOI: 10.1039/C9NR08705B.
119 J. Xia, H. Guo, G. Yu, *et al.*, 2D Vanadium Carbide (MXene) for Electrochemical Synthesis of Ammonia Under Ambient Conditions, *Catal. Lett.*, 2021, **151**(12), 3516–3522, DOI: 10.1007/s10562-021-03589-6.
120 W. Li, W. Fang, C. Wu, *et al.*, Bimetal–MOF nanosheets as efficient bifunctional electrocatalysts for oxygen evolution and nitrogen reduction reaction, *J. Mater. Chem. A*, 2020, **8**(7), 3658–3666, DOI: 10.1039/C9TA13473E.
121 H. Maimaitizi, A. Abulizi, T. Zhang, K. Okitsu and J.-j. Zhu, Facile photo-ultrasonic assisted synthesis of flower-like Pt/N-MoS2 microsphere as an efficient sonophotocatalyst for nitrogen fixation, *Ultrason. Sonochem.*, 2020, **63**, 104956, DOI: 10.1016/j.ultsonch.2019.104956.
122 H. Zeng, S. Terazono and T. Tanuma, A novel catalyst for ammonia synthesis at ambient temperature and pressure: Visible light responsive photocatalyst using localized surface plasmon resonance, *Catal. Commun.*, 2015, **59**, 40–44, DOI: 10.1016/j.catcom.2014.09.034.
123 N. H. Deissler, J. B. V. Mygind, K. Li, *et al.*, *Operando* investigations of the solid electrolyte interphase in the lithium mediated nitrogen reduction reaction, *Energy Environ. Sci.*, 2024, **17**(10), 3482–3492, DOI: 10.1039/D3EE04235A.
124 S. Yang, Y. Sohn, J. Chu, W. Kim and B. Shin, Unveiling the Mechanisms of Improved Stability and Performance via Tetraalkyl-Type Ionic Liquids: Suppression of Organic Solid Electrolyte Interface Formation in Lithium-Mediated Nitrogen Reduction, *ACS Appl. Mater. Interfaces*, 2025, **17**(48), 65590–65599, DOI: 10.1021/acsami.5c17012.
125 N. H. Deissler, J. B. V. Mygind, V. A. Niemann, *et al.*, Unveiling the mechanism of lithium-mediated nitrogen reduction *via operando* X-ray scattering in a flow cell with hydrogen oxidation, *Energy Environ. Sci.*, 2026, **19**(3), 849–859, DOI: 10.1039/D5EE06529A.
126 K. S. Ranjith, A. T. E. Vilian, S. M. Ghoreishian, R. Umapathi, Y. S. Huh and Y. K. Han, An ultrasensitive electrochemical sensing platform for rapid detection of rutin with a hybridized 2D-1D MXene-FeWO4

nanocomposite, *Sens. Actuators, B*, 2021, **344**, 130202, DOI: 10.1016/j.snb.2021.130202.

127 K. S. Ranjith, S. M. Ghoreishian, R. Umapathi, *et al.*, WS2-intercalated Ti3C2Tx MXene/TiO2-stacked hybrid structure as an excellent sonophotocatalyst for tetracycline degradation and nitrogen fixation, *Ultrason. Sonochem.*, 2023, **100**, 106623, DOI: 10.1016/j.ultsonch.2023.106623.

128 H. Ali, M. Masar, A. C. Guler, M. Urbanek, M. Machovsky and I. Kuritka, Heterojunction-based photocatalytic nitrogen fixation: principles and current progress, *Nanoscale Adv.*, 2021, **3**(22), 6358–6372, DOI: 10.1039/D1NA00565K.

129 H. J. Himmel and L. Manceron, Ni(N2)4 revisited: an analysis of the Ni–N2 bonding properties of this benchmark system on the basis of UV/Vis, IR and Raman spectroscopy, *Dalton Trans.*, 2005, (15), 2615, DOI: 10.1039/b504134a.

130 Y. Ohki, K. Uchida, M. Tada, R. E. Cramer, T. Ogura and T. Ohta, N2 activation on a molybdenum–titanium–sulfur cluster, *Nat. Commun.*, 2018, **9**(1), 3200, DOI: 10.1038/s41467-018-05630-6.

131 R. C. Vincent, A. K. Cheetham and R. Seshadri, Structure and lithium insertion in oxides of molybdenum, *APL Mater.*, 2023, **11**(1), 011102, DOI: 10.1063/5.0133518.

132 European Commission (CORDIS), Multi-Stakeholder Platform for a Secure Supply of Refractory Metals in Europe (MSP-REFRAM), available online, https://Cordis.Europa.Eu/Project/Id/688993, accessed on 3 September 2025, http://prometia.eu/msp-reframe.

133 V. Molahalli, A. Sharma, K. Bijapur, *et al. Properties, Synthesis, and Characterization of Cu-Based Nanomaterials*, 2024, pp. 1–33, DOI: 10.1021/bk-2024-1466.ch001.

134 J. A. Schwalbe, M. J. Statt, C. Chosy, *et al.*, A Combined Theory-Experiment Analysis of the Surface Species in Lithium-Mediated NH $_3$ Electrosynthesis, *ChemElectroChem*, 2020, **7**(7), 1542–1549, DOI: 10.1002/celc.201902124.

135 N. Lazouski, Z. J. Schiffer, K. Williams and K. Manthiram, Understanding Continuous Lithium-Mediated Electrochemical Nitrogen Reduction, *Joule*, 2019, **3**(4), 1127–1139, DOI: 10.1016/j.joule.2019.02.003.

136 L. Gao, Y. Cao, C. Wang, *et al.*, Domino Effect: Gold Electrocatalyzing Lithium Reduction to Accelerate Nitrogen Fixation, *Angew. Chem., Int. Ed.*, 2021, **60**(10), 5257–5261, DOI: 10.1002/anie.202015496.

137 X. Fu, J. B. Pedersen, Y. Zhou, *et al.*, Continuous-flow electrosynthesis of ammonia by nitrogen reduction and hydrogen oxidation, *Science*, 2023, **379**(6633), 707–712, DOI: 10.1126/science.adf4403.

138 X. Fu, J. B. Pedersen, Y. Zhou, *et al.*, Continuous-flow electrosynthesis of ammonia by nitrogen reduction and hydrogen oxidation, *Science*, 2023, **379**(6633), 707–712, DOI: 10.1126/science.adf4403.

139 N. Lazouski, M. Chung, K. Williams, M. L. Gala and K. Manthiram, Non-aqueous gas diffusion electrodes for rapid ammonia synthesis from nitrogen and water-splitting-derived hydrogen, *Nat. Catal.*, 2020, **3**(5), 463–469, DOI: 10.1038/s41929-020-0455-8.

140 O. Westhead, R. Tort, M. Spry, *et al.*, The origin of overpotential in lithium-mediated nitrogen reduction, *Faraday Discuss.*, 2023, **243**, 321–338, DOI: 10.1039/D2FD00156J.

141 P. V. Cherepanov, M. Krebsz, R. Y. Hodgetts, A. N. Simonov and D. R. MacFarlane, Understanding the Factors Determining the Faradaic Efficiency and Rate of the Lithium Redox-Mediated N $_2$ Reduction to Ammonia, *J. Phys. Chem. C*, 2021, **125**(21), 11402–11410, DOI: 10.1021/acs.jpcc.1c02494.

142 M. Spry, O. Westhead, R. Tort, *et al.*, Water Increases the Faradaic Selectivity of Li-Mediated Nitrogen Reduction, *ACS Energy Lett.*, 2023, **8**(2), 1230–1235, DOI: 10.1021/acsenergylett.2c02792.

143 K. Li, S. Z. Andersen, M. J. Statt, *et al.*, Enhancement of lithium-mediated ammonia synthesis by addition of oxygen, *Science*, 2021, **374**(6575), 1593–1597, DOI: 10.1126/science.abl4300.

144 S. Z. Andersen, M. J. Statt, V. J. Bukas, *et al.*, Increasing stability, efficiency, and fundamental understanding of lithium-mediated electrochemical nitrogen reduction, *Energy Environ. Sci.*, 2020, **13**(11), 4291–4300, DOI: 10.1039/D0EE02246B.

145 H. L. Du, K. Matuszek, R. Y. Hodgetts, *et al.*, The chemistry of proton carriers in high-performance lithium-mediated ammonia electrosynthesis, *Energy Environ. Sci.*, 2023, **16**(3), 1082–1090, DOI: 10.1039/D2EE03901J.

146 S. Li, Y. Zhou, K. Li, *et al.*, Electrosynthesis of ammonia with high selectivity and high rates via engineering of the solid-electrolyte interphase, *Joule*, 2022, **6**(9), 2083–2101, DOI: 10.1016/j.joule.2022.07.009.

147 K. Li, S. G. Shapel, D. Hochfilzer, *et al.*, Increasing Current Density of Li-Mediated Ammonia Synthesis with High Surface Area Copper Electrodes, *ACS Energy Lett.*, 2022, **7**(1), 36–41, DOI: 10.1021/acsenergylett.1c02104.

148 B. H. R. Suryanto, K. Matuszek, J. Choi, *et al.*, Nitrogen reduction to ammonia at high efficiency and rates based on a phosphonium proton shuttle, *Science*, 2021, **372**(6547), 1187–1191, DOI: 10.1126/science.abg2371.

149 P. V. Cherepanov, M. Krebsz, R. Y. Hodgetts, A. N. Simonov and D. R. MacFarlane, Understanding the Factors Determining the Faradaic Efficiency and Rate of the Lithium Redox-Mediated N $_2$ Reduction to Ammonia, *J. Phys. Chem. C*, 2021, **125**(21), 11402–11410, DOI: 10.1021/acs.jpcc.1c02494.

150 J. Y. Kim, P. Lindgren, Y. J. Zhang, *et al.*, Sulfur promotes hydrogen evolution on molybdenum carbide catalysts, *Mater. Adv.*, 2021, **2**(14), 4867–4875, DOI: 10.1039/D1MA00281C.

151 L. Zhang, X. Ji, X. Ren, *et al.*, Efficient Electrochemical N $_2$ Reduction to NH $_3$ on MoN Nanosheets Array under Ambient Conditions, *ACS Sustain. Chem. Eng.*, 2018, **6**(8), 9550–9554, DOI: 10.1021/acssuschemeng.8b01438.

152 L. Tian, J. Zhao, X. Ren, X. Sun, Q. Wei and D. Wu, MoS $_2$ -Based Catalysts for N $_2$ Electroreduction to NH $_3$ – An

Overview of MoS_2 Optimization Strategies, *ChemistryOpen*, 2021, **10**(10), 1041–1054, DOI: 10.1002/open.202100196.

153 C. Guo, J. Ran, A. Vasileff and S. Z. Qiao, Rational design of electrocatalysts and photo(electro)catalysts for nitrogen reduction to ammonia (NH_3) under ambient conditions, *Energy Environ. Sci.*, 2018, **11**(1), 45–56, DOI: 10.1039/C7EE02220D.

154 C. Liu, Y. Bai, W. Li, F. Yang, G. Zhang and H. Pang, In Situ Growth of Three-Dimensional MXene/Metal–Organic Framework Composites for High-Performance Supercapacitors, *Angew. Chem., Int. Ed.*, 2022, **61**(11), e202116282, DOI: 10.1002/anie.202116282.

155 B. Tahir, A. Alraeesi and M. Tahir, Metal-organic framework (MOF) integrated Ti3C2 MXene composites for CO2 reduction and hydrogen production applications: a review on recent advances and future perspectives, *Front. Chem.*, 2024, **12**, e202116282, DOI: 10.3389/fchem.2024.1448700.

156 D. Yan, H. Li, C. Chen, Y. Zou and S. Wang, Defect Engineering Strategies for Nitrogen Reduction Reactions under Ambient Conditions, *Small Methods*, 2019, **3**(6), 1800331, DOI: 10.1002/smtd.201800331.

157 Y. Zhang, W. Qiu, Y. Ma, *et al.*, High-Performance Electrohydrogenation of N_2 to NH_3 Catalyzed by Multishelled Hollow Cr_2O_3 Microspheres under Ambient Conditions, *ACS Catal.*, 2018, **8**(9), 8540–8544, DOI: 10.1021/acscatal.8b02311.

158 X. Zhang, Q. Liu, X. Shi, *et al.*, TiO_2 nanoparticles–reduced graphene oxide hybrid: an efficient and durable electrocatalyst toward artificial N_2 fixation to NH_3 under ambient conditions, *J. Mater. Chem. A*, 2018, **6**(36), 17303–17306, DOI: 10.1039/C8TA05627G.

159 T. Takashima, H. Fukasawa, T. Mochida and H. Irie, Cu-Doped Fe_2O_3 Nanorods for Enhanced Electrocatalytic Nitrogen Fixation to Ammonia, *ACS Appl. Nano Mater.*, 2023, **6**(24), 23381–23389, DOI: 10.1021/acsanm.3c04712.

160 X. Li, T. Li, Y. Ma, *et al.*, Boosted Electrocatalytic N_2 Reduction to NH_3 by Defect-Rich MoS_2 Nanoflower, *Adv. Energy Mater.*, 2018, **8**(30), 1801357, DOI: 10.1002/aenm.201801357.

161 A. Biswas, S. Bhardwaj, T. Boruah and R. S. Dey, Electrochemical ammonia synthesis: fundamental practices and recent developments in transition metal boride, carbide and nitride-class of catalysts, *Mater. Adv.*, 2022, **3**(13), 5207–5233, DOI: 10.1039/D2MA00279E.

162 S. Li, K. Cheng, L. Ma, L. Zhang, F. Li and Q. Cheng, Interface Engineering-Modulated Nanoscale Bimetallic CoFe-MIL-88A In-Situ-Grown on 2D V_2CT_x MXene for Electrocatalytic Nitrogen Reduction, *Inorg. Chem.*, 2024, **63**(18), 8366–8375, DOI: 10.1021/acs.inorgchem.4c00760.

163 A. Biswas, S. Bhardwaj, T. Boruah and R. S. Dey, Electrochemical ammonia synthesis: fundamental practices and recent developments in transition metal boride, carbide and nitride-class of catalysts, *Mater. Adv.*, 2022, **3**(13), 5207–5233, DOI: 10.1039/D2MA00279E.

164 L. Zhao, X. Kuang, C. Chen, X. Sun, Z. Wang and Q. Wei, Boosting electrocatalytic nitrogen fixation *via* energy-efficient anodic oxidation of sodium gluconate, *Chem. Commun.*, 2019, **55**(68), 10170–10173, DOI: 10.1039/C9CC04378K.

165 X. He, F. Yin, X. Yi, *et al.*, Defective UiO-66-NH_2 Functionalized with Stable Superoxide Radicals toward Electrocatalytic Nitrogen Reduction with High Faradaic Efficiency, *ACS Appl. Mater. Interfaces*, 2022, **14**(23), 26571–26586, DOI: 10.1021/acsami.1c23643.

166 Y. Goto, K.-i. Yamanaka, M. Ohashi, Y. Maegawa and S. Inagaki, Light-harvesting photocatalysis for H2 evolution by methylacridone-bridged periodic mesoporous organosilica, *Appl. Catal., B*, 2021, **287**, 119965, DOI: 10.1016/j.apcatb.2021.119965.

167 J. Duan, D. Shao, X. He, Y. Lu and W. Wang, Model MoS2@ZIF-71 interface acts as a highly active and selective electrocatalyst for catalyzing ammonia synthesis, *Colloids Surf., A*, 2021, **619**, 126529, DOI: 10.1016/j.colsurfa.2021.126529.

168 G. Lu, H. Zheng, J. Lv, G. Wang and X. Huang, Review of recent research work on CeO2-based electrocatalysts in liquid-phase electrolytes, *J. Power Sources*, 2020, **480**, 229091, DOI: 10.1016/j.jpowsour.2020.229091.

169 W. Qiu, X. Y. Xie, J. Qiu, *et al.*, High-performance artificial nitrogen fixation at ambient conditions using a metal-free electrocatalyst, *Nat. Commun.*, 2018, **9**(1), 3485, DOI: 10.1038/s41467-018-05758-5.

170 J. Han, Z. Liu, Y. Ma, *et al.*, Ambient N2 fixation to NH3 at ambient conditions: Using Nb2O5 nanofiber as a high-performance electrocatalyst, *Nano Energy*, 2018, **52**, 264–270, DOI: 10.1016/j.nanoen.2018.07.045.

171 J. Feng, G. Lang, T. Li, *et al.*, Enhanced electrochemical detection performance of C-Cr2O3 towards glucose and hydrazine by assembling Ni-MPN coating, *Appl. Surf. Sci.*, 2022, **604**, 154548, DOI: 10.1016/j.apsusc.2022.154548.

172 S. Zhao, H. X. Liu, Y. Qiu, *et al.*, An oxygen vacancy-rich two-dimensional Au/TiO_2 hybrid for synergistically enhanced electrochemical N_2 activation and reduction, *J. Mater. Chem. A*, 2020, **8**(14), 6586–6596, DOI: 10.1039/D0TA00658K.

173 S. Mahmood, S. Iqbal, Z. Wang, *et al.*, Emerging electrocatalysts for green ammonia production: Recent progress and future outlook, *Arabian J. Chem.*, 2024, **17**(10), 105950, DOI: 10.1016/j.arabjc.2024.105950.

174 Z. Wang, Y. Li, H. Yu, *et al.*, Ambient Electrochemical Synthesis of Ammonia from Nitrogen and Water Catalyzed by Flower-Like Gold Microstructures, *ChemSusChem*, 2018, **11**(19), 3480–3485, DOI: 10.1002/cssc.201801444.

175 Z. Fang, D. Fernandez, N. Wang, Z. Bai and G. Yu, Mo2C@3D ultrathin macroporous carbon realizing efficient and stable nitrogen fixation, *Sci. China:Chem.*, 2020, **63**(11), 1570–1577, DOI: 10.1007/s11426-020-9740-8.

176 D. Liu, G. Zhang, Q. Ji, Y. Zhang and J. Li, Synergistic Electrocatalytic Nitrogen Reduction Enabled by Confinement of Nanosized Au Particles onto a Two-Dimensional Ti_3C_2 Substrate, *ACS Appl. Mater. Interfaces*, 2019, **11**(29), 25758–25765, DOI: 10.1021/acsami.9b02511.

177 X. Xu, B. Sun, Z. Liang, H. Cui and J. Tian, High-Performance Electrocatalytic Conversion of N $_2$ to NH $_3$ Using 1T-MoS $_2$ Anchored on Ti $_3$ C $_2$ MXene under Ambient Conditions, *ACS Appl. Mater. Interfaces*, 2020, **12**(23), 26060–26067, DOI: 10.1021/acsami.0c06744.

178 G. Yu, H. Guo, S. Liu, *et al.*, Cr $_3$ C $_2$ Nanoparticle-Embedded Carbon Nanofiber for Artificial Synthesis of NH $_3$ through N $_2$ Fixation under Ambient Conditions, *ACS Appl. Mater. Interfaces*, 2019, **11**(39), 35764–35769, DOI: 10.1021/acsami.9b12675.

179 Y. Guo, T. Wang, Q. Yang, *et al.*, Highly Efficient Electrochemical Reduction of Nitrogen to Ammonia on Surface Termination Modified Ti $_3$ C $_2$ T $_x$ MXene Nanosheets, *ACS Nano*, 2020, **14**(7), 9089–9097, DOI: 10.1021/acsnano.0c04284.

180 T. Li, X. Yan, L. Huang, *et al.*, Fluorine-free Ti $_3$ C $_2$ T $_x$ (T = O, OH) nanosheets (~50–100 nm) for nitrogen fixation under ambient conditions, *J. Mater. Chem. A*, 2019, **7**(24), 14462–14465, DOI: 10.1039/C9TA03254A.

181 X. Qian, Y. Wei, M. Sun, *et al.*, Heterostructuring 2D TiO2 nanosheets in situ grown on Ti3C2T MXene to improve the electrocatalytic nitrogen reduction, *Chin. J. Catal.*, 2022, **43**(7), 1937–1944, DOI: 10.1016/S1872-2067(21)64020-2.

182 Z. Jin, C. Liu, Z. Liu, *et al.*, Rational Design of Hydroxyl-Rich Ti_3 C_2 T_x MXene Quantum Dots for High-Performance Electrochemical N_2 Reduction, *Adv. Energy Mater.*, 2020, **10**(22), 2000797, DOI: 10.1002/aenm.202000797.

183 H. Zhu, C. Wang, Y. He, *et al.*, Oxygen vacancies engineering in electrocatalysts nitrogen reduction reaction, *Front. Chem.*, 2022, **10**, 1039738, DOI: 10.3389/fchem.2022.1039738.

184 M. Cong, X. Chen, K. Xia, *et al.*, Selective nitrogen reduction to ammonia on iron porphyrin-based single-site metal–organic frameworks, *J. Mater. Chem. A*, 2021, **9**(8), 4673–4678, DOI: 10.1039/D0TA08741F.

185 H. He, H. K. Li, Q. Q. Zhu, C. P. Li, Z. Zhang and M. Du, Hydrophobicity modulation on a ferriporphyrin-based metal–organic framework for enhanced ambient electrocatalytic nitrogen fixation, *Appl. Catal., B*, 2022, **316**, 121673, DOI: 10.1016/j.apcatb.2022.121673.

186 X. Ren, G. Cui, L. Chen, *et al.*, Electrochemical N $_2$ fixation to NH $_3$ under ambient conditions: Mo $_2$ N nanorod as a highly efficient and selective catalyst, *Chem. Commun.*, 2018, **54**(61), 8474–8477, DOI: 10.1039/C8CC03627F.

187 S. Mahmood, S. Iqbal, Z. Wang, *et al.*, Emerging electrocatalysts for green ammonia production: Recent progress and future outlook, *Arabian J. Chem.*, 2024, **17**(10), 105950, DOI: 10.1016/j.arabjc.2024.105950.

188 A. Biswas, S. Bhardwaj, T. Boruah and R. S. Dey, Electrochemical ammonia synthesis: fundamental practices and recent developments in transition metal boride, carbide and nitride-class of catalysts, *Mater. Adv.*, 2022, **3**(13), 5207–5233, DOI: 10.1039/D2MA00279E.

189 W. Xiong, X. Cheng, T. Wang, *et al.*, Co3(hexahydroxytriphenylene)2: A conductive metal—organic framework for ambient electrocatalytic N2 reduction to NH3, *Nano Res.*, 2020, **13**(4), 1008–1012, DOI: 10.1007/s12274-020-2733-9.

190 R. Nakatani, S. Das and Y. Negishi, Metal–organic frameworks as promising electrocatalysts for the nitrogen reduction reaction: mapping the research landscape and identifying future trends, *J. Mater. Chem. A*, 2024, **12**(39), 26350–26366, DOI: 10.1039/D4TA04817B.

191 K. Chu, W. Gu, Q. Li, Y. Liu, Y. Tian and W. Liu, Amorphization activated FeB2 porous nanosheets enable efficient electrocatalytic N2 fixation, *J. Energy Chem.*, 2021, **53**, 82–89, DOI: 10.1016/j.jechem.2020.05.009.

192 C. F. Du, L. Yang, K. Tang, *et al.*, Ni nanoparticles/V $_4$ C $_3$ T $_x$ MXene heterostructures for electrocatalytic nitrogen fixation, *Mater. Chem. Front.*, 2021, **5**(5), 2338–2346, DOI: 10.1039/D0QM00898B.

193 S. Tan, B. M. Tackett, Q. He, J. H. Lee, J. G. Chen and S. S. Wong, Synthesis and electrocatalytic applications of flower-like motifs and associated composites of nitrogen-enriched tungsten nitride (W2N3), *Nano Res.*, 2020, **13**(5), 1434–1443, DOI: 10.1007/s12274-020-2687-y.

194 H. Wei, Q. Jiang, C. Ampelli, *et al.*, Enhancing N $_2$ Fixation Activity by Converting Ti $_3$ C $_2$ MXenes Nanosheets to Nanoribbons, *ChemSusChem*, 2020, **13**(21), 5614–5619, DOI: 10.1002/cssc.202001719.

195 D. Feng, L. Zhou, T. J. White, A. K. Cheetham, T. Ma and F. Wei, Nanoengineering Metal–Organic Frameworks and Derivatives for Electrosynthesis of Ammonia, *Nano-Micro Lett.*, 2023, **15**(1), 203, DOI: 10.1007/s40820-023-01169-4.

196 L. Zhao, J. Zhou, L. Zhang, *et al.*, Anchoring Au(111) on a Bismuth Sulfide Nanorod: Boosting the Artificial Electrocatalytic Nitrogen Reduction Reaction under Ambient Conditions, *ACS Appl. Mater. Interfaces*, 2020, **12**(50), 55838–55843, DOI: 10.1021/acsami.0c15987.

197 Z. Wang, K. Zheng, S. Liu, *et al.*, Electrocatalytic Nitrogen Reduction to Ammonia by Fe $_2$ O $_3$ Nanorod Array on Carbon Cloth, *ACS Sustain. Chem. Eng.*, 2019, **7**(13), 11754–11759, DOI: 10.1021/acssuschemeng.9b01991.

198 R. Cheng, T. Hu, J. Yang, *et al.*, Nitrogen and sulfur co-doped Ti $_3$ C $_2$ T $_x$ MXenes for high-rate lithium-ion batteries, *Phys. Chem. Chem. Phys.*, 2023, **25**(15), 10635–10646, DOI: 10.1039/D2CP05962B.

199 J. T. Ren, C. Y. Wan, T. Y. Pei, X. W. Lv and Z. Y. Yuan, Promotion of electrocatalytic nitrogen reduction reaction on N-doped porous carbon with secondary heteroatoms, *Appl. Catal., B*, 2020, **266**, 118633, DOI: 10.1016/j.apcatb.2020.118633.

200 X. Han, S. Yang and M. Schröder, Metal–Organic Framework Materials for Production and Distribution of Ammonia, *J. Am. Chem. Soc.*, 2023, **145**(4), 1998–2012, DOI: 10.1021/jacs.2c06216.

201 A. Maibam, I. B. Orhan, S. Krishnamurty, S. P. Russo and R. Babarao, Surface Electronic Properties-Driven Electrocatalytic Nitrogen Reduction on Metal-Conjugated Porphyrin 2D-MOFs, *ACS Appl. Mater. Interfaces*, 2024, **16**(7), 8707–8716, DOI: 10.1021/acsami.3c16406.

202 Y. Yao, K. Wei, S. Zhao, *et al.*, Highly Efficient Bifunctional NiFe-MOF Array Electrode for Nitrate Reduction to

Ammonia and Oxygen Evolution Reactions, *ACS Sustain. Chem. Eng.*, 2025, **13**(3), 1245–1252, DOI: 10.1021/acssuschemeng.4c07408.

203 Y. Lv, Y. Wang, M. Yang, *et al.*, Nitrogen reduction through confined electro-catalysis with carbon nanotube inserted metal–organic frameworks, *J. Mater. Chem. A*, 2021, **9**(3), 1480–1486, DOI: 10.1039/D0TA11797H.

204 S. Chen, F. Yin, X. He and J. Tan, The Preparation of UiO-66-NH_2/CNT Electrocatalyst and its High Catalytic Performance for Electrochemical Synthetic Ammonia in Neutral Electrolyte, *ChemistrySelect*, 2023, **8**(9), 202204988, DOI: 10.1002/slct.202204988.

205 X. Han, S. Yang and M. Schröder, Metal–Organic Framework Materials for Production and Distribution of Ammonia, *J. Am. Chem. Soc.*, 2023, **145**(4), 1998–2012, DOI: 10.1021/jacs.2c06216.

206 Y. Lv, Y. Wang, M. Yang, *et al.*, Nitrogen reduction through confined electro-catalysis with carbon nanotube inserted metal–organic frameworks, *J. Mater. Chem. A*, 2021, **9**(3), 1480–1486, DOI: 10.1039/D0TA11797H.

207 R. Zhang, X. Ren, X. Shi, *et al.*, Enabling Effective Electrocatalytic N_2 Conversion to NH_3 by the TiO_2 Nanosheets Array under Ambient Conditions, *ACS Appl. Mater. Interfaces*, 2018, **10**(34), 28251–28255, DOI: 10.1021/acsami.8b06647.

208 X. Zhao, X. Zhang, Z. Xue, W. Chen, Z. Zhou and T. Mu, Fe nanodot-decorated MoS_2 nanosheets on carbon cloth: an efficient and flexible electrode for ambient ammonia synthesis, *J. Mater. Chem. A*, 2019, **7**(48), 27417–27422, DOI: 10.1039/C9TA09264A.

209 H. Xie, X. Zheng, Q. Feng, *et al.*, Single-Step Synthesis of Fe—Fe_3O_4 Catalyst for Highly Efficient and Selective Electrochemical Nitrogen Reduction, *ChemSusChem*, 2022, **15**(21), 202200919, DOI: 10.1002/cssc.202200919.

210 A. Biswas, S. Bhardwaj, T. Boruah and R. S. Dey, Electrochemical ammonia synthesis: fundamental practices and recent developments in transition metal boride, carbide and nitride-class of catalysts, *Mater. Adv.*, 2022, **3**(13), 5207–5233, DOI: 10.1039/D2MA00279E.

211 S. Kang, J. Wang, S. Zhang, *et al.*, Plasma-etching enhanced titanium oxynitride active phase with high oxygen content for ambient electrosynthesis of ammonia, *Electrochem. Commun.*, 2019, **100**, 90–95, DOI: 10.1016/j.elecom.2019.01.028.

212 X. Liang, X. Ren, Q. Yang, *et al.*, A two-dimensional MXene-supported metal–organic framework for highly selective ambient electrocatalytic nitrogen reduction, *Nanoscale*, 2021, **13**(5), 2843–2848, DOI: 10.1039/D0NR08744K.

213 R. Nakatani, S. Das and Y. Negishi, Metal–organic frameworks as promising electrocatalysts for the nitrogen reduction reaction: mapping the research landscape and identifying future trends, *J. Mater. Chem. A*, 2024, **12**(39), 26350–26366, DOI: 10.1039/D4TA04817B.

214 Y. Cao, P. Li, T. Wu, M. Liu and Y. Zhang, Electrocatalysis of N_2 to NH_3 by HKUST-1 with High NH_3 Yield, *Chem.–Asian J.*, 2020, **15**(8), 1272–1276, DOI: 10.1002/asia.201901714.

215 J. Han, X. Ji, X. Ren, *et al.*, MoO_3 nanosheets for efficient electrocatalytic N_2 fixation to NH_3, *J. Mater. Chem. A*, 2018, **6**(27), 12974–12977, DOI: 10.1039/C8TA03974G.

216 D. Yang, T. Chen and Z. Wang, Electrochemical reduction of aqueous nitrogen (N_2) at a low overpotential on (110)-oriented Mo nanofilm, *J. Mater. Chem. A*, 2017, **5**(36), 18967–18971, DOI: 10.1039/C7TA06139K.

217 X. Cai, F. Yang, L. An, *et al.*, Evaluation of Electrocatalytic Activity of Noble Metal Catalysts Toward Nitrogen Reduction Reaction in Aqueous Solutions under Ambient Conditions, *ChemSusChem*, 2022, **15**(1), 202102234, DOI: 10.1002/cssc.202102234.

218 G. F. Chen, X. Cao, S. Wu, *et al.*, Ammonia Electrosynthesis with High Selectivity under Ambient Conditions via a Li^+ Incorporation Strategy, *J. Am. Chem. Soc.*, 2017, **139**(29), 9771–9774, DOI: 10.1021/jacs.7b04393.

219 H. Huang, L. Xia, X. Shi, A. M. Asiri and X. Sun, Ag nanosheets for efficient electrocatalytic N_2 fixation to NH_3 under ambient conditions, *Chem. Commun.*, 2018, **54**(81), 11427–11430, DOI: 10.1039/C8CC06365F.

220 M. A. Younis, S. Manzoor, A. Ali, *et al.*, Nitrogen-vacancy-rich molybdenum nitride nanosheets as highly efficient electrocatalysts for nitrogen reduction reaction, *Dalton Trans.*, 2024, **53**(4), 1809–1816, DOI: 10.1039/D3DT02761A.

221 L. Zhang, X. Ji, X. Ren, *et al.*, Efficient Electrochemical N_2 Reduction to NH_3 on MoN Nanosheets Array under Ambient Conditions, *ACS Sustain. Chem. Eng.*, 2018, **6**(8), 9550–9554, DOI: 10.1021/acssuschemeng.8b01438.

222 A. Rasyotra, A. Thakur, B. Gaykwad, R. Mandalia, R. Ranganathan and K. Jasuja, Vacancy Rich TiB_2 Nanosheets Promote Electrochemical Ammonia Synthesis, *ACS Appl. Mater. Interfaces*, 2024, **16**(19), 24473–24482, DOI: 10.1021/acsami.4c00253.

223 X. Zhang, R. M. Kong, H. Du, L. Xia and F. Qu, Highly efficient electrochemical ammonia synthesis *via* nitrogen reduction reactions on a VN nanowire array under ambient conditions, *Chem. Commun.*, 2018, **54**(42), 5323–5325, DOI: 10.1039/C8CC00459E.

224 X. Yang, J. Wan, H. Zhang and Y. Wang, *In situ* modification of the d-band in the core–shell structure for efficient hydrogen storage *via* electrocatalytic N_2 fixation, *Chem. Sci.*, 2022, **13**(37), 11030–11037, DOI: 10.1039/D2SC03975C.

225 W. Qiu, X. Y. Xie, J. Qiu, *et al.*, High-performance artificial nitrogen fixation at ambient conditions using a metal-free electrocatalyst, *Nat. Commun.*, 2018, **9**(1), 3485, DOI: 10.1038/s41467-018-05758-5.

226 M. Nazemi, S. R. Panikkanvalappil and M. A. El-Sayed, Enhancing the rate of electrochemical nitrogen reduction reaction for ammonia synthesis under ambient conditions using hollow gold nanocages, *Nano Energy*, 2018, **49**, 316–323, DOI: 10.1016/j.nanoen.2018.04.039.

227 X. Yi, X. He, F. Yin, T. Yang, B. Chen and G. Li, NH2–MIL-88B–Fe for electrocatalytic N2 fixation to NH3 with high Faradaic efficiency under ambient conditions in neutral electrolyte, *J. Mater. Sci.*, 2020, **55**(26), 12041–12052, DOI: 10.1007/s10853-020-04777-2.

228 W. Li, K. Li, Y. Ye, *et al.*, Efficient electrocatalytic nitrogen reduction to ammonia with aqueous silver nanodots, *Commun. Chem.*, 2021, **4**(1), 10, DOI: 10.1038/s42004-021-00449-7.

229 W. Cai, Y. F. Jiang, J. Zhang, *et al.*, Ruthenium/titanium oxide interface promoted electrochemical nitrogen reduction reaction, *Chem Catal.*, 2022, **2**(7), 1764–1774, DOI: 10.1016/j.checat.2022.05.009.

230 X. Yang, J. Nash, J. Anibal, *et al.*, Mechanistic Insights into Electrochemical Nitrogen Reduction Reaction on Vanadium Nitride Nanoparticles, *J. Am. Chem. Soc.*, 2018, **140**(41), 13387–13391, DOI: 10.1021/jacs.8b08379.

231 R. Zhang, Y. Xue, M. Ma, Y. Han and J. Tian, Cu–Bi Bimetallic Sulfides Loaded on Two-Dimensional $Ti_3C_2T_x$ MXene for Efficient Electrocatalytic Nitrogen Reduction under Ambient Conditions, *Nano Lett.*, 2024, **24**(33), 10297–10304, DOI: 10.1021/acs.nanolett.4c02869.

232 H. K. Lee, C. S. L. Koh, Y. H. Lee, *et al.*, Favoring the unfavored: Selective electrochemical nitrogen fixation using a reticular chemistry approach, *Sci. Adv.*, 2018, **4**(3), aar3208, DOI: 10.1126/sciadv.aar3208.

233 S. Y. Park, Y. J. Jang and D. H. Youn, A Review of Transition Metal Nitride-Based Catalysts for Electrochemical Nitrogen Reduction to Ammonia, *Catalysts*, 2023, **13**(3), 639, DOI: 10.3390/catal13030639.

234 Y. Yang, S. Wang, H. Wen, *et al.*, Nanoporous Gold Embedded ZIF Composite for Enhanced Electrochemical Nitrogen Fixation, *Angew. Chem., Int. Ed.*, 2019, **58**(43), 15362–15366, DOI: 10.1002/anie.201909770.

235 E. Y. Jeong, C. Y. Yoo, C. H. Jung, *et al.*, Electrochemical Ammonia Synthesis Mediated by Titanocene Dichloride in Aqueous Electrolytes under Ambient Conditions, *ACS Sustain. Chem. Eng.*, 2017, **5**(11), 9662–9666, DOI: 10.1021/acssuschemeng.7b02908.

236 X. Rong, F. Qiu, J. Yan, H. Zhao, X. Zhu and D. Yang, Coupling with a narrow-band-gap semiconductor for enhancement of visible-light photocatalytic activity: preparation of Bi_2S_3/g-C_3N_4 and application for degradation of RhB, *RSC Adv.*, 2015, **5**(32), 24944–24952, DOI: 10.1039/C4RA15715J.

237 L. Wang, J. Shang, W. Hao, *et al.*, A dye-sensitized visible light photocatalyst-Bi24O31Cl10, *Sci. Rep.*, 2014, **4**(1), 7384, DOI: 10.1038/srep07384.

238 A. H. Slavney, L. Leppert, D. Bartesaghi, *et al.*, Defect-Induced Band-Edge Reconstruction of a Bismuth-Halide Double Perovskite for Visible-Light Absorption, *J. Am. Chem. Soc.*, 2017, **139**(14), 5015–5018, DOI: 10.1021/jacs.7b01629.

239 D. A. Tolan, A. K. El-Sawaf, I. G. Alhindawy, *et al.*, Effect of bismuth doping on the crystal structure and photocatalytic activity of titanium oxide, *RSC Adv.*, 2023, **13**(36), 25081–25092, DOI: 10.1039/D3RA04034H.

240 Y. Liu, Z. Hu and J. C. Yu, Fe Enhanced Visible-Light-Driven Nitrogen Fixation on BiOBr Nanosheets, *Chem. Mater.*, 2020, **32**(4), 1488–1494, DOI: 10.1021/acs.chemmater.9b04448.

241 N. Zhang, L. Li, Q. Shao, T. Zhu, X. Huang and X. Xiao, Fe-Doped BiOCl Nanosheets with Light-Switchable Oxygen Vacancies for Photocatalytic Nitrogen Fixation, *ACS Appl. Energy Mater.*, 2019, **2**(12), 8394–8398, DOI: 10.1021/acsaem.9b01961.

242 S. Wang, X. Hai, X. Ding, *et al.*, Light-Switchable Oxygen Vacancies in Ultrafine Bi_5O_7Br Nanotubes for Boosting Solar-Driven Nitrogen Fixation in Pure Water, *Adv. Mater.*, 2017, **29**(31), 201701774, DOI: 10.1002/adma.201701774.

243 Z. Xing, W. Kong, T. Wu, *et al.*, Hollow Bi_2MoO_6 Sphere Effectively Catalyzes the Ambient Electroreduction of N_2 to NH_3, *ACS Sustain. Chem. Eng.*, 2019, **7**(15), 12692–12696, DOI: 10.1021/acssuschemeng.9b03141.

244 J. Cui, J. Hou, H. Pan and P. Kang, Self-supporting CuM LDH (M = Ni, Fe, Co) carbon cloth electrodes for selective electrochemical ammonia oxidation to nitrogen, *J. Electroanal. Chem.*, 2023, **940**, 117502, DOI: 10.1016/j.jelechem.2023.117502.

245 Q. Zeng, L. Ruan, X. Che, *et al.*, Synthesis of MoO_{3-x} nanosheets and its application in ascorbic acid detection of fruit and vegetables, *J. Food Sci.*, 2023, **88**(2), 837–847, DOI: 10.1111/1750-3841.16447.

246 Y. Fang, Z. Liu, J. Han, *et al.*, High-Performance Electrocatalytic Conversion of N_2 to NH_3 Using Oxygen-Vacancy-Rich TiO_2 In Situ Grown on $Ti_3C_2T_x$ MXene, *Adv. Energy Mater.*, 2019, **9**(16), 201803406, DOI: 10.1002/aenm.201803406.

247 Z. Yang, J. Wang, J. Wang, *et al.*, 2D WO_{3-x} Nanosheet with Rich Oxygen Vacancies for Efficient Visible-Light-Driven Photocatalytic Nitrogen Fixation, *Langmuir*, 2022, **38**(3), 1178–1187, DOI: 10.1021/acs.langmuir.1c02862.

248 Y. Zhang, T. Mori, J. Ye and M. Antonietti, Phosphorus-Doped Carbon Nitride Solid: Enhanced Electrical Conductivity and Photocurrent Generation, *J. Am. Chem. Soc.*, 2010, **132**(18), 6294–6295, DOI: 10.1021/ja101749y.

249 D. Ješić, B. Pomeroy, K. M. Kamal, Ž. Kovačič, M. Huš and B. Likozar, Photo- and Photoelectrocatalysis in Nitrogen Reduction Reactions to Ammonia: Interfaces, Mechanisms, and Modeling Simulations, *Adv. Energy Sustainability Res.*, 2024, **5**(9), 202400083, DOI: 10.1002/aesr.202400083.

250 J. Xiong, J. Li, H. Huang, *et al.*, Electronic state tuning over Mo-doped W18O49 ultrathin nanowires with enhanced molecular oxygen activation for desulfurization, *Sep. Purif. Technol.*, 2022, **294**, 121167, DOI: 10.1016/j.seppur.2022.121167.

251 S. Zhao, H. X. Liu, Y. Qiu, *et al.*, An oxygen vacancy-rich two-dimensional Au/TiO_2 hybrid for synergistically enhanced electrochemical N_2 activation and reduction, *J. Mater. Chem. A*, 2020, **8**(14), 6586–6596, DOI: 10.1039/D0TA00658K.

252 Y. Zhao, Y. Zhao, G. I. N. Waterhouse, *et al.*, Layered-Double-Hydroxide Nanosheets as Efficient Visible-Light-Driven Photocatalysts for Dinitrogen Fixation, *Adv. Mater.*, 2017, **29**(42), 201703828, DOI: 10.1002/adma.201703828.

253 X. Qian, X. Meng, J. Sun, *et al.*, Salt-Assisted Synthesis of 3D Porous g-C_3N_4 as a Bifunctional Photo- and

Electrocatalyst, *ACS Appl. Mater. Interfaces*, 2019, **11**(30), 27226–27232, DOI: 10.1021/acsami.9b08651.

254 C. Yang, Y. Zhang, F. Yue, *et al.*, Co doping regulating electronic structure of Bi2MoO6 to construct dual active sites for photocatalytic nitrogen fixation, *Appl. Catal., B*, 2023, **338**, 123057, DOI: 10.1016/j.apcatb.2023.123057.

255 L. Chen, Y. Chen, X. Tu, *et al.*, Fe/Zr-MOFs constructed by a sunlight-responsive ligand for efficient photocatalytic nitrogen fixation under ambient condition, *J. Colloid Interface Sci.*, 2023, **633**, 703–711, DOI: 10.1016/j.jcis.2022.11.129.

256 T. He, Z. Zhao, R. Liu, *et al.*, Porphyrin-Based Covalent Organic Frameworks Anchoring Au Single Atoms for Photocatalytic Nitrogen Fixation, *J. Am. Chem. Soc.*, 2023, **145**(11), 6057–6066, DOI: 10.1021/jacs.2c10233.

257 Z. Ding, X. Li and C. Kang, Single Ru atoms confined into MOF/C3N4 for dual improved photocatalytic carbon dioxide reduction and nitrogen fixation, *SSRN Electron. J.*, 2023, DOI: 10.2139/ssrn.4443548.

258 Y. Shiraishi, T. Kishimoto, S. Tanaka and T. Hirai, Photocatalytic Dinitrogen Fixation with Water on High-Phosphorus-Doped Carbon Nitride with Surface Nitrogen Vacancies, *Langmuir*, 2022, **38**(23), 7137–7145, DOI: 10.1021/acs.langmuir.2c00336.

259 D. Sun, N. Li, K. Wang, *et al.*, In-MOF derived In2S3-X@ZnS heterojunction with rich sulfur vacancies for enhanced performance in photocatalytic nitrogen fixation, *Appl. Surf. Sci.*, 2024, **656**, 159658, DOI: 10.1016/j.apsusc.2024.159658.

260 A. Shehzad, L. Geng and Z. Luo, Electrocatalytic Nitrogen Reduction to Ammonia Using TiO_2-Supported $Cu_4Cl_4(PPh_3)_4$ and $Ag_4Cl_4(PPh_3)_4$ Nanoclusters, *J. Phys. Chem. Lett.*, 2025, **16**(22), 5538–5545, DOI: 10.1021/acs.jpclett.5c00866.

261 X. H. Li, W. L. Chen, H. Q. Tan, *et al.*, Reduced State of the Graphene Oxide@Polyoxometalate Nanocatalyst Achieving High-Efficiency Nitrogen Fixation under Light Driving Conditions, *ACS Appl. Mater. Interfaces*, 2019, **11**(41), 37927–37938, DOI: 10.1021/acsami.9b12328.

262 C. He, X. Li, D. Qiu, Y. Chen, Y. Lu and X. Cui, Nonlinear optical polarization and heterostructure synergistically boosted the built-in electric field of CeF3/LiNbO3 for a higher photocatalytic nitrogen reduction activity, *Appl. Surf. Sci.*, 2021, **556**, 149753, DOI: 10.1016/j.apsusc.2021.149753.

263 Z. Zhao, R. Tan, Y. Kong, *et al.*, Defect Pyrochlore-Type Mott–Schottky Photocatalysts for Enhanced Ammonia Synthesis at Low Pressure, *Angew. Chem., Int. Ed.*, 2023, **62**(26), e202303629, DOI: 10.1002/anie.202303629.

264 M. A. Khan, S. Mutahir, I. Shaheen, Y. Qunhui, M. Bououdina and M. Humayun, Recent advances over the doped g-C3N4 in photocatalysis: A review, *Coord. Chem. Rev.*, 2025, **522**, 216227, DOI: 10.1016/j.ccr.2024.216227.

265 S. Chen, D. Fang, Z. Zhou, Z. Dai and J. Shi, Theoretical study of the nitrogen reduction reaction catalyzed by a B-doped MoO_2 six-membered ring, *Phys. Chem. Chem. Phys.*, 2024, **26**(17), 13405–13411, DOI: 10.1039/D3CP05342C.

266 P. Martins, S. Kappert, H. Nga Le, *et al.*, Enhanced Photocatalytic Activity of Au/TiO2 Nanoparticles against Ciprofloxacin, *Catalysts*, 2020, **10**(2), 234, DOI: 10.3390/catal10020234.

267 Y. Guo, J. Yang, D. Wu, *et al.*, Au nanoparticle-embedded, nitrogen-deficient hollow mesoporous carbon nitride spheres for nitrogen photofixation, *J. Mater. Chem. A*, 2020, **8**(32), 16218–16231, DOI: 10.1039/D0TA03793A.

268 J. Yuan, X. Yi, Y. Tang, M. Liu and C. Liu, Efficient Photocatalytic Nitrogen Fixation: Enhanced Polarization, Activation, and Cleavage by Asymmetrical Electron Donation to N≡N Bond, *Adv. Funct. Mater.*, 2020, **30**(4), 201906983, DOI: 10.1002/adfm.201906983.

269 Y. Liu, Z. Hu and J. C. Yu, Fe Enhanced Visible-Light-Driven Nitrogen Fixation on BiOBr Nanosheets, *Chem. Mater.*, 2020, **32**(4), 1488–1494, DOI: 10.1021/acs.chemmater.9b04448.

270 P. Li, Z. Zhou, Q. Wang, *et al.*, Visible-Light-Driven Nitrogen Fixation Catalyzed by Bi_5O_7Br Nanostructures: Enhanced Performance by Oxygen Vacancies, *J. Am. Chem. Soc.*, 2020, **142**(28), 12430–12439, DOI: 10.1021/jacs.0c05097.

271 Y. Zhang, S. Gu, X. Zhou, *et al.*, Boosted photocatalytic nitrogen fixation by bismuth and oxygen vacancies in Bi_2MoO_6/BiOBr composite structures, *Catal. Sci. Technol.*, 2021, **11**(14), 4783–4792, DOI: 10.1039/D1CY00539A.

272 M. Lan, N. Zheng, X. Dong, C. Hua, H. Ma and X. Zhang, Bismuth-rich bismuth oxyiodide microspheres with abundant oxygen vacancies as an efficient photocatalyst for nitrogen fixation, *Dalton Trans.*, 2020, **49**(26), 9123–9129, DOI: 10.1039/D0DT01332C.

273 S. Zhang, Y. Zhao, R. Shi, *et al.*, Efficient Photocatalytic Nitrogen Fixation over $Cu^{\delta+}$-Modified Defective ZnAl-Layered Double Hydroxide Nanosheets, *Adv. Energy Mater.*, 2020, **10**(8), 201901973, DOI: 10.1002/aenm.201901973.

274 S. Sultana, S. Mansingh and K. M. Parida, Phosphide protected FeS_2 anchored oxygen defect oriented CeO_2 NS based ternary hybrid for electrocatalytic and photocatalytic N_2 reduction to NH_3, *J. Mater. Chem. A*, 2019, **7**(15), 9145–9153, DOI: 10.1039/C8TA11437D.

275 H. Xu, Y. Wang, X. Dong, N. Zheng, H. Ma and X. Zhang, Fabrication of In2O3/In2S3 microsphere heterostructures for efficient and stable photocatalytic nitrogen fixation, *Appl. Catal., B*, 2019, **257**, 117932, DOI: 10.1016/j.apcatb.2019.117932.

276 M. Liu, Y. Wang, X. Kong, *et al.*, Efficient Nitrogen Fixation Catalyzed by Gallium Nitride Nanowire Using Nitrogen and Water, *iScience*, 2019, **17**, 208–216, DOI: 10.1016/j.isci.2019.06.032.

277 S. Sun, X. Li, W. Wang, L. Zhang and X. Sun, Photocatalytic robust solar energy reduction of dinitrogen to ammonia on ultrathin MoS2, *Appl. Catal., B*, 2017, **200**, 323–329, DOI: 10.1016/j.apcatb.2016.07.025.

278 K. Li, C. Sun, Z. Chen, H. Qu, H. Xie and Q. Zhong, Fe-carbon dots enhance the photocatalytic nitrogen fixation

activity of TiO2@CN heterojunction, *Chem. Eng. J.*, 2022, **429**, 132440, DOI: 10.1016/j.cej.2021.132440.

279 S. Shang, W. Xiong, C. Yang, *et al.*, Atomically Dispersed Iron Metal Site in a Porphyrin-Based Metal–Organic Framework for Photocatalytic Nitrogen Fixation, *ACS Nano*, 2021, **15**(6), 9670–9678, DOI: 10.1021/acsnano.0c10947.

280 H. Kim, S. Hong, H. Kim, Y. Jun, S. Y. Kim and S. H. Ahn, Recent progress in Pt-based electrocatalysts for ammonia oxidation reaction, *Appl. Mater. Today*, 2022, **29**, 101640, DOI: 10.1016/j.apmt.2022.101640.

281 N. Zhang, L. Li, Q. Shao, T. Zhu, X. Huang and X. Xiao, Fe-Doped BiOCl Nanosheets with Light-Switchable Oxygen Vacancies for Photocatalytic Nitrogen Fixation, *ACS Appl. Energy Mater.*, 2019, **2**(12), 8394–8398, DOI: 10.1021/acsaem.9b01961.

282 C. Xiao, H. Hu, X. Zhang and D. R. MacFarlane, Nanostructured Gold/Bismutite Hybrid Heterocatalysts for Plasmon-Enhanced Photosynthesis of Ammonia, *ACS Sustain. Chem. Eng.*, 2017, **5**(11), 10858–10863, DOI: 10.1021/acssuschemeng.7b02788.

283 L. Li, Y. Wang, S. Vanka, X. Mu, Z. Mi and C. Li, Nitrogen Photofixation over III-Nitride Nanowires Assisted by Ruthenium Clusters of Low Atomicity, *Angew. Chem., Int. Ed.*, 2017, **56**(30), 8701–8705, DOI: 10.1002/anie.201703301.

284 K. Shu, B. Guan, L. Zhu, *et al.*, A Comprehensive Review of Transition Metal Catalysts in Ammonia Catalytic Oxidation: Recent Advances and Future Perspectives, *Energy Fuels*, 2025, **39**(34), 15919–15960, DOI: 10.1021/acs.energyfuels.5c01534.

285 R. Bariki, S. K. Pradhan, S. Panda, S. K. Nayak, A. R. Pati and B. G. Mishra, Hierarchical UiO-66(−NH $_2$)/CuInS $_2$ S-Scheme Photocatalyst with Controlled Topology for Enhanced Photocatalytic N $_2$ Fixation and H $_2$ O $_2$ Production, *Langmuir*, 2023, **39**(22), 7707–7722, DOI: 10.1021/acs.langmuir.3c00519.

286 T. Liu, L. Sun, Z. Cao, *et al.*, Construction of FeIn2S4/Palygorskite nanocomposite for photocatalytic nitrogen fixation coupled with biomass conversion, *J. Alloys Compd.*, 2023, **962**, 171181, DOI: 10.1016/j.jallcom.2023.171181.

287 Y. Zhang, L. Guo, Y. Wang, *et al.*, In-situ anion exchange based Bi2S3/OV-Bi2MoO6 heterostructure for efficient ammonia production: A synchronized approach to strengthen NRR and OER reactions, *J. Mater. Sci. Technol.*, 2022, **110**, 152–160, DOI: 10.1016/j.jmst.2021.09.009.

288 T. Gao, S. Yu, Y. Chen, *et al.*, Regulating the thickness of the carbon coating layer in iron/carbon heterostructures to enhance the catalytic performance for oxygen evolution reaction, *J. Colloid Interface Sci.*, 2023, **642**, 120–128, DOI: 10.1016/j.jcis.2023.03.067.

289 Z. Liu, X. Li, S. Su, *et al.*, Enhancing photocatalytic nitrogen fixation performance of Co-doped bismuth molybdate through band engineering tuning, *Appl. Surf. Sci.*, 2023, **611**, 155627, DOI: 10.1016/j.apsusc.2022.155627.

290 J. Wang, C. Zhao, S. Yuan, *et al.*, One-step fabrication of Cu-doped Bi2MoO6 microflower for enhancing performance in photocatalytic nitrogen fixation, *J. Colloid Interface Sci.*, 2023, **638**, 427–438, DOI: 10.1016/j.jcis.2023.02.005.

291 L. Zhang, X. Zhou, S. Liu, *et al.*, Two birds, one stone: Rational design of Bi-MOF/g-C3N4 photocatalyst for effective nitrogen fixation and pollutants degradation, *J. Cleaner Prod.*, 2023, **425**, 138912, DOI: 10.1016/j.jclepro.2023.138912.

292 X. Huang, Y. Shi, C. Liu, *et al.*, Enhanced photocatalytic nitrogen fixation on Cu2O clusters/MIL-100(Fe) heterojunction, *Appl. Surf. Sci.*, 2023, **640**, 158443, DOI: 10.1016/j.apsusc.2023.158443.

293 P. Li, H. Wu, C. Zhang, *et al.*, Rational design of BiOBr/Ov-TiO2-Cu photocatalyst for efficient nitrogen reduction to ammonia, *J. Alloys Compd.*, 2024, **982**, 173809, DOI: 10.1016/j.jallcom.2024.173809.

294 K. Guan, J. Li, W. Lei, *et al.*, Synthesis of sulfur doped g-C3N4 with enhanced photocatalytic activity in molten salt, *J. Materiomics*, 2021, **7**(5), 1131–1142, DOI: 10.1016/j.jmat.2021.01.008.

295 H. Wang, L. Zhang, K. Wang, X. Sun and W. Wang, Enhanced photocatalytic CO2 reduction to methane over WO3·0.33H2O via Mo doping, *Appl. Catal., B*, 2019, **243**, 771–779, DOI: 10.1016/j.apcatb.2018.11.021.

296 V. H. Nguyen, M. Mousavi, J. B. Ghasemi, *et al.*, High-impressive separation of photoinduced charge carriers on step-scheme ZnO/ZnSnO3/Carbon dots heterojunction with efficient activity in photocatalytic NH3 production, *J. Taiwan Inst. Chem. Eng.*, 2021, **118**, 140–151, DOI: 10.1016/j.jtice.2021.01.012.

297 S. Z. Zhao, Y. Lu, R. Lu, Y. D. Hu, R. D. Rodriguez and J. J. Chen, Constructing BiOBr/TiO2 heterostructure nanotubes for enhanced adsorption/photocatalytic performance, *J. Water Process Eng.*, 2023, **54**, 103972, DOI: 10.1016/j.jwpe.2023.103972.

298 D. Zhang, M. Wu, J. Hao, *et al.*, Construction of Z-scheme heterojunction by coupling Bi2Sn2O7 and BiOBr with abundant oxygen vacancies: Enhanced photodegradation performance and mechanism insight, *J. Colloid Interface Sci.*, 2022, **612**, 550–561, DOI: 10.1016/j.jcis.2021.12.152.

299 Z. Liu, M. Luo, S. Yuan, *et al.*, Boron-doped graphene quantum dot/bismuth molybdate composite photocatalysts for efficient photocatalytic nitrogen fixation reactions, *J. Colloid Interface Sci.*, 2023, **650**, 1301–1311, DOI: 10.1016/j.jcis.2023.07.085.

300 J. Chen, S. Zang, K. Gao, C. Zhang, X. Wang and H. Liu, Efficient photocatalytic nitrogen fixation over novel 2D/2D Bi12O17Br2/ZnCr layered double hydroxide heterojunction, *Appl. Surf. Sci.*, 2023, **639**, 158216, DOI: 10.1016/j.apsusc.2023.158216.

301 X. Huang, M. Sun, M. Humayun, *et al.*, In-situ synthesis of efficient N-graphyne/Bi/BiOBr photocatalysts for contaminants removal and nitrogen fixation, *J. Alloys Compd.*, 2024, **976**, 173025, DOI: 10.1016/j.jallcom.2023.173025.

302 W. Ding, X. Li, S. Su, *et al.*, Cationic vacancy engineering of p-TiO $_2$ for enhanced photocatalytic nitrogen fixation,

Nanoscale, 2023, **15**(8), 4014–4021, DOI: 10.1039/D2NR06821D.

303 C. Chen, R. Ji, X. Xia, *et al.*, Dispersed Bi2S3 site in a porphyrin-based metal–organic framework for photocatalytic nitrogen fixation, *Appl. Energy*, 2024, **357**, 122508, DOI: 10.1016/j.apenergy.2023.122508.

304 Y. Sun, H. Ji, Y. Sun, *et al.*, Synergistic Effect of Oxygen Vacancy and High Porosity of Nano MIL-125(Ti) for Enhanced Photocatalytic Nitrogen Fixation, *Angew. Chem., Int. Ed.*, 2024, **63**(3), e202316973, DOI: 10.1002/anie.202316973.

305 T. Shan, H. Luo, S. Wu, *et al.*, In situ formation of a covalent organic framework on g-C3N4 encapsulated with nanocellulosic carbon for enhanced photocatalytic N2-to-NH3 conversion, *Fuel*, 2024, **358**, 130157, DOI: 10.1016/j.fuel.2023.130157.

306 R. Gupta, U. Alam and N. Verma, Efficient photofixation of nitrogen to ammonia over an S-scheme-based NiSnO3-g-C3N4 heterojunction, *Chem. Eng. J.*, 2024, **479**, 147644, DOI: 10.1016/j.cej.2023.147644.

307 Z. Zhao, S. Hong, C. Yan, *et al.*, Efficient visible-light driven N_2 fixation over two-dimensional Sb/TiO_2 composites, *Chem. Commun.*, 2019, **55**(50), 7171–7174, DOI: 10.1039/C9CC02291K.

308 Y. Xue, X. Kong, Y. Guo, Z. Liang, H. Cui and J. Tian, Synthesis of porous few-layer carbon nitride with excellent photocatalytic nitrogen fixation, *J. Materiomics*, 2020, **6**(1), 128–137, DOI: 10.1016/j.jmat.2020.01.006.

309 Y. Xue, Y. Guo, Z. Liang, H. Cui and J. Tian, Porous g-C3N4 with nitrogen defects and cyano groups for excellent photocatalytic nitrogen fixation without co-catalysts, *J. Colloid Interface Sci.*, 2019, **556**, 206–213, DOI: 10.1016/j.jcis.2019.08.067.

310 Z. Ding, S. Wang, X. Chang, D. H. Wang and T. Zhang, Nano-MOF@defected film C_3N_4 Z-scheme composite for visible-light photocatalytic nitrogen fixation, *RSC Adv.*, 2020, **10**(44), 26246–26255, DOI: 10.1039/D0RA03562A.

311 S. Cao, B. Fan, Y. Feng, H. Chen, F. Jiang and X. Wang, Sulfur-doped g-C3N4 nanosheets with carbon vacancies: General synthesis and improved activity for simulated solar-light photocatalytic nitrogen fixation, *Chem. Eng. J.*, 2018, **353**, 147–156, DOI: 10.1016/j.cej.2018.07.116.

312 L. Shi, Z. Li, L. Ju, *et al.*, Promoting nitrogen photofixation over a periodic WS_2 @TiO_2 nanoporous film, *J. Mater. Chem. A*, 2020, **8**(3), 1059–1065, DOI: 10.1039/C9TA12743G.

313 W. Wang, H. Zhou, Y. Liu, *et al.*, Formation of B–N–C Coordination to Stabilize the Exposed Active Nitrogen Atoms in g-C_3N_4 for Dramatically Enhanced Photocatalytic Ammonia Synthesis Performance, *Small*, 2020, **16**(13), 201906880, DOI: 10.1002/smll.201906880.

314 C. Liang, H. Y. Niu, H. Guo, *et al.*, Insight into photocatalytic nitrogen fixation on graphitic carbon nitride: Defect-dopant strategy of nitrogen defect and boron dopant, *Chem. Eng. J.*, 2020, **396**, 125395, DOI: 10.1016/j.cej.2020.125395.

315 X. Li, C. He, S. Zuo, *et al.*, Photocatalytic nitrogen fixation over fluoride/attapulgite nanocomposite: Effect of upconversion and fluorine vacancy, *Sol. Energy*, 2019, **191**, 251–262, DOI: 10.1016/j.solener.2019.08.063.

316 J. Fan, M. Zuo, Z. Ding, Z. Zhao, J. Liu and B. Sun, A readily synthesis of oxygen vacancy-induced In(OH)3/carbon nitride 0D/2D heterojunction for enhanced visible-light-driven nitrogen fixation, *Chem. Eng. J.*, 2020, **396**, 125263, DOI: 10.1016/j.cej.2020.125263.

317 J. Luo, X. Bai, Q. Li, *et al.*, Band structure engineering of bioinspired Fe doped SrMoO4 for enhanced photocatalytic nitrogen reduction performance, *Nano Energy*, 2019, **66**, 104187, DOI: 10.1016/j.nanoen.2019.104187.

318 D. Sun, L. Li, Y. Yu, *et al.*, B and cyano groups co-doped g-C3N4 with multiple defects for photocatalytic nitrogen fixation in ultrapure water without hole scavengers, *J. Colloid Interface Sci.*, 2021, **600**, 639–648, DOI: 10.1016/j.jcis.2021.05.075.

319 X. Chen, P. Xing, S. Wei, H. Luo, L. Dai and Y. Wang, Electrochemical co-reduction of N2 and CO2 to urea using In2S3 anchored on S-doped reduced graphene oxide, *J. Electroanal. Chem.*, 2024, **969**, 118516, DOI: 10.1016/j.jelechem.2024.118516.

320 X. Li, C. He, S. Zuo, *et al.*, Photocatalytic nitrogen fixation over fluoride/attapulgite nanocomposite: Effect of upconversion and fluorine vacancy, *Sol. Energy*, 2019, **191**, 251–262, DOI: 10.1016/j.solener.2019.08.063.

321 L. Tan, N. Yang, X. Huang, *et al.*, Synthesis of ammonia *via* electrochemical nitrogen reduction on high-index faceted Au nanoparticles with a high faradaic efficiency, *Chem. Commun.*, 2019, **55**(96), 14482–14485, DOI: 10.1039/C9CC06132K.

322 Y. Feng, Z. Zhang, K. Zhao, S. Lin, H. Li and X. Gao, Photocatalytic nitrogen fixation: Oxygen vacancy modified novel micro-nanosheet structure Bi2O2CO3 with band gap engineering, *J. Colloid Interface Sci.*, 2021, **583**, 499–509, DOI: 10.1016/j.jcis.2020.09.089.

323 A. Bjelajac, R. Petrović, M. Popović, *et al.*, Doping of TiO2 nanotubes with nitrogen by annealing in ammonia for visible light activation: Influence of pre- and post-annealing in air, *Thin Solid Films*, 2019, **692**, 137598, DOI: 10.1016/j.tsf.2019.137598.

324 I. Hong, H. S. Moon, B. J. Park, *et al.*, Band alignment modulation of g-C3N4 by tuning structural defects for selective ammonia photosynthesis from nitrate reduction under visible light irradiation, *Chem. Eng. J.*, 2024, **484**, 149506, DOI: 10.1016/j.cej.2024.149506.

325 F. Li, H. Liu, W. Chen, *et al.*, Light induced ammonia synthesis by crystalline polyoxometalate-based hybrid frameworks coupled with the Sv-1T MoS_2 cocatalyst, *Inorg. Chem. Front.*, 2022, **9**(15), 3828–3838, DOI: 10.1039/D2QI01003H.

326 Y. Cao, S. Hu, F. Li, *et al.*, Photofixation of atmospheric nitrogen to ammonia with a novel ternary metal sulfide catalyst under visible light, *RSC Adv.*, 2016, **6**(55), 49862–49867, DOI: 10.1039/C6RA08247E.

327 P. Zhang, N. Zhang, Z. Liu and C. Du, Synthesis of $Zn_{0.1}Sn_{0.1}Cd_{0.8}S_x$ Solid Solutions for Photocatalytic Reduction of

Cr(VI): Bandgap Structure and Sulfur Vacancy Regulation, *Chem.–Asian J.*, 2023, **18**(10), 202300089, DOI: 10.1002/asia.202300089.

328 J. Ge, L. Zhang, J. Xu, Y. Liu, D. Jiang and P. Du, Nitrogen photofixation on holey g-C3N4 nanosheets with carbon vacancies under visible-light irradiation, *Chin. Chem. Lett.*, 2020, **31**(3), 792–796, DOI: 10.1016/j.cclet.2019.05.030.

329 Q. Zhang, S. Hu, Z. Fan, *et al.*, Preparation of g-C $_3$ N $_4$/ZnMoCdS hybrid heterojunction catalyst with outstanding nitrogen photofixation performance under visible light via hydrothermal post-treatment, *Dalton Trans.*, 2016, **45**(8), 3497–3505, DOI: 10.1039/C5DT04901F.

330 L. Li, X. Lv, L. Jin, *et al.*, Facile synthesis of Sn-doped MOF-5 catalysts for efficient photocatalytic nitrogen fixation, *Appl. Catal., B*, 2024, **344**, 123586, DOI: 10.1016/j.apcatb.2023.123586.

331 K. Pournemati, A. Habibi-Yangjeh and A. Khataee, TiO $_2$ Quantum Dots/Fe $_3$ S $_4$ Heterojunction Nanocomposites for Efficient Ammonia Production through Nitrogen Fixation upon Simulated Sunlight, *ACS Appl. Nano Mater.*, 2024, **7**(2), 2200–2213, DOI: 10.1021/acsanm.3c05517.

332 S. Hu, W. Zhang, J. Bai, G. Lu, L. Zhang and G. Wu, Construction of a 2D/2D g-C $_3$ N $_4$/rGO hybrid heterojunction catalyst with outstanding charge separation ability and nitrogen photofixation performance via a surface protonation process, *RSC Adv.*, 2016, **6**(31), 25695–25702, DOI: 10.1039/C5RA28123G.

333 S. Yuan, J. Wang, C. Zhao, *et al.*, S-scheme Bi2O3/CdMoO4 hybrid with highly efficient charge separation for photocatalytic N2 fixation and tetracycline Degradation: Fabrication, catalytic Optimization, physicochemical studies, *Sep. Purif. Technol.*, 2023, **325**, 124665, DOI: 10.1016/j.seppur.2023.124665.

334 Z. Dong, H. Feng, L. Li, Y. Hu, T. Yang and S. Xue, Photocatalytic nitrogen fixation by g-C3N4/MoS2/PbTiO3 with synergistic electric field, *J. Alloys Compd.*, 2023, **968**, 172226, DOI: 10.1016/j.jallcom.2023.172226.

335 L. Yue, J. Zhang, Z. Zeng, *et al.*, In Situ Fabrication of an S-Scheme NaNbO $_3$/Bi $_2$ O $_2$ CO $_3$ Heterojunction for Enhanced Performance in Photocatalytic Nitrogen Fixation, *Langmuir*, 2023, **39**(37), 13267–13278, DOI: 10.1021/acs.langmuir.3c01725.

336 K. Pournemati, A. Habibi-Yangjeh and A. Khataee, Outstanding photocatalytic nitrogen fixation performance of TiO2 QDs modified by Bi2O3/NaBiS2 nanostructures upon simulated sunlight, *J. Colloid Interface Sci.*, 2023, **641**, 1000–1013, DOI: 10.1016/j.jcis.2023.03.122.

337 T. Sun, P. Gao, Y. He, Z. Wu, J. Liu and X. Rong, Dual Z-scheme TCN/ZnS/ZnIn2S4 with efficient separation for photocatalytic nitrogen fixation, *J. Colloid Interface Sci.*, 2024, **654**, 602–611, DOI: 10.1016/j.jcis.2023.10.023.

338 X. Gao, Y. Shang, L. Liu and F. Fu, Multilayer ultrathin Ag-δ-Bi2O3 with ultrafast charge transformation for enhanced photocatalytic nitrogen fixation, *J. Colloid Interface Sci.*, 2019, **533**, 649–657, DOI: 10.1016/j.jcis.2018.08.091.

339 G. Wu, L. Yu, Y. Liu, J. Zhao, Z. Han and G. Geng, One step synthesis of N vacancy-doped g-C3N4/Ag2CO3 heterojunction catalyst with outstanding "two-path" photocatalytic N2 fixation ability via in-situ self-sacrificial method, *Appl. Surf. Sci.*, 2019, **481**, 649–660, DOI: 10.1016/j.apsusc.2019.03.112.

340 C. He, D. Chen and W. X. Zhang, Machine learning-driven shortening the screening process towards high-performance nitrogen reduction reaction electrocatalysts with four-step screening strategy, *J. Colloid Interface Sci.*, 2024, **676**, 22–32, DOI: 10.1016/j.jcis.2024.07.109.

341 M. Kim, B. C. Yeo, Y. Park, H. M. Lee, S. S. Han and D. Kim, Artificial Intelligence to Accelerate the Discovery of N $_2$ Electroreduction Catalysts, *Chem. Mater.*, 2020, **32**(2), 709–720, DOI: 10.1021/acs.chemmater.9b03686.

342 P. J. Rousseeuw, *Silhouettes: A Graphical Aid to the Interpretation and Validation of Cluster Analysis*, vol. 20, 1987.

343 P. Semnani, M. Bogojeski, F. Bley, *et al.*, A Machine Learning and Explainable AI Framework Tailored for Unbalanced Experimental Catalyst Discovery, *J. Phys. Chem. C*, 2024, **128**(50), 21349–21367, DOI: 10.1021/acs.jpcc.4c05332.

344 A. S. Mishra, V. G. Lade, J. R. Barmar, A. B. Bindwal and R. P. Birmod, A mini review on revolutionizing hydrogenation catalysis: unleashing transformative power of artificial intelligence, *J. Mol. Model.*, 2025, **31**(5), 152, DOI: 10.1007/s00894-025-06376-x.

345 L. G. de Araujo, L. Vilcocq, P. Fongarland and Y. Schuurman, Recent developments in the use of machine learning in catalysis: A broad perspective with applications in kinetics, *Chem. Eng. J.*, 2025, **508**, 160872, DOI: 10.1016/j.cej.2025.160872.

346 O. Capron and L. D. Couto, An Efficient Methodology Combining K-Means Machine Learning and Electrochemical Modelling for the Determination of Ionic Diffusivity and Kinetic Properties in Battery Electrodes, *Materials*, 2023, **16**(14), 5146, DOI: 10.3390/ma16145146.